



UNIVERSITY  
OF MANITOBA

# Investigation on Seat Structural Integrity and Occupant Safety in Coach Rollover

by

Hamid Giahi

A thesis submitted to the Faculty of Graduate Studies of

The University of Manitoba

in partial fulfillment of the requirements for the degree of

MASTER OF SCIENCE

Department of Mechanical Engineering

University of Manitoba

Winnipeg, Manitoba, Canada

Copyright © 2016 by Hamid Giahi

---

## **ABSTRACT**

Motor coaches are an integral part of the transportation system. It was observed that occupant fatalities and serious injuries occur in rollover more frequently than in any other type of accidents for these vehicles. Several regulations such as Economic Commission for Europe Regulation 66 (ECE R66) are issued to minimize the catastrophic consequences of rollover accidents. Passing “Motorcoach safety plan” which is based on a complete vehicle rollover test of ECE R66 will be mandatory in North America in the near future. However, the cost of a single physical test encourages researchers to perform numerical simulations prior to a complete vehicle rollover test.

In this thesis, the integrity of a coach seat and the effects of different restraint configurations on the safety of passengers in rollover are numerically studied. To perform this research, a new modeling approach, which is computationally effective and highly suitable for parametric studies, is proposed. Firstly, a detailed model of two seats of a coach is developed and validated against experimental results. Anthropomorphic Test Devices are then introduced to the model and acceleration history of a physical rollover test is imposed on the system. The model is solved using non-linear explicit dynamic Finite Element code LS-DYNA<sup>®</sup>. Injury criteria values are extracted and compared to the experimental results. An acceptable level of correlation is achieved that confirms the validity of the model and the reliability of the modeling approach. The integrity of the seat in a rollover is analyzed showing the necessity of an anchorage test prior to a whole coach rollover test. The results of a parametric study on the safety of passengers reveal the high probability of partial ejection if the retractor does not lock properly in a rollover. It is also shown that the safety of occupants can be improved if retractor pretensioners be introduced to coaches.

## **ACKNOWLEDGEMENTS**

I would like to express my appreciation to both my advisors Dr. Igor Telichev and Dr. Christine Wu whose instructions, guidance, helps, and kindness were motivating me through this research. Without their support, I would not be able to conduct this study.

Thank you to Anton Kuznetcov for his advice, guidance, and, software training.

Special thanks to my parents and wife for their supports and encouragements over the years.

# TABLE OF CONTENTS

Abstract .....	ii
Acknowledgements.....	iii
Table of Contents .....	iv
List of Tables .....	vii
List of Figures .....	ix
1 Introduction .....	1
1.1 Problem Statement .....	1
1.1.1 Motivation.....	1
1.1.2 Problem Definition.....	2
1.1.3 Proposed Solution .....	3
1.2 Thesis Formulation.....	4
1.2.1 Thesis objective .....	4
1.2.2 Research Questions .....	4
1.2.3 Scope of the Thesis .....	5
1.2.4 Organization of the Thesis .....	5
2 Background Information.....	8
2.1 Introduction .....	8
2.2 Regulations and Standards .....	10
2.2.1 FMVSS 220 Standard .....	11
2.2.2 ECE R66 Regulation.....	12
2.2.3 Comparison of FMVSS 220 and ECE R66.....	14

2.2.4	Motorcoach Safety Plan .....	15
2.3	Previous Researches .....	16
2.3.1	Structural Performance .....	16
2.3.2	Occupant Kinematics .....	18
2.3.3	Restraint System .....	20
2.4	Verification, Validation, and Calibration .....	22
3	Research Methodology .....	25
3.1	Modeling Approach.....	25
3.2	Software and Hardware .....	26
4	Model Development .....	30
4.1	Parts Development .....	30
4.2	Mesh Generation .....	33
4.3	Assembly and Connection.....	35
4.4	Boundary Condition .....	39
4.5	Material Properties .....	40
4.6	Elements Formulation .....	50
4.7	ATDs Positioning.....	51
4.8	Seat Belt .....	54
4.8.1	Overview.....	54
4.8.2	Seat Belt Material Property.....	55
4.8.3	Retractor.....	59
4.9	Loading Condition.....	60
4.10	Sub-model .....	62

4.10.1	Geometry.....	63
4.10.2	Mesh & Element Formulation .....	64
4.10.3	Assembly and Connection .....	66
4.10.4	Bolt Pre-stress .....	66
4.10.5	Boundary Condition.....	68
4.10.6	Material Properties.....	69
4.10.7	Loading Condition .....	69
5	Model Verification and Validation.....	71
5.1	Seat Structure Validation .....	71
5.2	ATDs' Kinematics, Verification, and Validation.....	75
6	Results and Discussion .....	85
6.1	Seat Structural Integrity .....	85
6.1.1	Kinematics of Occupants .....	85
6.1.2	Sub-model.....	87
6.1.3	Mesh convergence .....	99
6.2	Sensitivity Analysis of Restrain Properties .....	99
7	Summary and Future Work .....	107
7.1	Overview .....	107
7.2	Conclusions .....	109
7.3	Answers to the Research Questions .....	109
7.4	Future Work .....	110
	References.....	111

## LIST OF TABLES

Table 2-1 Occupant injury severity in 21 severe intercity bus collision in Canada 2002 [5].....	8
Table 2-2 Injury distribution in coach accidents, Spain 1995-2000 [6] .....	9
Table 2-3 Energy configurations for rollover test conditions of ECE R66 and FMVSS 220 .....	14
Table 2-4 Comparison metrics and acceptance criteria [26] .....	24
Table 4-1 Summary of mesh statistics .....	34
Table 4-2 Summary of mesh control .....	35
Table 4-3 Elastic materials' properties .....	40
Table 4-4 Rigid materials' properties .....	41
Table 4-5 Steel St34 material properties.....	42
Table 4-6 Steel SS304 material properties.....	43
Table 4-7 Steel S355 material properties.....	44
Table 4-8 Steel St-14 material properties .....	45
Table 4-9 Steel QSTE 460 material properties .....	46
Table 4-10 Steel St52-3 material properties .....	47
Table 4-11 Aluminum AA6060T4 material properties .....	48
Table 4-12 Foam material properties .....	49
Table 4-13 Fabric belt material properties.....	56
Table 4-14 Segment belt material properties .....	58
Table 4-15 Bolt and nut material properties .....	69
Table 5-1 Head acceleration* .....	77
Table 5-2 Chest acceleration*.....	78

Table 5-3 Pelvis acceleration* .....	78
Table 5-4 Upper neck forces in local CS* .....	79
Table 5-5 Summarized metrics' results .....	84
Table 6-1 Resultant stress for different bolt preload .....	91
Table 6-2 Maximum stress and strain for different load scenarios.....	97
Table 6-3 Retractor Configurations .....	100
Table 6-4 Injury risk comparison.....	105



## LIST OF FIGURES

Figure 2-1 Number of occupant fatalities [2] .....	9
Figure 2-2 Number of rollover fatalities by ejection status .....	10
Figure 2-3 FMVSS 220 test .....	11
Figure 2-4 Residual Space .....	12
Figure 2-5 Vehicle on the tilting platform .....	13
Figure 2-6 Seat positioning.....	19
Figure 2-7 Schematic of the verification processes .....	22
Figure 2-8 Schematic of the validation processes.....	23
Figure 3-1 Flowchart of research methodology.....	27
Figure 3-2 Employed commercial software.....	28
Figure 4-1 Provided 3d model .....	31
Figure 4-2 Sample of the provided drawings.....	31
Figure 4-3 Solid to shell conversion .....	31
Figure 4-4 Shell parts.....	32
Figure 4-5 Solid parts.....	32
Figure 4-6 Whole seat model.....	32
Figure 4-7 Final Model .....	33
Figure 4-8 Shell elements .....	34
Figure 4-9 Solid elements .....	34
Figure 4-10 A sample CNRB.....	36
Figure 4-11 A sample spot-weld.....	36

Figure 4-12 Whole model welding .....	36
Figure 4-13 Transversal beam to frame tied contact .....	38
Figure 4-14 Leg to rail frictional contact.....	38
Figure 4-15 a) floor rail BC b) bolt head BC c) side rail end BC.....	39
Figure 4-16 Steel St34 stress vs. plastic strain curve.....	42
Figure 4-17 Steel SS304 stress vs. plastic strain curve.....	43
Figure 4-18 Steel S355 stress vs. plastic strain curve.....	44
Figure 4-19 Steel St-14 stress vs. plastic strain curve .....	45
Figure 4-20 Steel QSTE 460 stress vs. plastic strain curve .....	46
Figure 4-21 Steel St52-3 stress vs. plastic strain curve .....	47
Figure 4-22 Aluminum AA6060T4 stress vs. plastic strain curve.....	48
Figure 4-23 Foam stress vs. strain curve .....	49
Figure 4-24 Contact instability caused by foam material property.....	50
Figure 4-25 Implemented ATD .....	52
Figure 4-26 a) Before the application of gravity b) After the application of gravity .....	53
Figure 4-27 Compressed cushions .....	53
Figure 4-28 Implemented ATD in the simulation vs. the test.....	54
Figure 4-29 Seat belt.....	55
Figure 4-30 Stress versus strain curve for fabric belt a) longitudinal b) lateral .....	57
Figure 4-31 Force versus strain curve for segment belt.....	59
Figure 4-32 Force vs. pull out for retractor.....	60
Figure 4-33 Accelerometers' locations .....	61
Figure 4-34 Mid-floor accelerometer data .....	61

Figure 4-35 a) Anchorage system in the whole model b) Sub-model .....	63
Figure 4-36 Sub-model geometry .....	64
Figure 4-37 Fine mesh .....	65
Figure 4-38 Final meshed model .....	65
Figure 4-39 Bolt pre-stress vs. time curve .....	67
Figure 4-40 Damping coefficient vs. time curve .....	67
Figure 4-41 Symmetry condition .....	68
Figure 4-42 Fixed points in the perpendicular direction.....	68
Figure 4-43 Section A-A in the whole model.....	70
Figure 4-44 Section A-A in the sub-model.....	70
Figure 5-1 Test setup .....	72
Figure 5-2 Applied load measured from the test .....	72
Figure 5-3 Experiment vs. simulation front view .....	73
Figure 5-4 Experiment vs. simulation rear view.....	73
Figure 5-5 Stroke displacement vs. time.....	74
Figure 5-6 Metrics results for seat structure validation .....	75
Figure 5-7 ATDs kinematics.....	76
Figure 5-8 Energy balance .....	77
Figure 5-9 Head Z (G's) vs. time (s) .....	80
Figure 5-10 Chest Z (G's) vs. time (s) .....	80
Figure 5-11 Pelvis Z (G's) vs. time (s).....	81
Figure 5-12 Neck FZ (N) vs. time (s) .....	81
Figure 5-13 Neck MY (Nm) vs. time (s) .....	82

Figure 5-14 Head Y (G's) vs. time (s) .....	82
Figure 5-15 Chest Y (G's) vs. time (s) .....	83
Figure 5-16 Pelvis Y (G's) vs. time (s).....	83
Figure 5-17 Neck FY (N) vs. time (s).....	84
Figure 6-1 the moment with the highest imposed load.....	85
Figure 6-2 Plastic strain distribution.....	86
Figure 6-3 Extracted load from the cut boundary .....	87
Figure 6-4 Sub-model before bolt pre-stress .....	88
Figure 6-5 Sub-model after bolt pre-stress, Displacement scale factor: 10.....	88
Figure 6-6 Contact force .....	89
Figure 6-7 Damped kinetic energy .....	89
Figure 6-8 Stress distribution in bolts.....	90
Figure 6-9 Stress concentration locations .....	90
Figure 6-10 Bolts pre-load application .....	91
Figure 6-11 Load and lock steps.....	91
Figure 6-12 Resultant stress for different bolt preload .....	92
Figure 6-13 Sub-model loading face.....	93
Figure 6-14 Von misses stress distribution.....	93
Figure 6-15 Stress distribution in each part .....	94
Figure 6-16 Plastic strain distribution.....	95
Figure 6-17 Contact Force between bracket and rail .....	96
Figure 6-18 Maximum stress .....	97
Figure 6-19 Plastic strain .....	98

Figure 6-20 Component test setup .....	98
Figure 6-21 Stress distribution for different element sizes a) 4mm b) 2mm c) 1 mm.....	99
Figure 6-22 Force vs. pull out for unlocked retractor.....	100
Figure 6-23 Force vs. pull out for unlocked retractor.....	101
Figure 6-24 Unlocked retractor performance .....	102
Figure 6-25 a) Unlocked retractor b) Locked retractor.....	103
Figure 6-26 Locked retractor performance .....	104
Figure 6-27 Pretensioner performance.....	104
Figure 6-28 Chest deflection comparison.....	106

# 1 INTRODUCTION

## 1.1 PROBLEM STATEMENT

### 1.1.1 Motivation

Rollover is one of the worst accident that may happen to any vehicles [1]. For coaches, rollover causes the most fatality and serious injuries. To improve the safety of occupants in a rollover, several safety regulations are proposed. These regulations enforce the bus manufacturers to analyze and, if necessary, redesign their products in order to increase the chance of occupant survival in a rollover accident. “Motorcoach safety plan” [2] is a regulation which will be mandatory in North America in the near future. According to Motorcoach safety plan [2], the rollover test must be performed on a whole coach, and specific requirements must be met. One of the requirements is that none of the seat anchorages can completely separate from their mounting structure. If even one seat anchorage fails, the bus does not pass the standard, and the whole coach rollover test must be repeated.

In the rollover test, 68 kg ballasts should be restrained to designated seats. As an alternative to ballasts, Anthropomorphic Test Devices (ATDs) are used in physical tests performed to date. In addition to providing the realistic loading for the structure, instrumented ATDs can be used to extract injury data to evaluate the injury risk of passengers in a coach rollover.

The cost of a single physical test motivates researchers to perform numerical simulation prior to a physical test. The aim of numerical simulations is first, to predict the response of different parts of

---

the structure in the rollover test and secondly, investigate the passenger's safety in a rollover accident. Moreover, significant findings from rollover accidents data show that occupant can be injured from poor seat and seat belt anchorages allowing the seat and belts to come loose [3].

The motivation of this research is thus to develop a numerical model to predict the seat structural integrity and, at the same time, investigate the safety of the restrained passengers in the rollover.

### 1.1.2 Problem Definition

In order to develop a numerical simulation tool which can evaluate the seat structural response in a rollover, a detailed model of the seat and an accurate loading condition are required. The imposed load on the seat is dependent on the occupant mass and the kinematics of the occupants in a rollover. An accurate kinematics of ATDs not only provides the realistic loading for the seat but also yields injury data of the passengers in a rollover. The obtained injury data can further be used to evaluate the passengers' safety during a coach rollover accident.

In all of the reviewed studies, to model the kinematics of occupants in a rollover, a whole coach or a bay section rollover simulation is performed. Since a complete vehicle or even a bay section rollover simulation is a computationally expensive task, the researchers have highly simplified the developed models. Simplifying the model would cause two issues. Firstly, a highly simplified seat model cannot numerically predict the integrity of the seat in the rollover. Secondly, in the majority of simplified models, the effects of the seat and seat belt parameters on the injury risk of passengers are ignored.

To evaluate the seat structural integrity in a rollover and to investigate the effects of seat belt parameters on the safety of passengers, having a detailed seat and seat belt models and, at the same

time, an accurate kinematics are essential. As discussed previously, performing the whole coach simulation to capture an accurate kinematics cannot be combined with a detailed model of seat and seat belt system due to the complexity of a whole coach simulation. Thus, the problem of this thesis is to find an alternative way to simulate the kinematics of occupant without dealing with the complexity of a coach rollover simulation.

### 1.1.3 Proposed Solution

In the present study, the kinematics of occupants in a rollover is simulated using just one row of seats with restrained ATDs, subjected to the acceleration history of a physical rollover test. By this new modeling approach, the desired accurate seat structure is implemented, and yet, the complex model of a coach or a bay section is completely omitted from the model. By having the accurate model of the seat, the required seat structural integrity analysis is carried out. Furthermore, omitting the complexity of a bay section or a whole coach rollover simulation yields the alternative model that has a high level of computational efficiency. Comparing the run-time of the new modeling approach with the reported run-time of the traditional methods shows that the run-time has decreased by a factor of 10. This level of efficiency makes the model perfectly suitable for further parametric studies on passengers' safety. In this study, by benefiting from the accurate seat belt model, a parametric study of the effects of different restraint system configurations on the injury risk of passengers is carried out.

To prove that the kinematics can be accurately modeled by the proposed modeling approach, the injury criteria of the ATD [4] is extracted and compared with experimental results. An acceptable level of agreement is achieved that confirms the validity of both the model and the proposed modeling approach.



## 1.2 THESIS FORMULATION

### 1.2.1 Thesis objective

The primary objectives of this thesis are to analyze the integrity of a coach seat in rollover and investigate the safety of restrained passengers. In order to achieve the main objectives, the following tasks have been pursued and completed step by step:

- Developing a Finite Element model of a row of coach seats in detail.
- Validating the developed model of the seat structure against experimental results.
- Introducing restrained ATDs to the model and simulating the kinematics of occupants in a rollover by imposing an acceleration history of a physical rollover test on the model.
- Validating both the proposed modeling approach and the kinematics of occupants by comparing injury risk data with experimental results.
- Analyzing the structural response of the seat anchorage under the imposed inertial force of occupants in the rollover.
- Performing a parametric study of the effects of retractor performance on the injury risk of passengers.

### 1.2.2 Research Questions

The following question is going to be answered through this thesis:

- Is the proposed modeling approach a valid substitute for a complete vehicle rollover simulation allowing to get an accurate kinematics?
- How can the new modeling approach be justified and validated?

- For the validation of the model, what level of correlation is acceptable? What criterion should be used to quantitatively compare the simulation and the experimental results?
- Is the new modeling approach more computationally effective when compared to the traditional approach?
- Can the developed model be used for further parametric studies on passenger safety in a rollover?

### 1.2.3 Scope of the Thesis

In this thesis, the seat structural response under the inertial force of occupants is investigated. To consider the worst case scenario, a row of seats opposite to the impact side is studied. The anchorage of the seats opposite to the impact side is the worst one since the mass of restrained occupants are imposed on the anchorages during the rollover. In this study, the side wall deformation around the seat mounting structure is not considered. However, the deformation can be added to the model as a boundary condition.

At the time of writing this thesis, the sidewall deformation is unknown; however, other members of the group are investigating a complete vehicle rollover simulation that will yield the sidewall deformation time history once completed.

### 1.2.4 Organization of the Thesis

This thesis is divided into seven chapters. The first chapter is dedicated to an introduction to this thesis. The importance of this research is firstly presented followed by the thesis problem and the proposed solution. The objectives of this study are then clearly stated. Afterward, the questions

associated with the proposed solution are provided. The scope of the thesis is then presented that specifies the boundary of this study.

The second chapter starts with a review of the existent regulations for bus rollover. The regulations are compared, and the one which will be mandatory in North America is described in detail. This is followed by a background information about the relevant research conducted to date. Chapter two finishes with an overview of the criterion used in this study for quantitative validation.

The research methodology will subsequently be presented in chapter three. The modeling approach is explained in detail, and the software and hardware used to solve the model are introduced. This chapter also includes an introduction about explicit dynamic, as the solving method for the model, and its pros and cons.

In chapter four, the model development is described in a step-by-step fashion. The procedure for the part development and assembly is firstly described. The properties of the assigned material to the parts are then provided. The implemented elements' formulations are explained as well. ATDs are then introduced, and the positioning process is described. In this chapter, the necessity of sub-modeling the anchorage system is stated, and the sub-model's development procedure is finally expressed.

Afterward, the model is validated, and the results of validation are presented in chapter five. The validation is divided into two stages. In the first stage, the seat structure is validated against a quasi-static test, and the results are presented. Secondly, the results of verification and validation of the kinematics of an occupant under rollover are shown. To have a quantitative validation, two comparison metrics are used, and the findings are presented in this chapter.

Chapter six is dedicated to results and discussions. It consists of two sub-sections. Firstly, the total deformation of the seat structure under the imposed load is shown. The critical location with maximum stress is found, and the necessity of sub-molding the anchorage is justified. The results of the sub-model simulation are then shown and based on the sub-model results, a component test is designed and proposed to the bus manufacturer. Secondly, the result of a parametric study on the influence of the retractor performance on the injury risks of passengers is presented. It is shown that the model can effectively be used toward increasing the passenger's safety in a rollover.

This study ends up with the conclusion and future works. The conclusion part summarizes the findings of the thesis and answers the thesis questions. How the model can be used for a future study on the passenger's safety is described in the future work section.

## 2 BACKGROUND INFORMATION

### 2.1 INTRODUCTION

Traveling by bus is now one of the safest types of transportation [5]. In Canada, only 0.3% of all road fatalities comes from the accidents involving busses, and in Europe, this number is less than 0.25% [5]. However, even a single accident may lead to a significant number of casualties. Among all kind of accidents that happen for buses in Canada, rollover causes the most fatalities and serious injuries. In 21 intercity bus collisions in Canada, 28.3% of the occupants faced severe, critical and fatal injuries in rollover accidents. For non-rollover accidents, the value is only 8.1% [5] (Table 2-1).

*Table 2-1 Occupant injury severity in 21 severe intercity bus collision in Canada 2002 [5]*

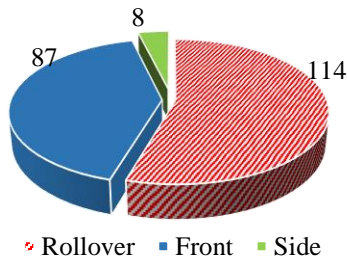
	No Injury	Minor	Moderate	Serious	Severe	Critical	Death	Not specified	Total Passengers
Rollover	26	113	12	6	9	1	52	5	219
Non-Rollover	179	92	30	16	10	1	17	1	346

Based on Fatality Analysis Reporting System (FARS) data for buses, in the 10-year period of 2000 to 2009, rollovers account for more than half of the occupant fatalities in the US [2] (Figure 2-1).

Injury distribution in intercity buses in Spain showed that although the total number of occupants involved in rollover accidents is not high, the risk of fatalities in a rollover is about five times

higher than all other accidents [6] (Table 2-2). Moreover, analysis of the data from more than 300 events in Hungary showed that the average casualty rate per accident for rollover is 25, while it is 17 for frontal collision [7].

*Table 2-2 Injury distribution in coach accidents, Spain  
1995-2000 [6]*



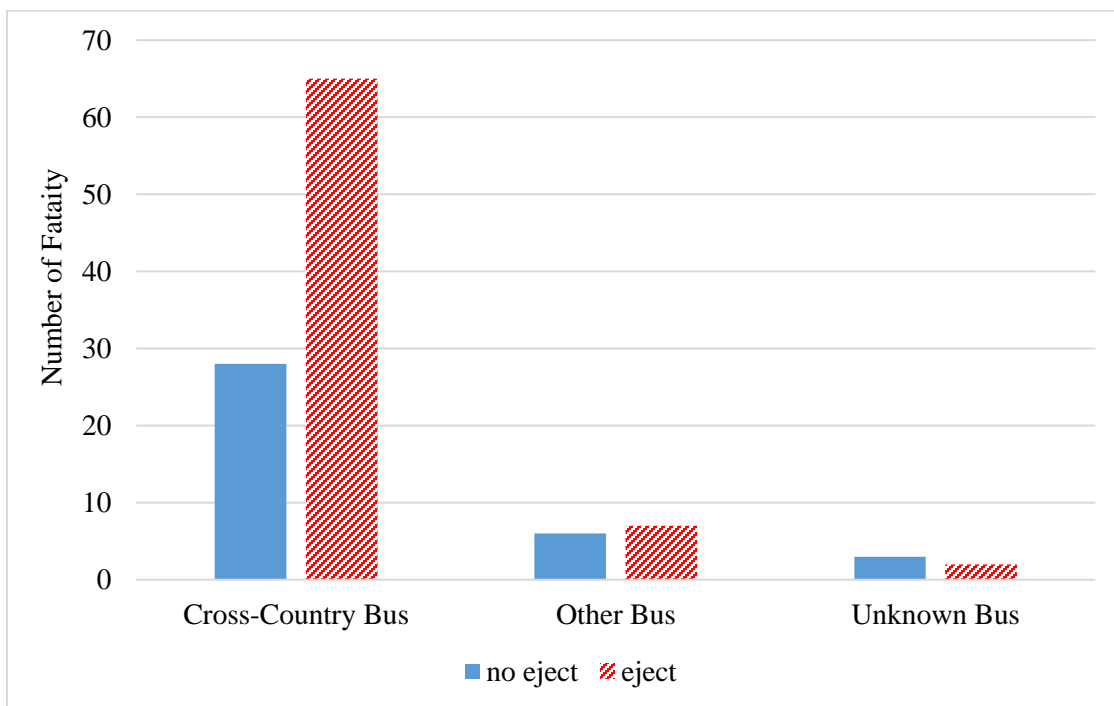
*Figure 2-1 Number of occupant fatalities [2]*

Injury Severity	Rollover	Others
Fatalities	9.6 %	2.5%
Serious injured	32.1%	7.7%
Minor injured	55.6%	43.3%
Not injured	2.6%	46.5%
Total number of occupants	1037	14151

Further examination of FARS data shows that two third of fatalities in a rollover is related to ejected occupant [2] (Figure 2-2).

Consequently, regulations like Federal Motor Vehicle Safety Standard (FMVSS) 220 [8] and Economic Commission for Europe Regulation 66 (ECE R66) [9] with the aim of minimizing catastrophic consequences of rollover accidents are established. The proposal of these regulations forced the manufacturers to analyze their products and, if necessary, redesign the structure to increase the chance of occupant's survival in a rollover accident.

Tripped and untripped are two types of rollovers [10]. Tripped rollover happens when the vehicle leaves the roadway, and after an impact with an external object like a barrier or a curb, it starts to roll several times. On the other hand, untripped rollover happens due to high-speed collision avoidance maneuvers, severe turn or rapid lane changes. In an untripped rollover, the vehicle rotates 90 degrees, and the sidewall hits the ground. The consequences of the untripped rollover are more dependent on the characteristics of the bus structure rather than the accident situation; therefore, the regulations are mainly targeted toward occupant safety in an untripped rollover.



*Figure 2-2 Number of rollover fatalities by ejection status*

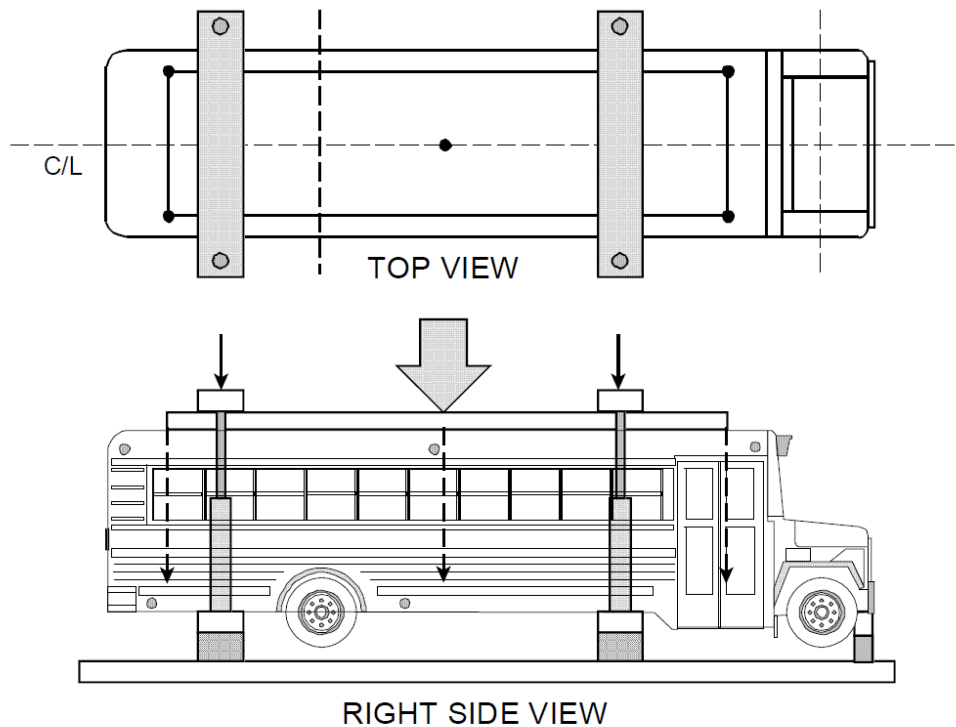
## 2.2 REGULATIONS AND STANDARDS

In 1977, the American Department of Transportation established the FMVSS 220 standard for school buses [8]. In 1987, the Economic Commission for Europe enforced Regulation No 66 [9].

In ECE R66, the bus superstructure must be reinforced in a way to ensure that a predefined survival space remains untouched in a rollover test. In 2014, National Highway Traffic Safety Administration (NHTSA) issued a notice of proposed rulemaking for North America [2]. It states that a bus should meet specific requirements after a complete vehicle rollover test based on ECE R66. In this section, each regulation is briefly introduced.

### 2.2.1 FMVSS 220 Standard

FMVSS 220 [8] was enforced in 1977 by the United States Department of Transportation for school bus rollover protection. The FMVSS 220 states that a force equal to 1.5 times of the unloaded vehicle weight should be applied to the roof of the vehicle's body structure through a flat, rigid, rectangular force application plate. Figure 2-3 shows how the test must be performed.



*Figure 2-3 FMVSS 220 test*



The vehicle can get the approval if the downward vertical movement of the plate does not exceed the specific distance of 130.175 mm. The emergency exits must be operable during the full application of the force and after the release of the force.

### 2.2.2 ECE R66 Regulation

The ECE R66 regulation [9] is enforced by the Economic Commission in 1978 for Europe after series of severe rollover accidents. It applies to single-decked vehicles constructed for carrying more than 22 passengers, seated or standing, in addition to the driver and crew. The superstructure is the main load bearing and energy absorbing part of the structure. It refers to coherent components which contribute to the strength of the bus structure. The regulation states that the superstructure design must ensure that a predefined survival space (residual space) inside the bus remains unaffected during and after a rollover test. It means that no intrusion to the survival space by the parts which was out of the survival space is acceptable. Moreover, no parts which were in the survival space can project outside. The survival space is a longitudinal envelope inside the bus with predefined dimensions. In Figure 2-4 the shaded area illustrates the survival space.

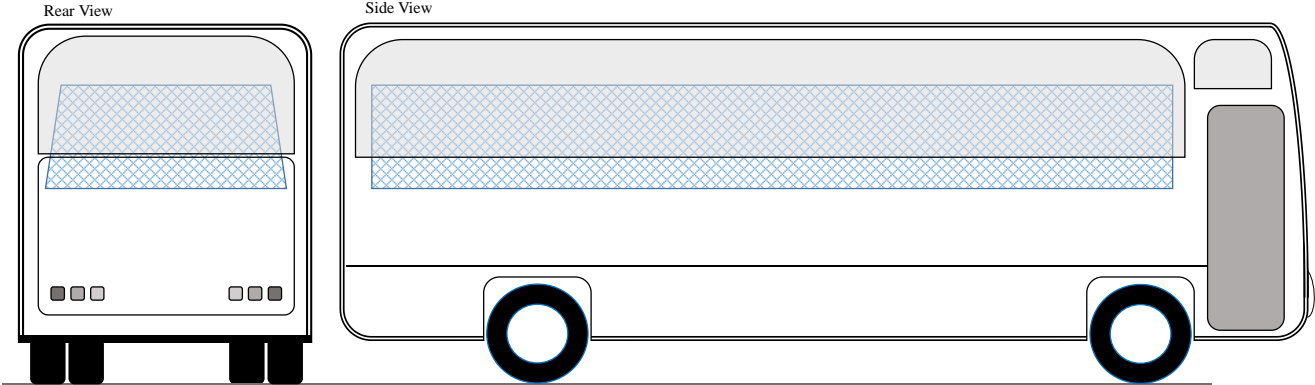
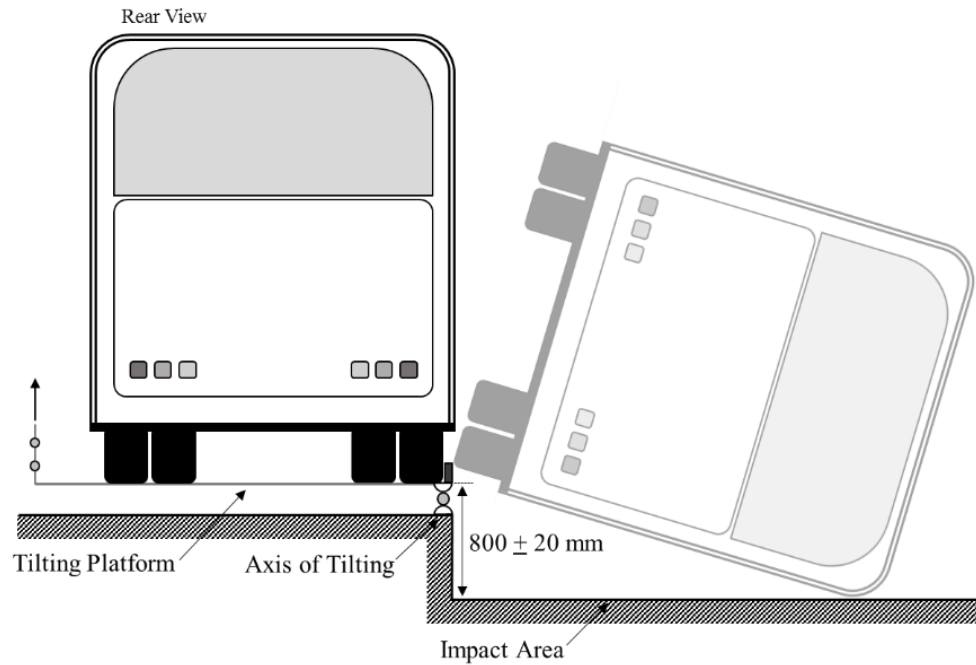


Figure 2-4 Residual Space

In the rollover test, the vehicle should be tipped over from an 800 mm raised platform onto a level ground surface made of concrete. Figure 2-5 shows vehicle on the tilting platform and after it touches the ground surface.



*Figure 2-5 Vehicle on the tilting platform*

There are totally five equivalent approval tests. A bus must successfully pass at least one of the following tests to get the approval:

- a) Complete vehicle rollover test;
- b) Rollover tests on body sections which are representative of the complete vehicle;
- c) Quasi-static loading tests of body sections;
- d) Quasi-static calculations based on the results of component tests;
- e) Computer simulation - via dynamic calculations - of the basic rollover test on a complete vehicle.

In these tests, it is assumed that passenger mass is self-arresting. Therefore, the required energy which should be absorbed by the superstructure of the coach depends exclusively on the unladen mass of the vehicle.

### 2.2.3 Comparison of FMVSS 220 and ECE R66

Liang et al. [11] compared FMVSS 220 and ECE R66 regulations through a finite element analysis of a bus superstructure. The distortion distribution of the vehicle superstructure through the absorbed energy was investigated. It was found that these two regulations are quite different in terms of distortion configuration which indicates that they are representative for different accident scenarios. In the ECE R66, the side wall section of the vehicle superstructure had the highest distortion (57.16%) while the roof section in FMVSS 220 consumes the most energy by a distortion of 50.01%. Table 2-3 shows the energy configuration of the vehicle under both test procedures.

*Table 2-3 Energy configurations for rollover test conditions of ECE R66 and FMVSS 220 [11]*

Vehicle & Section	ECE R66		FMVSS 220	
	Energy Absorbed (KJ)	Rate (%)	Energy Absorbed (KJ)	Rate (%)
Whole vehicle	66.55	100	1.33	100
Front section	6.35	9.55	0.23	17.50
Rear section	8.03	12.07	0.11	8.27
Roof section	13.34	20.04	0.67	<b>50.01</b>
Side wall section	38.04	<b>57.16</b>	0.30	22.80
Others	0.79	1.18	0.02	1.42

It was concluded that the European standard is more related to a lateral rollover accident; whereas the US standard deals with an accident in which the roof compresses under the impact of the roof with the ground or under the weight of the vehicle itself. Furthermore, it was shown that survival space was more in danger of being intruded in the lateral rollover testing condition.

#### 2.2.4 Motorcoach Safety Plan

National Highway Traffic Safety Administration (NHTSA) issued a notice of proposed rulemaking with the aim of increasing rollover structural integrity for buses in North America [2]. The test procedure is based on the ECE R66. After the test, the following requirements should be met:

1. Intrusion into the “survival space,” demarcated in the vehicle interior, by any part of the vehicle outside the survival space is prohibited;
2. Each anchorage of the seats and overhead luggage racks must not completely separate from its mounting structure;
3. Emergency exits must remain shut during the test and must be operable after the test;
4. Each side window glazing opposite the impacted side of the vehicle must remain attached to its mounting such that there is no opening that will allow the passage of a 102 mm diameter sphere.

In the rollover test, 68 kg ballasts should be restrained to designated seats by the provided seat belt system. Occupant mass imposes a more realistic load on both the vehicle structure and the seat anchorages.

Although passing the new proposal is based on complete vehicle rollover test and no computer simulation is acceptable, the expenses of a single physical test encourage researchers to simulate

the rollover process before the test. Meeting the regulation's requirements in the first complete vehicle rollover test is desirable for any bus manufacturer.

As an alternative to ballasts, Anthropomorphic Test Devices (ATDs) can be used to evaluate the injury risks of passengers in the rollover test. This yields valuable research data about the safety of passengers in a rollover. Although the regulation does not require any injury criteria data extraction from ATDs, the main goal of the regulation is to improve the safety of passengers in a rollover. Consequently, NHTSA used the ATDs in all physical tests performed to date.

## 2.3 PREVIOUS RESEARCHES

After the proposal of aforementioned regulations, researchers have analyzed a variety of buses. Structural performance and occupant kinematics are the two major fields that are under investigation by the researchers. Structural analysis can predict the performance of a bus in rollover and kinematics of occupants yields valuable research data about the safety of passengers in a rollover.

### 2.3.1 Structural Performance

The structural analysis mainly demonstrates whether the survival space (explained in subsection 2.2.2) is intruded or not. The results can be used as a guideline for bus manufacturers to improve their products.

Guler et al. [12] studied the influences of the seat structure, passengers, and luggage weight on the structural response of a bus following ECE R66. A Finite Element model of a bus superstructure in LS-DYNA code was used in this study. It was demonstrated that introduction of a simplified seat frame to the bus baseline model strengthened the whole structure and decreased the distance

between the sidewall and survival space by 20%. However, passengers' weight caused the survival space to be intruded, and moreover, the inclusion of the luggage mass caused a further increase in the deformation of the superstructure. It was concluded that a bus structure which passes the ECE R66 regulation without considering the passenger mass might fail after adding the weight of passengers. Therefore, it was recommended to include the passenger mass analysis in the next revision of the regulation.

Anderson et al. [13] found the percentage of occupant mass that should be coupled to the structural mass during the ECE R66 test in order to better reproduce the real accident. The percentage was found for different types of provided restraint systems on the bus. It was shown that 71% of the passenger mass for lap-belts, 93% for 3-point belts and 18% for unrestrained passengers should be coupled to the structure during a rollover. The research findings confirm the recommendation by Guler [12]. The study emphasized that although introducing the passengers mass to the vehicle is not requested by ECE R66, it can have a great influence on the structural response of the whole coach.

In another research performed by Chirwa et al. [14], a Finite Element model of a 32-seat bus superstructure was developed to pass the ECE R66 regulation virtually. The stiffness and energy absorption capability of the model were validated through a quasi-static and a pendulum impact experimental testing of a roof joint. In that study, the parts in the structure that significantly affect the crashworthiness capability of the whole structure in rollover were identified.

In other research conducted by Bojanowski et al. [15], ECE R66 rollover test was introduced to paratransit buses and a new measure of safety margin was proposed in rollover test of these

vehicles. It was shown that a multi-objective optimization on the structural strength increased the distance between the structure and the survival space from 16% to 29%.

### 2.3.2 Occupant Kinematics

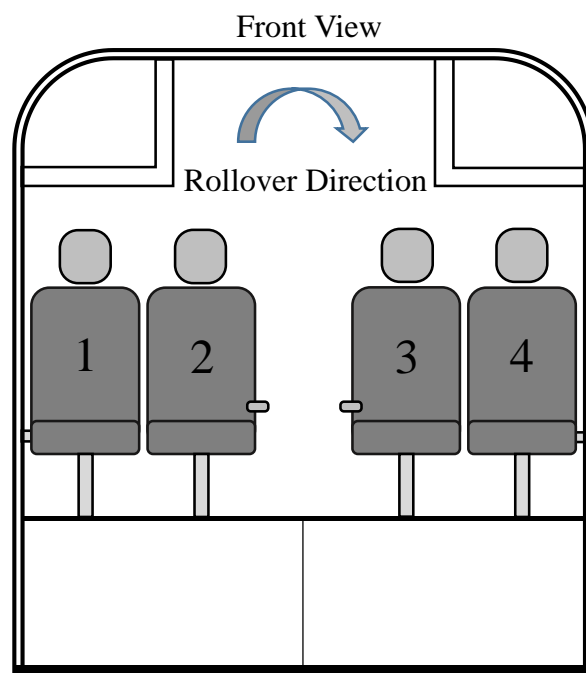
In addition to bus structural analysis, modeling the kinematics of an occupant in a rollover for evaluation of the injury risk is among researchers' interests. Significant findings from accidents data showed that occupant could be injured as a result of poor seat and seat belt anchorages allowing the seat and belts to come loose [3]. This motivates the development of a numerical simulation of the occupant kinematics to improve the safety of passengers in a rollover.

Guler et al. [16] used a bus baseline structure from [12] and introduced eight ATDs to the model. To understand the effects of different seat belt system, a whole coach rollover simulation was performed for ATDs with no seat belt, 2-point, and 3-point seat belts respectively. The injury criteria values were extracted from ATDs, and the 2-point seat belt was recommended. Only Head Injury Criteria (HIC) and neck force were extracted in the research and the seat structure, and seat belt models were simplified.

Martinez et al. [6] used a numerical model of a bay section to investigate the injury risk of the passenger in a rollover. It was shown that a 2-point seat belt could reduce the injury risk for all occupants except those sitting in position four (Figure 2-6). It was concluded that lateral airbags could reduce the injury risk of a passenger by preventing the hard contact of the passenger's head with the sidewall.

Belingardi et al. [17] also built a bay section numerical model using a combination of multibody (MB) and Finite Element approach with simplified seat models and one ATD. A parametric study

was performed to understand the effects of occupant size, restraint system and structural strength on the injury risk of passengers. It was concluded that a 2-point seat belt is ineffective for an ATD in position three (Figure 2-6) since it cannot prevent the impact between the ATD's head and the side window. But the use of a 3-point seat belt can effectively decrease the head injury of the mentioned occupant. It was also shown that an ATD seated in position four does not benefit from any kind of seat belt and the head injury always exceeds the acceptable value.



*Figure 2-6 Seat positioning*

As mentioned previously, Anderson et al. [13] stated that a bus might fail after considering the passengers' mass. Belingardi et al. [18] suggested that bus structures should be reinforced to pass the regulation after considering the presence of passengers. Then the influences of this reinforcement on the injury risk of the passengers were studied. To study the injury risk, a detailed model of the seat structure was added to the base model. An accurate model of the seats is added



to consider the effects of ATD's interaction with the seats. The seat structure was modeled using a hybrid multibody-finite element method. Comparing the results of the detailed model with a simulation that has a simplified seat structure showed that the seat modeling approach has a great influence on the injury risk of passengers. In this research, two different bus structure, regular strength and increased strength, were studied. It was concluded that reinforcement increases the risk of injuries if adequate restraint system (3-point seat belt) is not used. Some components in the model were simplified, and as it was shown in the paper, the simplifications affect the injury risk results [18].

In a study conducted by Deshmukh [19], firstly, a detailed model of a transit bus is developed for a rollover analysis of the structure. However, a separate highly simplified model is developed for performing a parametric study on injury risk of seated and standing passengers. As it can be seen in this study, performing a complete vehicle rollover simulation for a parametric study on injury risk of passengers is not feasible.

### 2.3.3 Restraint System

Retractor is one of the key parts of a 3-point seat belt system. Different types of retractors are developed to improve the occupant protection in frontal and side impacts. All retractors come with an Emergency Locking Mechanism (ELM) which locks the webbing under vehicle deceleration in crashes. Some others have pretensioner which deploys even prior to the crash and tighten the belt to keep the occupant in the safest position. More advanced one, Energy Management Retractor (EMR), benefits from a load limiter that allows webbing to be pulled out in a controlled way to minimize load on passenger's chest. Since the retractors are designed for the frontal crashes, its

behavior in the rollover is an open question and has been under investigation for passenger cars for several years.

Hare et al. [20] investigated the performance of seat belt with and without pretensioner in 8 rollover tests of SUVs. A modified FMVSS 208 [4] rollover test was used in the study. Although their tests were not repeatable, the desired performance of seat belt was confirmed. It was concluded that pretensioner does not have great influence on reducing the injury risk of SUV's occupants in a rollover.

Michael E. Klima et al. [21] analyzed seat belt retractor performance in a passenger car based on a new repeatable test method. It was shown that for the simulated rollover test, the retractor remains locked.

It is observed from real world evidence that restraint system cannot prevent the head of passenger cars' driver from being partially ejected in a rollover [22]. In a research conducted by Friedman [23], it was discussed that hard contact of the drivers head with the ground, due to the partial ejection, can cause fatal head injury. Two roof design modifications were suggested to strength the car structure in a way to eliminate or minimize the hard contact of the head with the ground [24].

Although the performance of seat belt's retractor in passenger cars is under investigation over the years, its performance in a coach rollover is not fully understood.

## 2.4 VERIFICATION, VALIDATION, AND CALIBRATION

A computer simulation should pass a verification and validation procedure to be considered acceptable and accurate [24]. Based on American Society of Mechanical Engineer definition [25], verification, validation, and calibration of a computer simulation are defined as follow:

1. **Verification:** The process of determining that a computational model accurately represents the underlying mathematical model and its solution.
2. **Validation:** The process of determining the degree to which a model is an accurate representation of the real world from the perspective of the intended uses of the model.
3. **Calibration:** The process of adjusting physical modeling parameters in the computational model to improve agreement with experimental data.

The purpose of verification is to compare the discrete numerical approximation with the mathematical solution. In crashworthiness analysis, the numerical solution is usually performed in a Finite Element software and the mathematical solution is achieved analytically solving the differential equation. Figure 2-7 shows the schematic of the verification process.

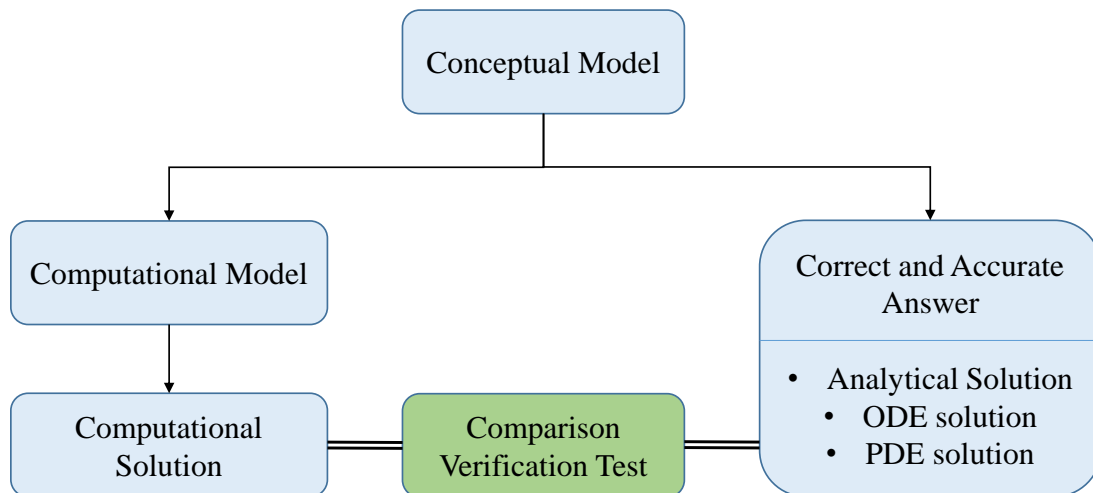


Figure 2-7 Schematic of the verification processes

On the other hand, validation is the process of comparison of the numerical and experimental results. The verification test can vary from a component test to a full-scale crash test. Figure 2-8 shows the schematic of the validation process.

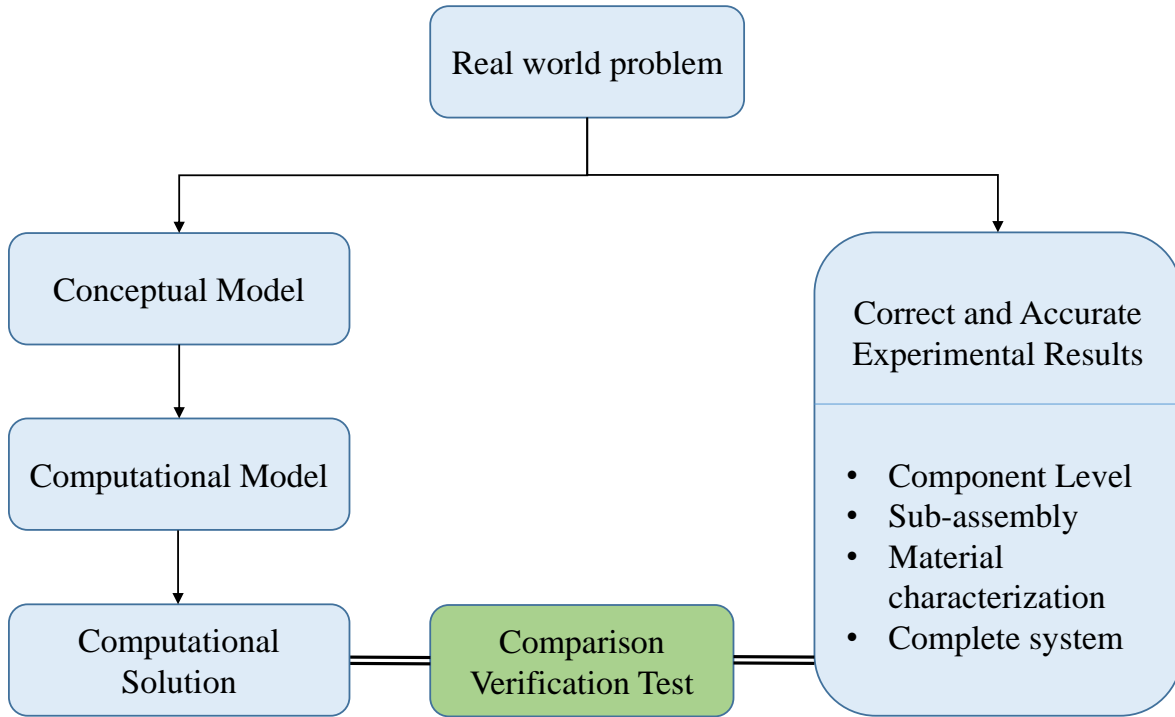


Figure 2-8 Schematic of the validation processes

In this thesis, the verification of the simulation is performed by checking the energy balance. To provide a quantitative validation, Roadside Safety Verification and Validation Program (RSVVP) [26] is used. RSVVP is developed to compare the similarity between two curves by computing the comparison metrics. Two metrics are evaluated for each pair of curves, namely, the Magnitude-Phase-Composite (MPC) and analysis of variance (ANOVA). MPC metric compares the magnitude and phase of a pair of curves and then combines them into a single composite value. In the current research Sprague & Geers metric [27] is chosen, and its analytical description is presented in Table 2-4. In the table  $m_i$  and  $c_i$  indicate measured, and computed quantities

respectively and  $i$  refers to a specific instant in time. ANOVA metrics [28] is used as the second comparison metrics. The criterion compares time domain signal of a finite element simulation with the physical test to see if they can be determined as the same event. The analytical definition of ANOVA metrics and the acceptance criteria suggested by National Cooperative Highway Research Program (NCHRP) can be found in Table 2-4.

Table 2-4 Comparison metrics and acceptance criteria [26]

Metrics	Metrics' Terms	Equations	Acceptance criteria, %
Sprague & Geers [26]	Magnitude	$M = \sqrt{\frac{\sum c_i^2}{\sum m_i^2}} - 1$	$\leq 40$
	Phase	$P = \frac{1}{\pi} \cos^{-1} \frac{\sum c_i m_i}{\sqrt{\sum c_i^2 \sum m_i^2}}$	$\leq 40$
	Comprehensive	$\sqrt{M^2 + P^2}$	$\leq 40$
ANOVA [26]	Average Residual	$\bar{e}^r = \frac{\sum(m_i - c_i)}{m_{max}} \frac{1}{n}$	$\leq 0.5$
	Standard Deviation	$\sigma^r = \sqrt{\frac{1}{n} \sum (m_i - c_i - \bar{e}^r)^2}$	$\leq 35$

## 3 RESEARCH METHODOLOGY

### 3.1 MODELING APPROACH

Investigating the integrity of a bus seat structure in a rollover is one of the requirements in the newly proposed “Motorcoach safety plan.” To investigate the structural integrity of the seat, in addition to a detailed model of seat, an accurate kinematics of occupants in a rollover is needed. A precise occupant’s kinematics not only impose a realistic load to the seat structure but also provide useful data about passengers’ safety in a coach rollover.

In this study, a detailed model of seat structure is developed. All the required details that may influence the kinematics are considered. The developed seat structure model is then validated against experimental results. Afterward, ATDs are introduced to the model. To simulate the kinematics of occupants, instead of assembling seats in either a bay section or a complete bus structure, acceleration history of a physical NHTSA’s complete vehicle rollover test is applied directly to the system. The proposed method can save considerable cost and computational resources. However, the new modeling approach needs to be validated. In order to do that, the ATD injury risks in the physical, and the numerical tests are compared. This comparison not only confirms the reliability of the modeling approach but also shows the validity of the model.

Afterward, the critical anchorage with the highest probability of failure is found. This anchorage is sub-modeled to include all features of design for capturing an accurate stress distribution. In the sub-model simulation, the probability of failure of the anchorage in a rollover is investigated. Based on the sub-model simulation results, a component test is designed and proposed to the bus

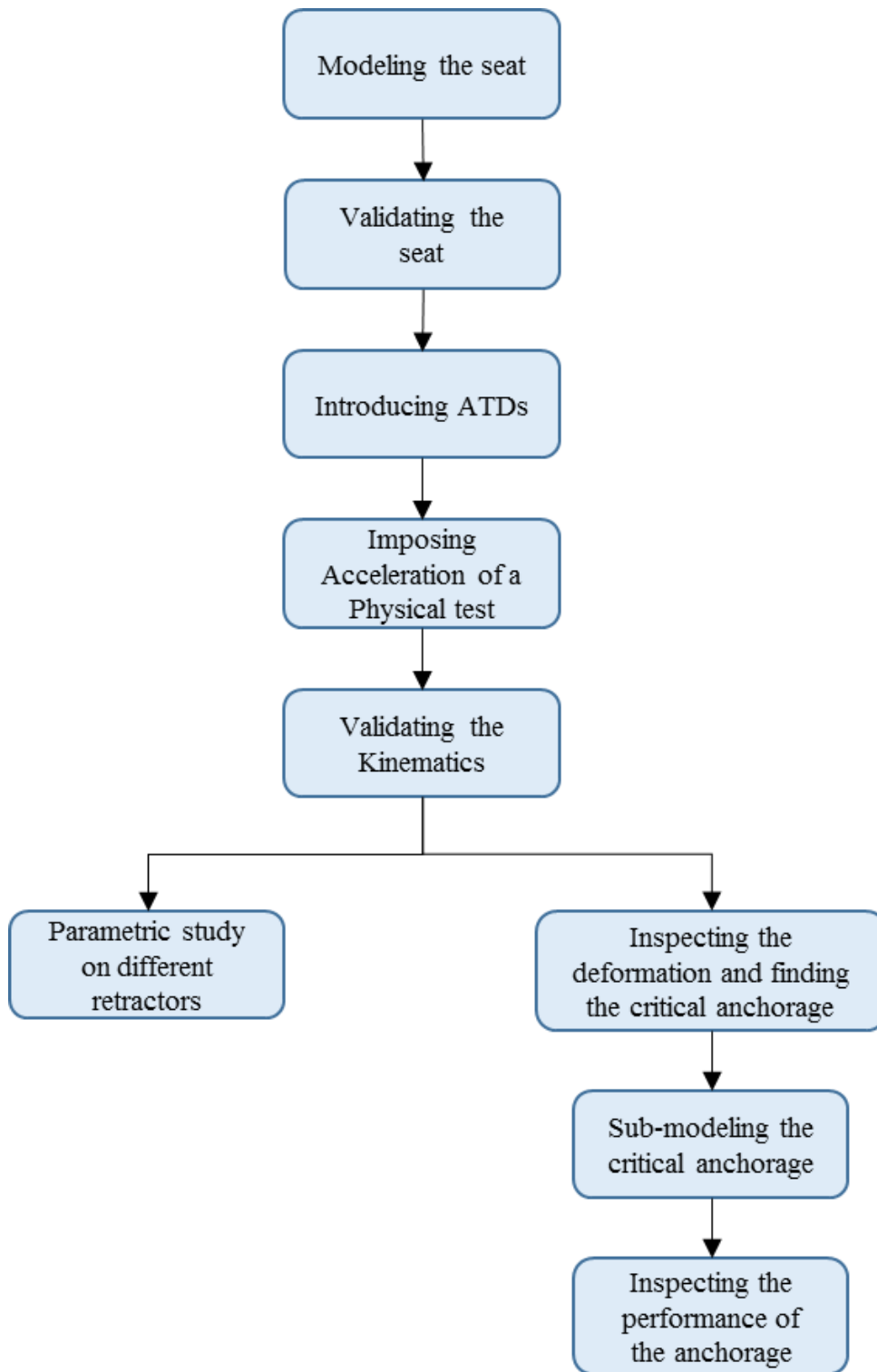
manufacturer to be performed prior to a complete vehicle rollover test. Comparing the results of this study with the component test can accurately predict the behavior of the anchorage system in a rollover.

Moreover, the developed model is used for a parametric study on the effects of different retractor types (Retractor with ELM, retractor with pretensioner, and EMR) and their performance on the injury risk of passengers. Figure 3-1 shows the research methodology in a flowchart format.

### 3.2 SOFTWARE AND HARDWARE

In this research, the Finite Element seat structure is modeled based on drawings and 3D CAD files of the seat provided by the seat manufacturer. ANSYS Mechanical<sup>®</sup> [29] and workbench LS-DYNA<sup>®</sup> [30] are used to simplify the geometries and create parts. Eligible 3D geometries are simplified as shell parts, and the model meshed manually, The Finite Element parts are imported to LS-PP<sup>®</sup> [31] for assembly and material assigning. The key file of the fully developed model is extracted and solved by LS-DYNA<sup>®</sup> explicit dynamic solver. The results are read by LS-PP for post processing and data extraction. Figure 3-2 shows an overview of methodology with the employed commercial software.

The pre and post processing of the model is performed using a workstation with 4 GB RAM and four cores 2.67 GHz processor. However, the simulations are performed using supercomputing facility, GREX, with 8 to 16 cores for different simulations.



*Figure 3-1 Flowchart of research methodology*



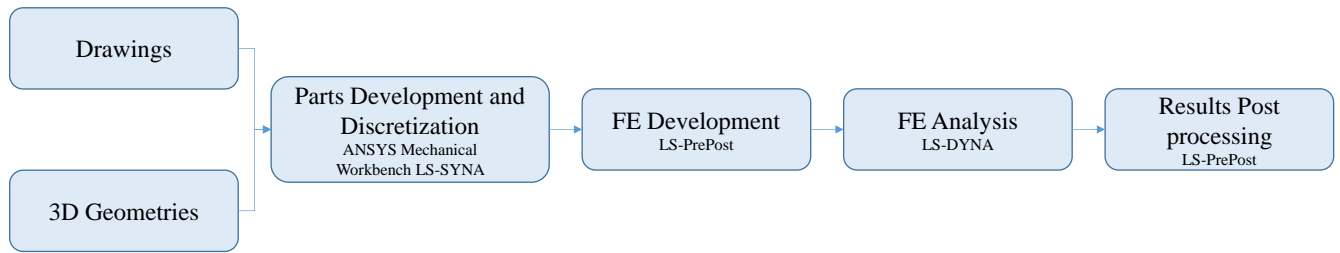


Figure 3-2 Employed commercial software

In dynamic explicit solver, nodal accelerations are obtained directly (explicitly, not iteratively). Once nodal accelerations are known, the central difference integration rule is used to update the velocity at time  $t + \frac{\Delta t}{2}$  and displacements at time  $t + \Delta t$ . No iterations are required in the equation solver to update the accelerations, velocities, and displacements. From the displacements, strain and stress can be found, and the cycle will be repeated.

Nodal accelerations are solved by multiplying the easily inverted diagonal mass matrix with the net nodal force vector (Equation 3-1). Nodal force includes all external forces which can come from body force, applied pressure, contact and element stress, damping, bulk viscosity, and hourglass control [32].

$$\ddot{\mathbf{x}}|_t = [\mathbf{M}]^{-1} \cdot (\mathbf{F}_i - \mathbf{F}_e)|_t \quad \text{Equation 3-1}$$

Where  $\ddot{\mathbf{x}}$  = acceleration vector of length  $n$ ,  $[\mathbf{M}] = n \times n$  mass matrix,  $\mathbf{F}_e$  = body force and external load vector of length  $n$ ,  $\mathbf{F}_i$  = internal force vector of length  $n$ .

Central difference integration rule (Equation 3-2) is used to explicitly find the displacement at the next time step from already found nodal acceleration.

$$\begin{cases} \dot{x}|_{t+\frac{\Delta t}{2}} = \dot{x}|_{t-\frac{\Delta t}{2}} + \ddot{x}|_t \Delta t \\ x|_{t+\Delta t} = x|_t + \dot{x}|_{t+\frac{\Delta t}{2}} \Delta t \end{cases} \quad \text{Equation 3-2}$$

In the explicit analysis, the time step should be less than the time required for a sound wave to travel across an element. Equation 3-3 shows the time step of an explicit analysis.

$$\Delta t = \frac{L_s}{c} \quad \text{Equation 3-3}$$

Where  $L_s$  is characteristic length of element and  $c$  is sound speed in the material.

Sound speed in a material can be found from Equation 3-4.

$$c = \sqrt{\frac{E}{\rho(1 - \nu^2)}} \quad \text{Equation 3-4}$$

Where  $E$  is material's Young modulus,  $\rho$  is density, and  $\nu$  is Poisson's ratio.

As it can be seen in Equation 3-3 time step is a function of element size and material property. It can be concluded that each element has a time step and the governing global time step for the whole simulation is controlled by the element with the smallest time step [33]. As a result, a single small element can cause the global time step to be unreasonably small. Utilizing mass scale is a remedy that can keep the explicit time step in a reasonable range. Mass-scaling refers to a feature in which nonphysical mass is added to small elements in order to achieve a larger time step [32]. The amount of added mass can be tracked through the simulation. The percentage of the added mass must be small enough to keep the effects of the added mass insignificant.

## 4 MODEL DEVELOPMENT

### 4.1 PARTS DEVELOPMENT

The provided 3D CAD geometries by the seat manufacturer consisted of solid parts with all the detailed features (Figure 4-1). However, no material properties were assigned to them. To make the parts compatible with a Finite Element analysis, unnecessary details are simplified. The parts that are theoretically qualified to be modeled as shell parts are simplified to shell. In order to do that, mid-surface of each part is extracted. The rest of the parts which are not eligible to be modeled as shell remain solid. Solid parts are cushion foam, hand-rest, and bolts. Few parts that do not play any role in the total stiffness of the structure are not considered in the modeling process. All dimensions of the components in the CAD file are compared to the provided drawings (Figure 4-2 as an example) to increase the rigorousness of the model.

Figure 4-3 shows an example of the converting solid parts to shell components. A gap equal to half of the thickness is considered between the surfaces to avoid initial penetration.

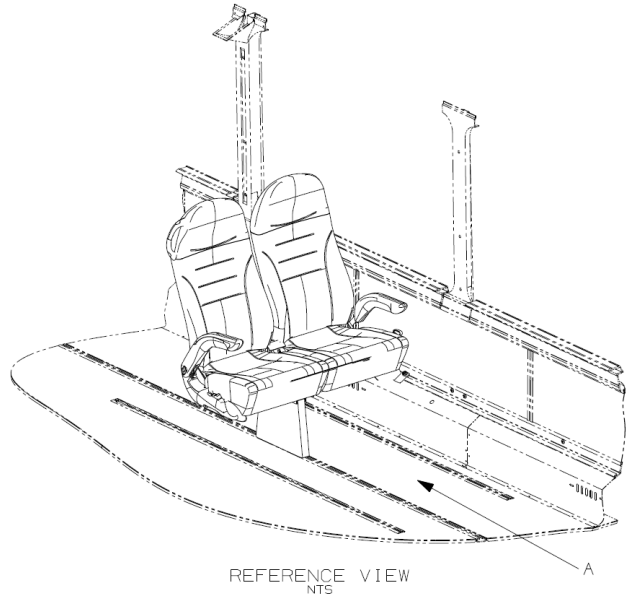
The model consists of 81 parts, 54 shell parts, 23 solids, and 4 beams. The beams are used to model the recliner mechanism.

Figure 4-4 shows the parts which are modeled as a shell. In Figure 4-5 parts which are modeled as solid components can be seen. The whole assembly model of the seat can be found in Figure 4-6.

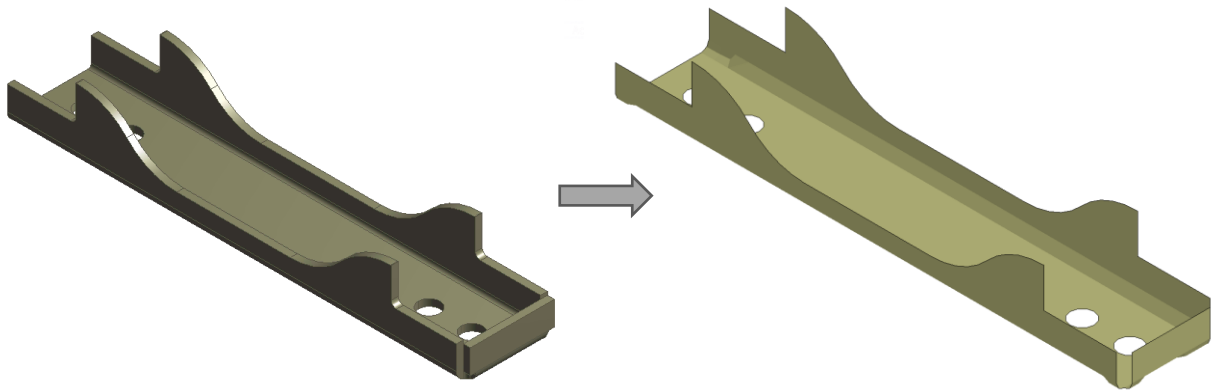
To be able to analyze the anchorage performance, part of the sidewall and floor rail are added to the model. Three rigid walls which represent the sidewall and floor are introduced to the assembly. The final model is shown in Figure 4-7.



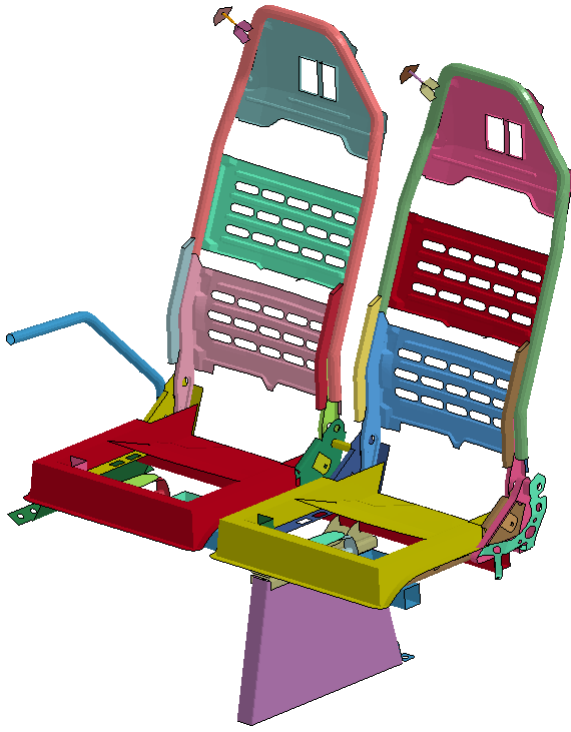
*Figure 4-1 Provided 3d model*



*Figure 4-2 Sample of the provided drawings*



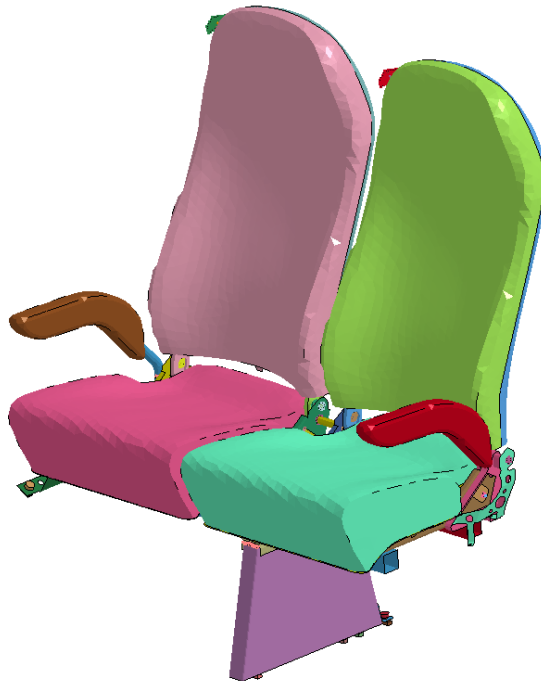
*Figure 4-3 Solid to shell conversion*



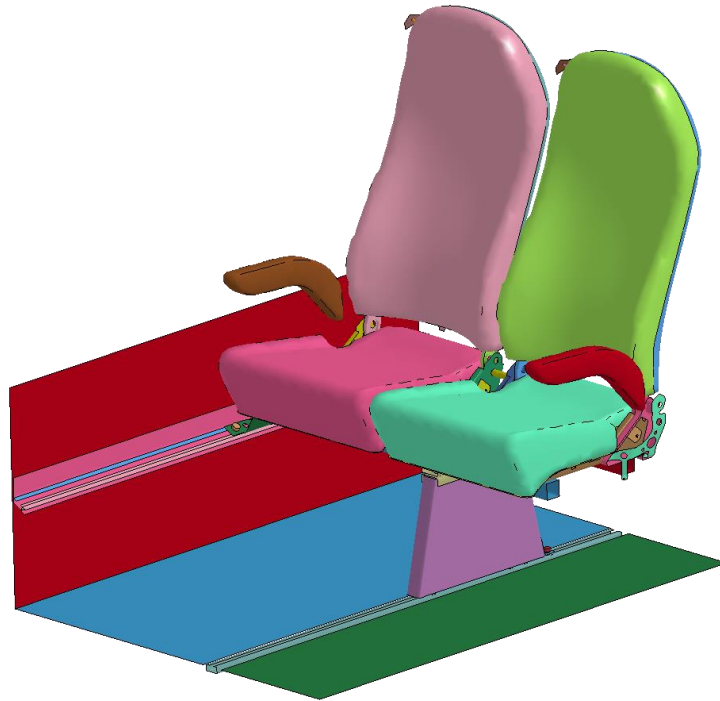
*Figure 4-4 Shell parts*



*Figure 4-5 Solid parts*



*Figure 4-6 Whole seat model*



*Figure 4-7 Final Model*

## 4.2 MESH GENERATION

Shell parts are dominantly discretized to quadrilateral shell elements; however, few areas with triangle shell elements can be found in the model.

Pyramid elements, which are created in the transition from hexahedron to tetrahedron elements, are not acceptable in the explicit dynamic simulation. As a result, solid parts should be exclusively discretized by either hexahedron or tetrahedron elements. Hexahedron is preferred to tetrahedron elements since the same volume can be meshed with fewer elements; however, the geometric complexity of the parts enforces tetrahedron elements to be used as well. Table 4-1 shows the summary of the generated mesh for the model.

Table 4-1 Summary of mesh statistics

<i>Specification</i>	<i>Triangle/ Tetrahedron</i>	<i>Quadrilateral/ Hexahedron</i>	<i>Total</i>
Number of 2d elements	946	68,085	69,031
Number of 3d elements	119,955	1,464	121,419
Number of nodes	-	-	146176

Figure 4-8 and Figure 4-9 illustrate the generated mesh for shell and solid parts respectively.

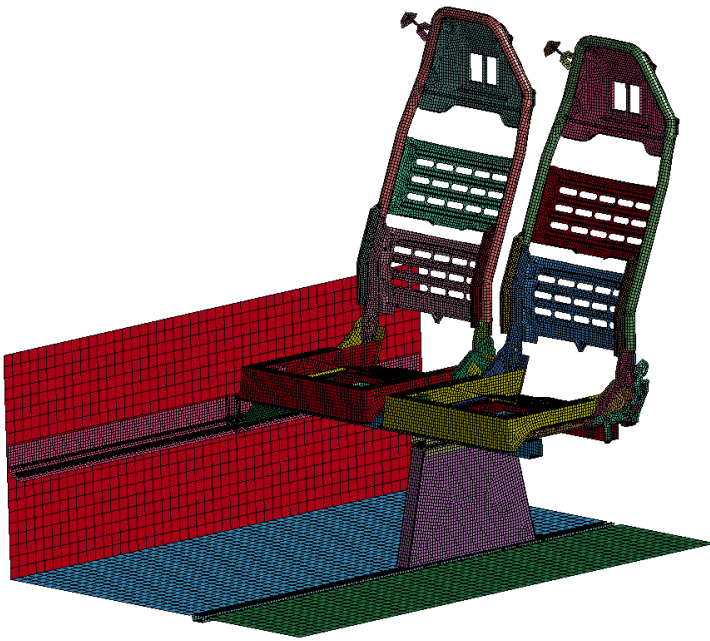


Figure 4-8 Shell elements



Figure 4-9 Solid elements

Mesh quality is checked by the common criteria for 2d and 3d elements. Less than 5% low-quality elements in the non-load bearing parts are considered to be acceptable. Attempts to improve the mesh quality further decrease the efficiency of the model since the time step is a function of element size. Keeping the mesh size in an acceptable range while having a good quality of mesh leads to approximate size of 6 mm, 20 mm, and 2 mm for shell elements, foam hexahedron elements, and solid parts, respectively. Table 4-2 shows the percentage of failed elements based on some mesh quality control criteria for 2d and 3d elements.

*Table 4-2 Summary of mesh control*

<i>Criterion</i>	<i>Failed 2d elements</i>		<i>Failed 3d elements</i>	
Jacobian	4%		0%	
Min. angle	<i>Quadrilateral</i>	1%	<i>hexahedron</i>	0%
	<i>triangle</i>	1%	<i>triangle</i>	3%
Max. angle	<i>Quadrilateral</i>	1%	<i>hexahedron</i>	1%
	<i>triangle</i>	5%	<i>triangle</i>	4%
Warpage	1%		0%	
Aspect ratio	0%		0%	

### 4.3 ASSEMBLY AND CONNECTION

The structure of the real seat is primarily assembled by butt welding. In the model, these connections are implemented using Tied Contacts and Constraint Nodal Rigid Bodies (CNRB).



Few parts are connected by the spot-weld and extra-node keyword. A sample weld, which is modeled by CNRB, can be found in Figure 4-10. Figure 4-11 shows a spot-weld that connect the retractor to the seat frame. Figure 4-12 shows all CNRB in the model.

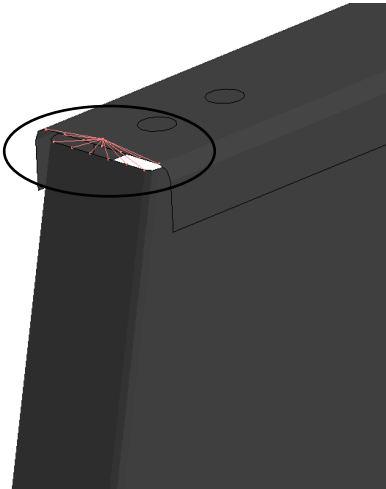


Figure 4-10 A sample CNRB

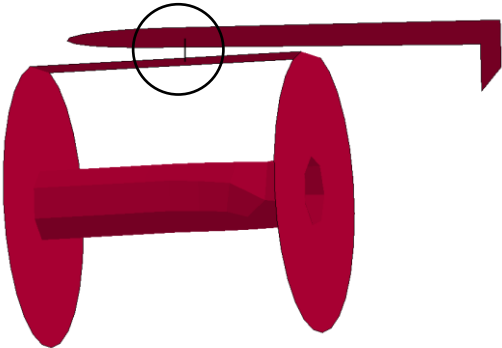


Figure 4-11 A sample spot-weld

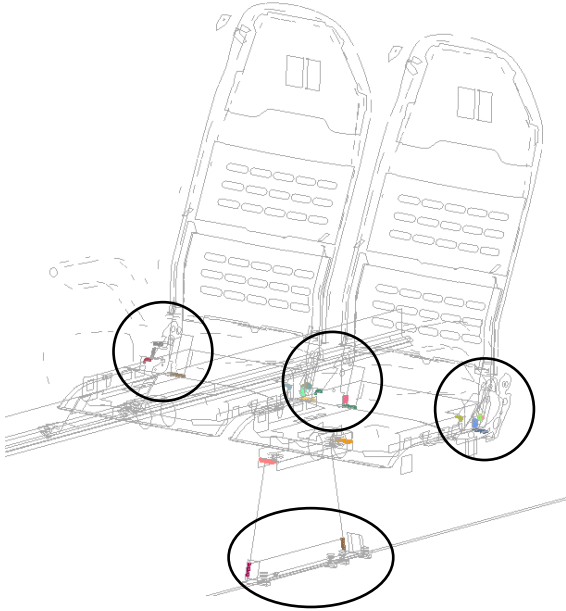


Figure 4-12 Whole model CNRB

The model consists of more than 100 contacts in total. Contacts are either frictional or tied. The frictional contacts are Surface-to-Surface with the static coefficient of friction of 0.6. A 10% of critical viscous damping coefficient is considered in contacts to make contacts more stable.

For the contacts with wide variation in the elastic bulk modulus between the two pairs of the contact, a segment based contact definition is used [33]. As an example, cushion foam and seat frame can be mentioned. In the default penalty-based approach, the contact stiffness is calculated based on the material properties of the pairs (Equation 4-1). However, when dissimilar materials with different bulk modules come into contact, the stiffness become small. The reason is that the stiffness is calculated based on the minimum bulk modules of the pairs [33]. A small contact stiffness causes the contact to break down easily. On the other hand, the contact stiffness in a segment based contact is defined using the nodal mass and the global time step (Equation 4-2). Consequently, the segment based contact is ideal when the soft and hard material come to contact.

$$k = \frac{SF \times Area \times K}{Minimum\ Diagonal} \quad \text{Equation 4-1}$$

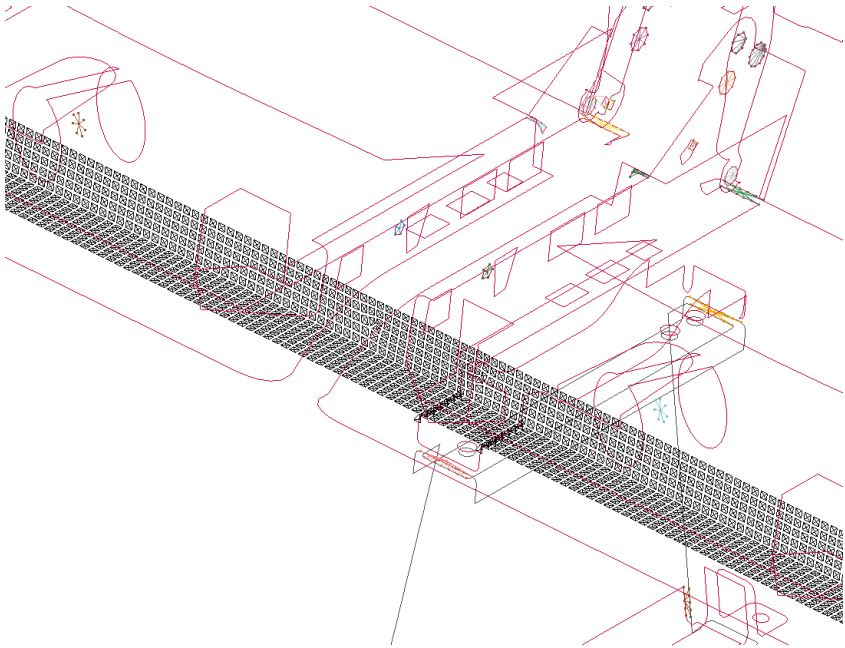
Where  $SF$  is a scale factor, and  $K$  is the bulk moduli.

$$k = SF \frac{m}{\Delta t^2} \quad \text{Equation 4-2}$$

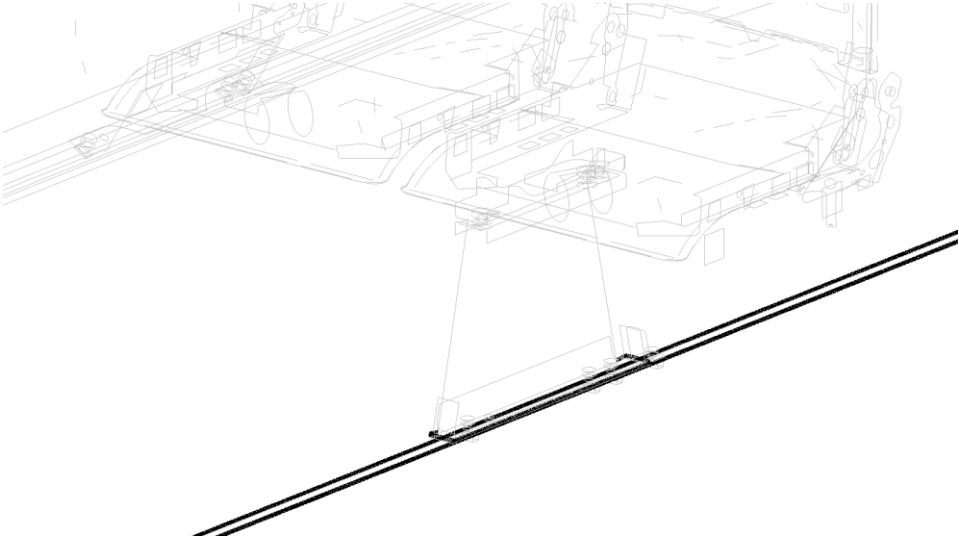
where  $m$  is the nodal mass, and  $\Delta t$  is the global time step.

The tied contacts, which is used to model welds, are “Node to Surface” with an offset between the contact pairs. The offset is considered to avoid initial penetration. Any initial undetected penetration is ignored in the contact control card. The same 10% viscous damping is used for the tied contact.

Shaded area in Figure 4-13 shows an example of frictional contact and a sample of tied contact can be seen by two lines in Figure 4-14.



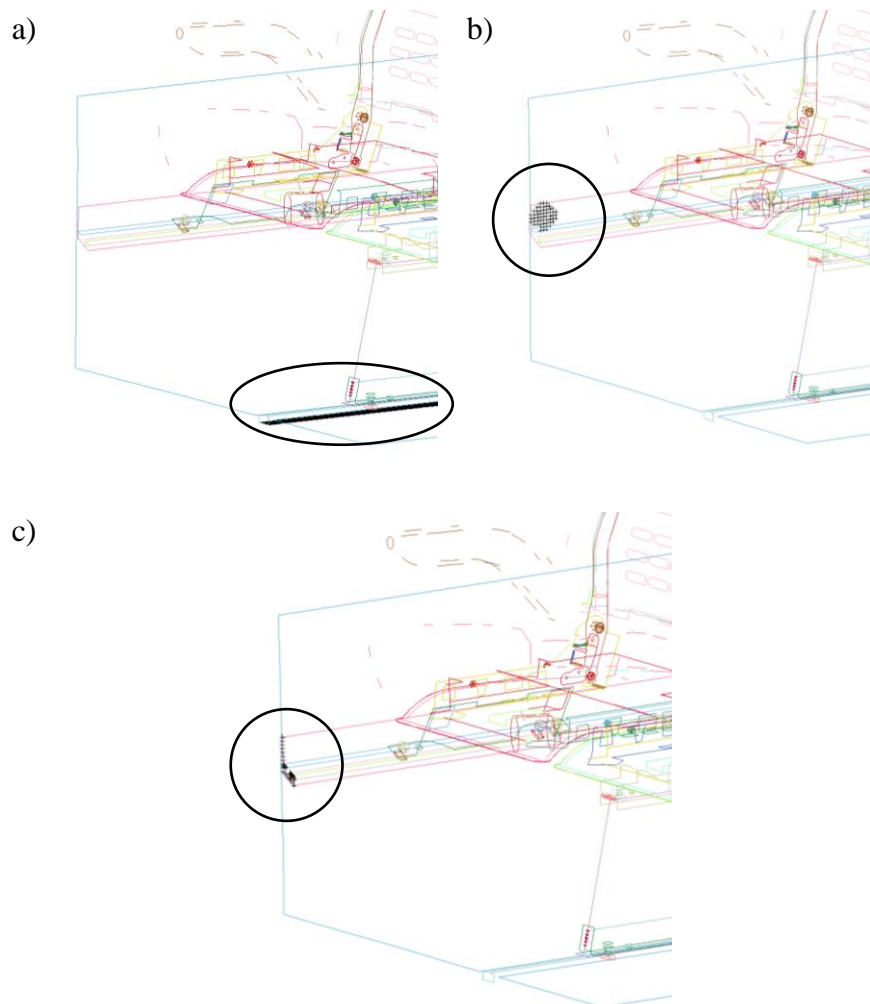
*Figure 4-13 Transversal beam to frame tied contact*



*Figure 4-14 Leg to rail frictional contact*

#### 4.4 BOUNDARY CONDITION

In the coach, the seat is bolted to the floor and side rail. The floor rail is welded, and the side rail is bolted to the superstructure. In the Finite Element model, the lower surface of floor rail is fully constrained to represent the welding between the floor rail and the superstructure. To model the side rail connections, the area which is underneath the bolt heads in the coach are fixed in the Finite Element model. Symmetric conditions are applied to the two ends of rails to consider the continuation of the rail along the coach. In Figure 4-15 boundary conditions are shaded in black.



*Figure 4-15 a) floor rail BC b) bolt head BC c) side rail end BC*

## 4.5 MATERIAL PROPERTIES

To have a robust Finite Element model, material properties of components should be modeled accurately. The model consists of more than 10 different material types. The material properties are extracted from the literature. Elastic steel, elastic nylon, rigid material, three different nonlinear elastic-plastic steel, nonlinear elastic-plastic aluminum and two different low-density foam are used in the model. The seat model is fully deformable; the sidewall and floor are rigid since they do not play any role in the stiffness of the seat.

Two elastic materials are used in the model. Elastic steel is used to model bolts and four beams in the recliner mechanism modeling. Elastic nylon properties are extracted from literature to model cushion frame. Table 4-3 shows the properties of the elastic material.

*Table 4-3 Elastic materials' properties*

Material type	Material	Mass density (ton/mm <sup>3</sup> )	Young's modulus (N/mm <sup>2</sup> )	Poisson's ratio	Used for
Elastic	Steel	7.85e-9	2.1e5	0.3	Bolts
Elastic	Nylon	1.5e-9	1.1e4	0.4	Cushion Frame

Sidewall, floor and hand rest are considered rigid. A hard nylon based rigid material is assumed for the hand rests. Table 4-4 shows the properties of the rigid material.

Table 4-4 Rigid materials' properties

Material type	Material	Mass density (ton/mm <sup>3</sup> )	Young's modulus (N/mm <sup>2</sup> )	Poisson's ratio	Used for
Rigid	Steel	7.85e-9	2.1e5	0.3	Sidewall, Floor
Rigid	Foam	1.5e-9	2.1e5	0.3	Hand-rest

The material of the load bearing parts of the seat is modeled using piecewise linear plastic steel and piecewise linear plastic aluminum. For piecewise linear plastic which is an elastoplastic material, an arbitrary stress-strain curve and strain rate dependency can be defined. Cowper and Symonds is the assumed strain rate dependency method for steel as recommended for crashworthiness analysis in LS-DYNA theory manual [33]. Cowper and Symonds scale the yield stress of the material by a  $K$  factor that is shown in Equation 4-3 [33].

$$K = 1 + \left(\frac{\dot{\epsilon}}{C}\right)^{1/p} \quad \text{Equation 4-3}$$

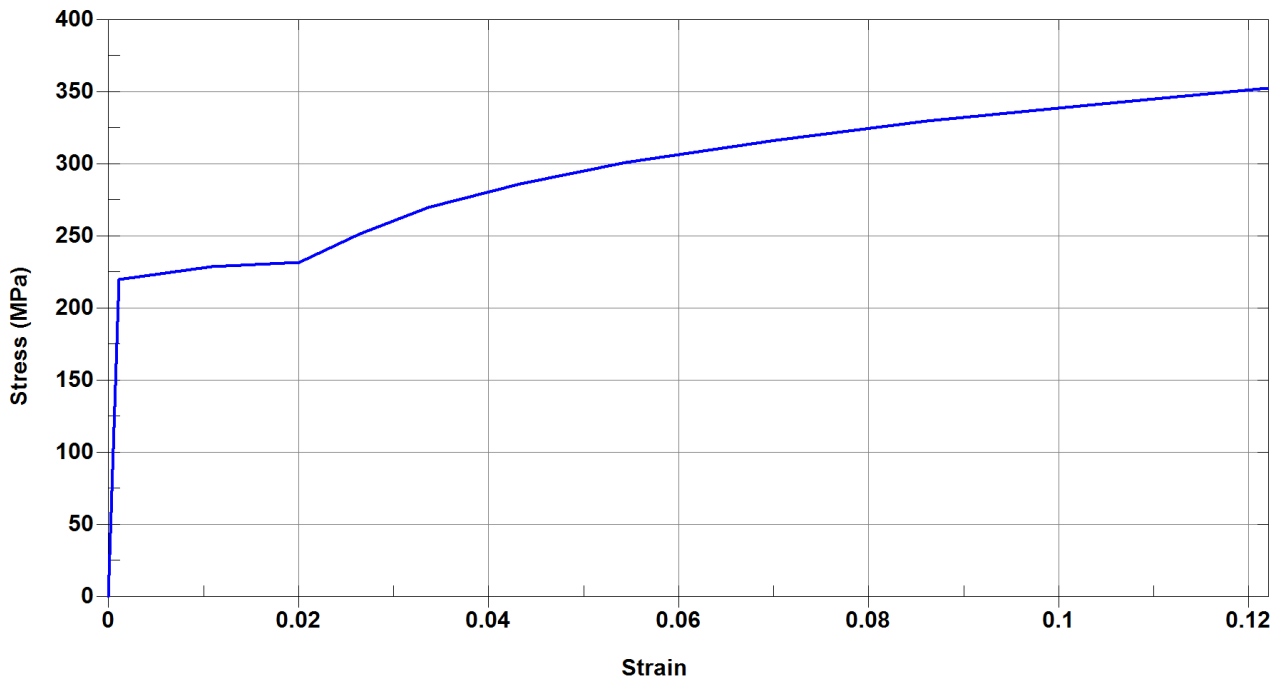
Where  $\dot{\epsilon}$  is the strain rate,  $\dot{\epsilon} = \sqrt{\dot{\epsilon}_{ij}\dot{\epsilon}_{ij}}$ .  $C$  and  $P$  are material constants.

Steel St34 is used to model transversal beams and Steel SS304 is assumed for the leg brackets. Steel S355 is the material of the brackets underneath the cushion frame and also retractor's components. Seatback membranes are made of Steel St-14, and Steel QSTE 460 is assumed for seatback brackets. Steel St52-3 is used for seatback tubes, and the rails are made of Aluminum

alloy AA6060T4. All material properties and  $C$  and  $P$  constants for strain rate dependency of steels are presented in Table 4-5 to Table 4-11. Stress vs. plastic strain curve for each material is shown in Figure 4-16 to Figure 4-21.

*Table 4-5 Steel St34 material properties*

Material type	Material	Mass density (ton/mm <sup>3</sup> )	Young's modulus (N/mm <sup>2</sup> )	Poisson's ratio	Yield stress (MPa)	Used for	C	P
Piecewise Linear Plasticity	St34	7.85e-9	1.95e5	0.3	220	Seat beams	80	4



*Figure 4-16 Steel St34 stress vs. plastic strain curve*

Table 4-6 Steel SS304 material properties

Material type	Material	Mass density (ton/mm <sup>3</sup> )	Young's modulus (N/mm <sup>2</sup> )	Poisson's ratio	Yield stress (MPa)	Used for	C	P
Piecewise Linear Plasticity	SS304	7.85e-9	1.95e5	0.3	258	leg brackets	100	10

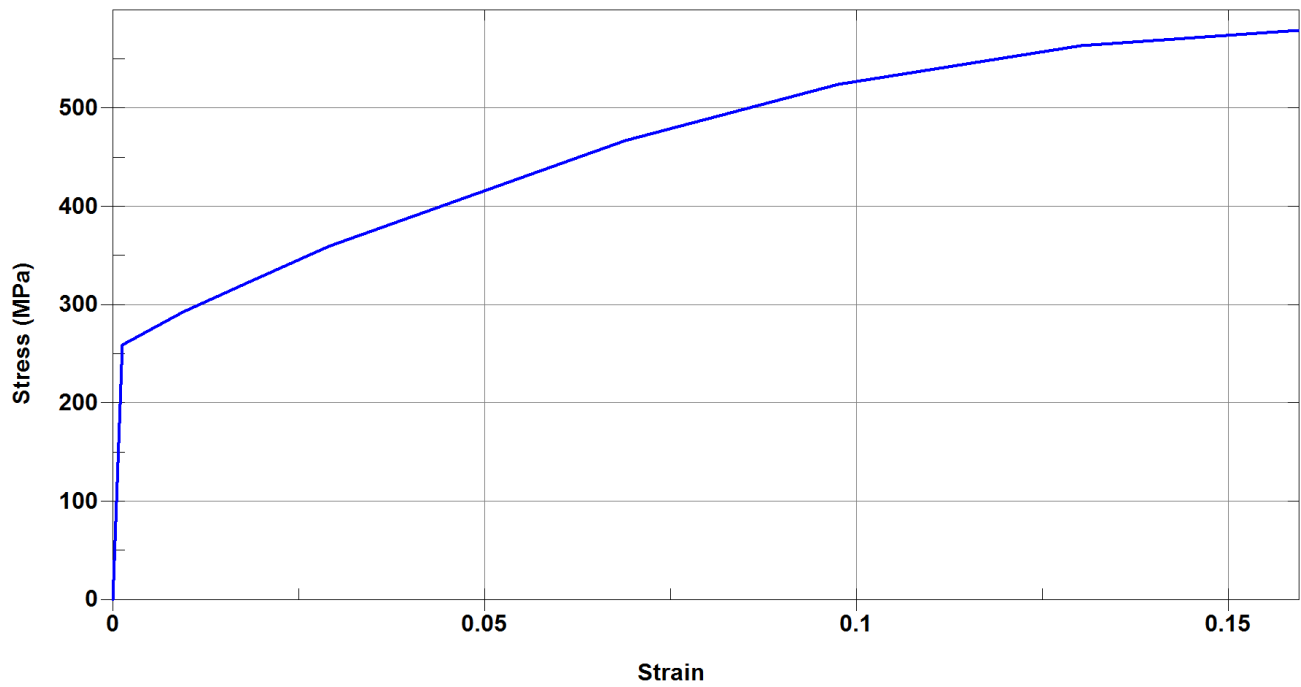


Figure 4-17 Steel SS304 stress vs. plastic strain curve



Table 4-7 Steel S355 material properties

Material type	Material	Mass density (ton/mm <sup>3</sup> )	Young's modulus (N/mm <sup>2</sup> )	Poisson's ratio	Yield stress (MPa)	Used for	C	P
Piecewise Linear Plasticity	SS304	7.85e-9	2.1e5	0.3	391	Frame brackets	80	4

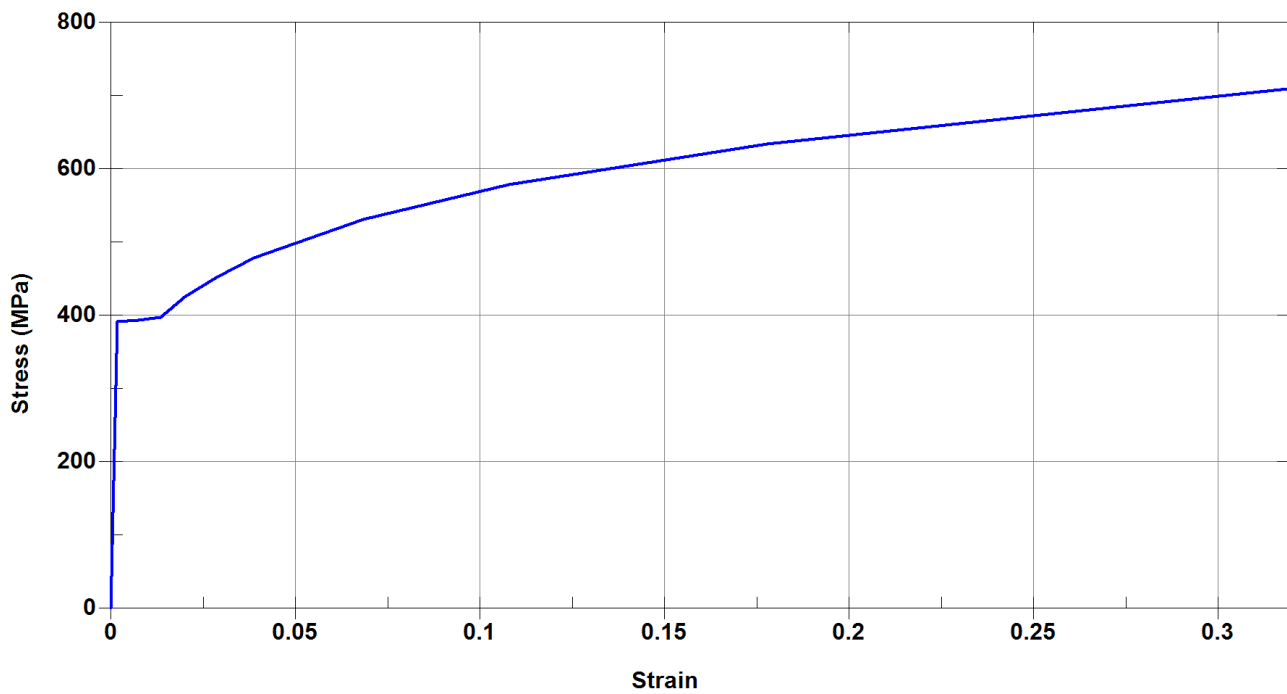


Figure 4-18 Steel S355 stress vs. plastic strain curve

Table 4-8 Steel St-14 material properties

Material type	Material	Mass density (ton/mm <sup>3</sup> )	Young's modulus (N/mm <sup>2</sup> )	Poisson's ratio	Yield stress (MPa)	Used for	C	P
Piecewise Linear Plasticity	St-14	7.85e-9	1.8e5	0.3	159	Seatback membranes	80	4

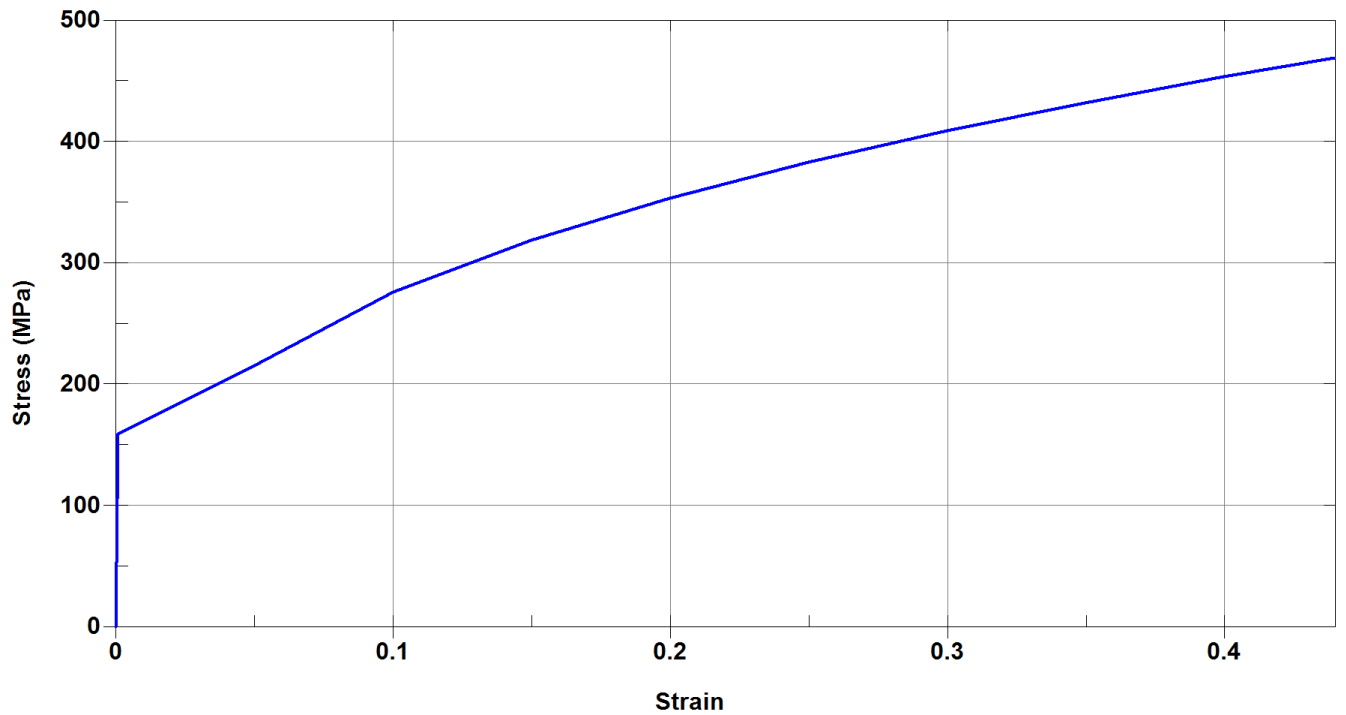


Figure 4-19 Steel St-14 stress vs. plastic strain curve

Table 4-9 Steel QSTE 460 material properties

Material type	Material	Mass density (ton/mm <sup>3</sup> )	Young's modulus (N/mm <sup>2</sup> )	Poisson's ratio	Yield stress (MPa)	Used for	C	P
Piecewise Linear Plasticity	QSTE 460	7.85e-9	2.1e5	0.3	456	Seatback brackets	40	5

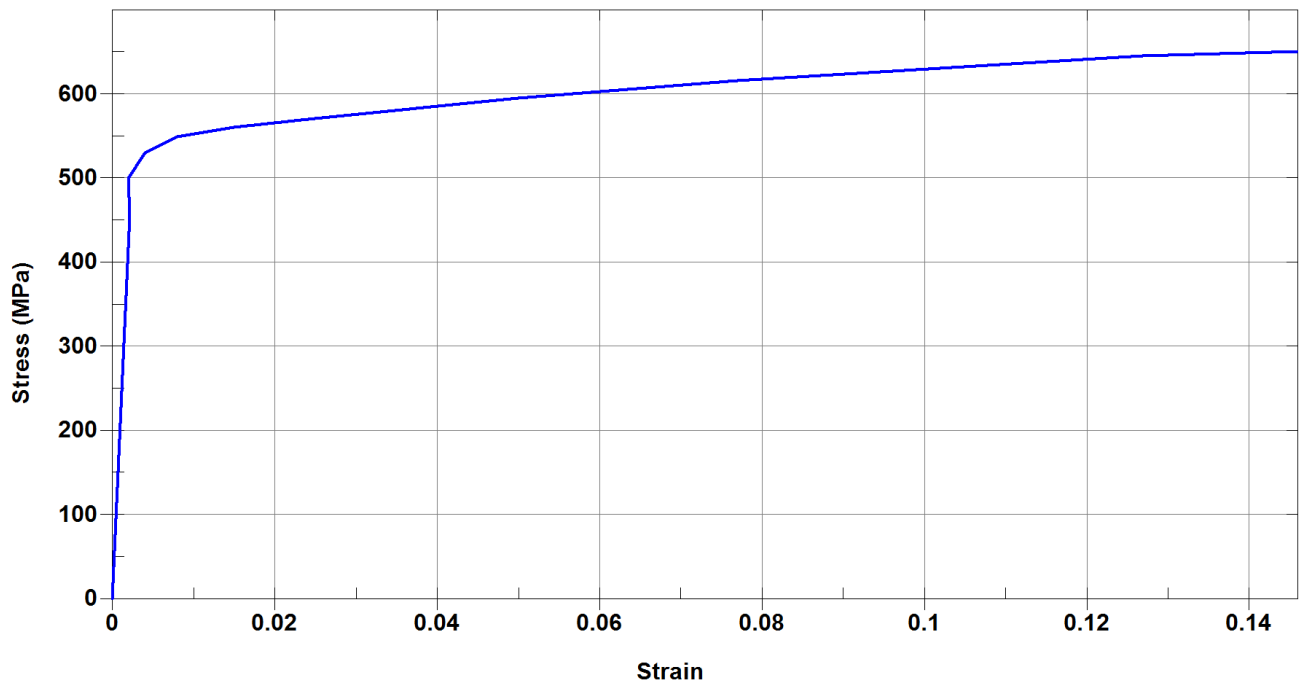


Figure 4-20 Steel QSTE 460 stress vs. plastic strain curve

Table 4-10 Steel St52-3 material properties

Material type	Material	Mass density (ton/mm <sup>3</sup> )	Young's modulus (N/mm <sup>2</sup> )	Poisson's ratio	Yield stress (MPa)	Used for	C	P
Piecewise Linear Plasticity	St52-3	7.85e-9	2.1e5	0.3	355	seatback tubes	80	4

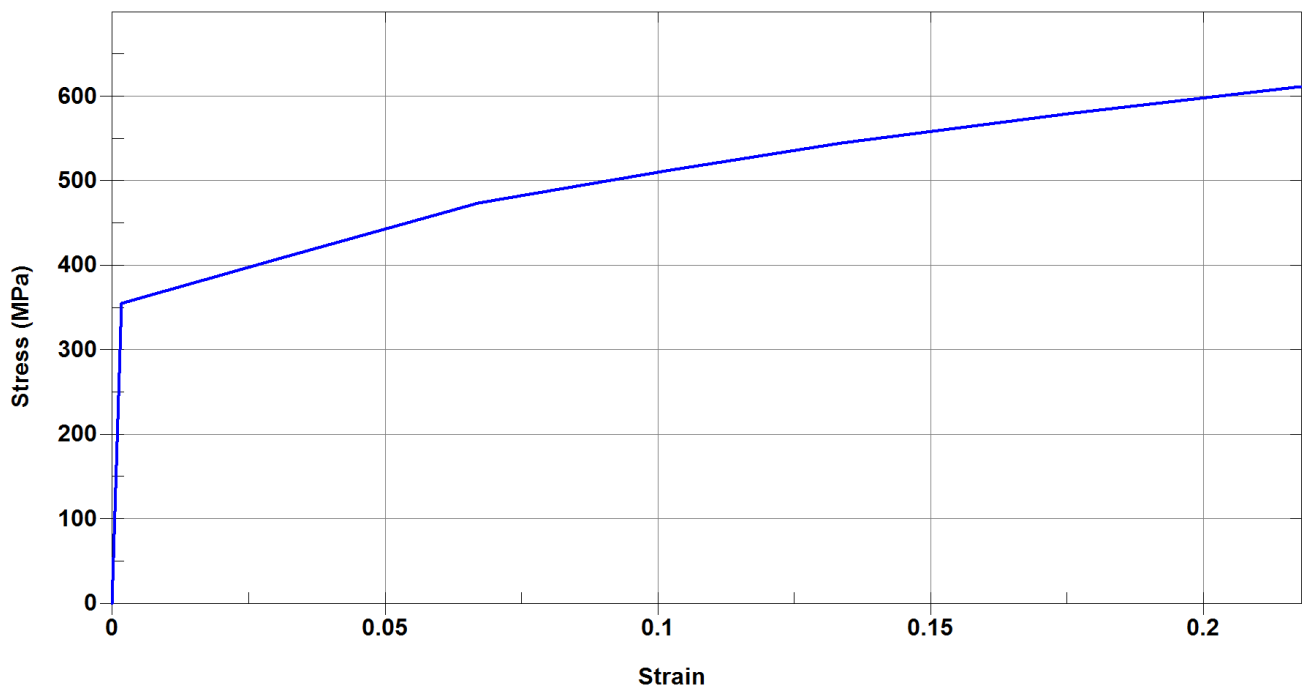


Figure 4-21 Steel St52-3 stress vs. plastic strain curve

Table 4-11 Aluminum AA6060T4 material properties

Material type	Material	Mass density (ton/mm <sup>3</sup> )	Young's modulus (N/mm <sup>2</sup> )	Poisson's ratio	Yield stress (MPa)	Used for
Piecewise Linear Plasticity	Aluminum AA6060T4	2.7e-9	6.82e4	0.33	80.58	Rails

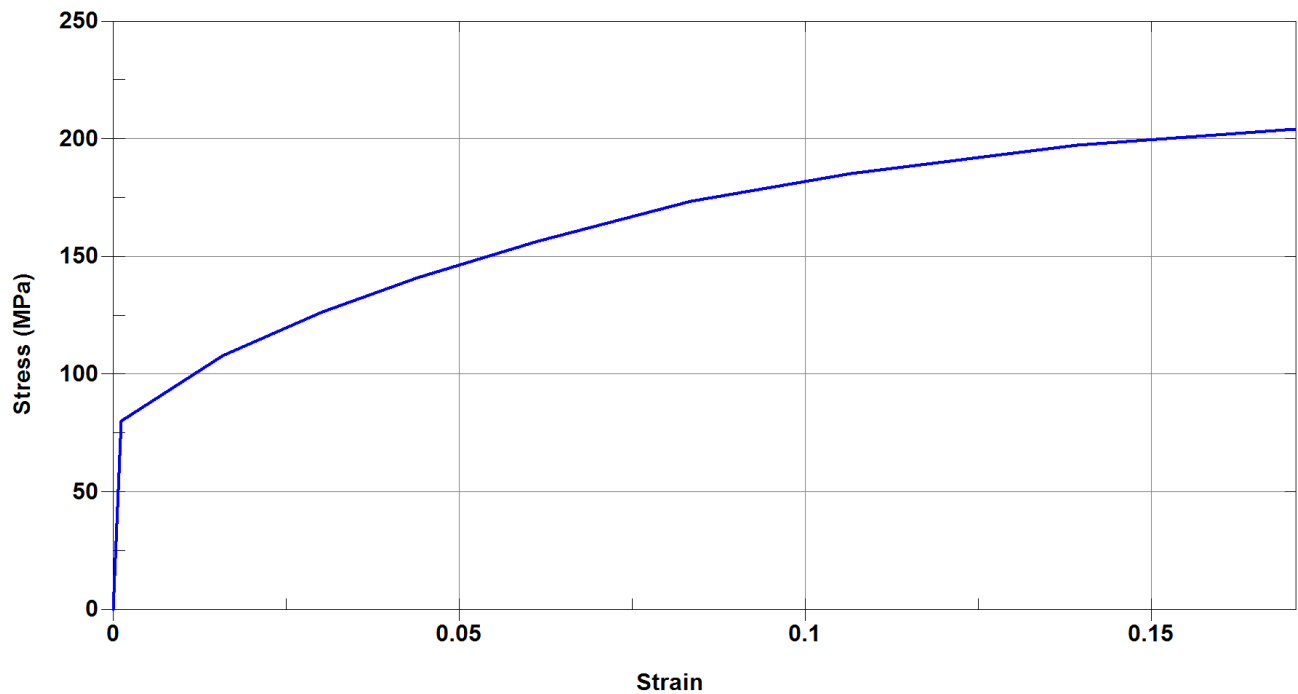


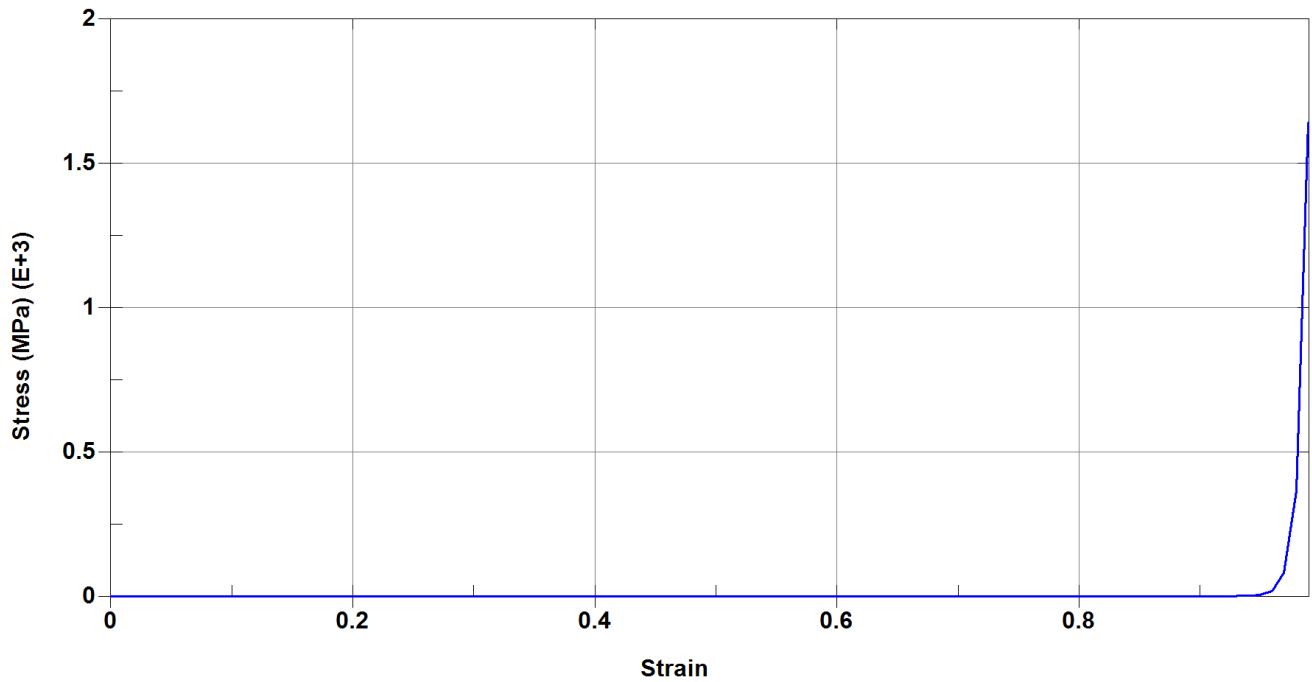
Figure 4-22 Aluminum AA6060T4 stress vs. plastic strain curve

A low-density foam is used to model the cushion and the seatback foam. This material can be used to model highly compressible foam, like the one which is used for seats' cushions. Table 4-12

shows the material property of the foam used in the model and Figure 4-23 shows the nominal stress vs. strain curve.

*Table 4-12 Foam material properties*

Material type	Material	Mass density (ton/mm <sup>3</sup> )	Young's modulus (N/mm <sup>2</sup> )	KCON (N/mm <sup>2</sup> )	Used for
Low Density Foam	Foam	4.8e-11	1	100	Cushion Foam

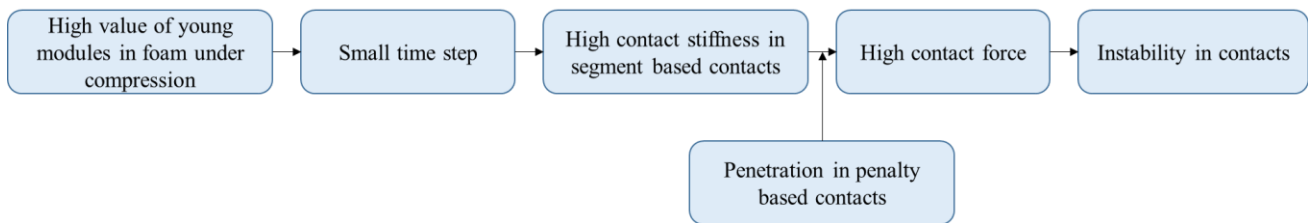


*Figure 4-23 Foam stress vs. strain curve*

As it can be seen in Figure 4-23, stress goes to infinity when the foam is fully compressed (strain equals to one). As a result, the Young's modulus of the foam tends to infinity when foams' elements are highly compressed. High value of Young's modulus of elements create two problems for the simulation:

First, the global time step of the simulation decreases since it is inversely proportional to the Young's modulus based on Equation 3-3 and Equation 3-4. Small time step causes the simulation to run longer.

Secondly, in segment based contacts of the model contact stiffness increases quadratically with the time step decay (Equation 4-2). In penalty based contacts, the high value of contact stiffness may lead to instability of the contact. It can be described by the fact that the high value of the contact stiffness yields an unreasonable force in contact which destroys the contact. Figure 4-24 summarizes how the stiffness of the foam under compression may lead to a contact failure in another part of the simulation.



*Figure 4-24 Contact instability caused by foam material property*

As a remedy, an arbitrary stiffness (KCON) is defined, and the contact stiffness is calculated based on the KCON value regardless of the deformation of the foams' elements. The KCON value should be found by trial to eliminate all contacts instabilities. The KCON value defined for the foam can be seen in Table 4-12.

#### 4.6 ELEMENTS FORMULATION

The developed Finite Element model is mainly created using shell elements. Out of totally 81 parts, 58 components in the model are shell parts. All shell parts are modeled with 4-noded Belytschko-

Tsay shell elements with three integration points through the shell thickness. Reduced integration Belytschko-Tsay (LS-DYNA type 2 shell element formulation) is the shell formulation. It is a dominant shell formulation for crashworthiness analysis [34] [35] [36]. It is chosen for this kind of analysis because of the high efficiency of the reduced integration due to the mathematical simplifications behind it. The drawback of this formulation is that it cannot capture some sort of element distortion. This distortion causes the artificial hourglass energy to be produced. The solution is to change formulation from reduced integration to full integration. However, this remedy increases the computational time. Since the hourglass energy in the Finite Element model of this study is kept under the acceptable limit, the reduced integration is used as the single type of formulation for shell parts.

For solid parts with hexahedron element geometries, the default constant stress solid element formulation is assumed. The default formulation is under-integrated constant stress. The under-integrated formulation increases the efficiency of the model. However, the hourglass must be checked to be less than the acceptable limit. This is checked in the verification section of the thesis.

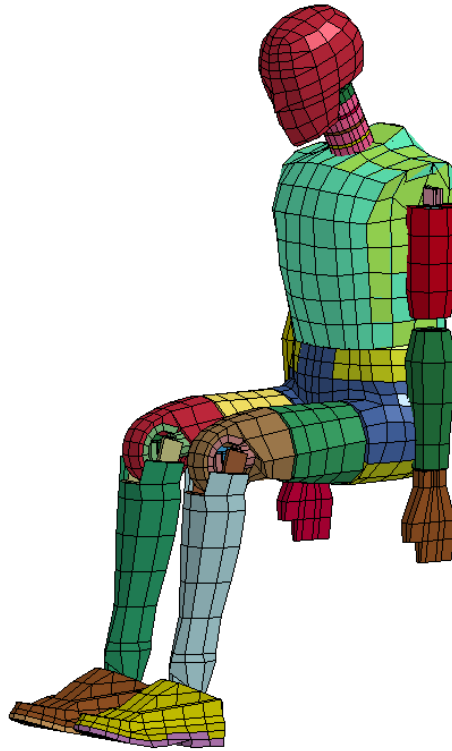
For components with tetrahedron element geometries (mainly the foams), 1 point constant stress tetrahedron formulation is chosen. The four node tetrahedron element with one point integration is a highly recommended simple, fast and stable element for modeling low-density foams with high compressibility [33].

#### 4.7 ATDs POSITIONING

Two Hybrid III 50<sup>th</sup> Fast Dummy from Livermore Software Technology Corp. (LSTC) [37] online resources are downloaded and positioned in the model. The ATDs are already validated against



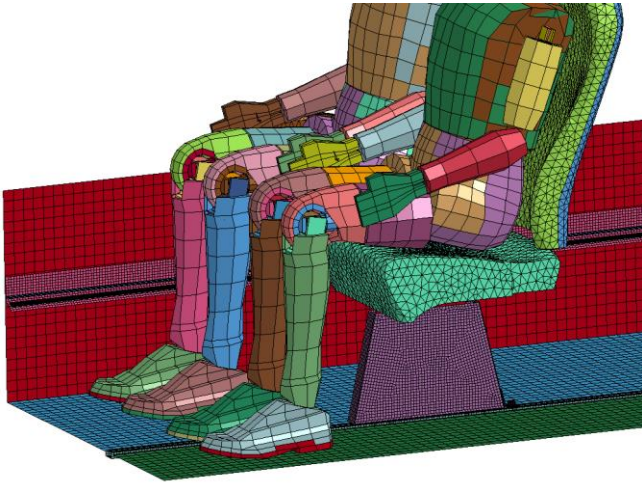
experimental results, and the comparison graphs can be found in [37]. Each ATD weights 78kg which is the lightest available ATD heavier than the proposed 68 kg. Figure 4-25 shows the implemented ATD. Two ATDS are introduced to the model to impose the weight of the occupants on the anchorage completely.



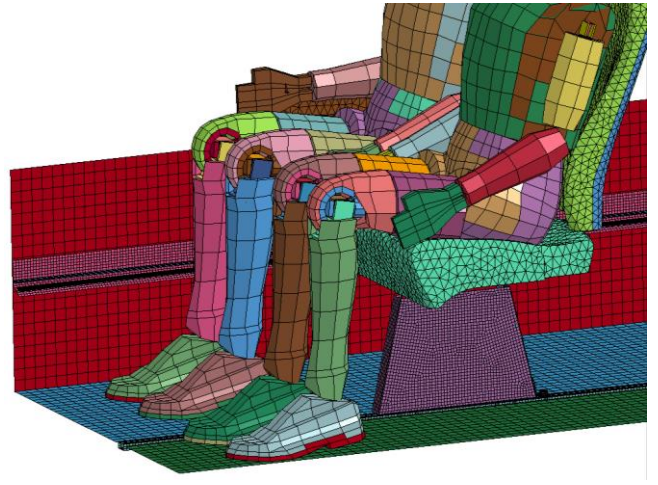
*Figure 4-25 Implemented ATD*

ATDs are initially positioned few centimeters above the seat cushion. The numerical procedure starts the search of the ATD position under a load of gravity and finally, the ATDs rest on the seat (Figure 4-26). As a result, the cushion is formed by the shape of ATDs' hips, and legs. Afterward, the geometry of the cushion is saved. This geometry is applied to the final model as the reference geometry for the foam. The reference geometry creates a pre-compression initial condition for the foam. Figure 4-27 shows the compressed cushions under the load of ATDs.

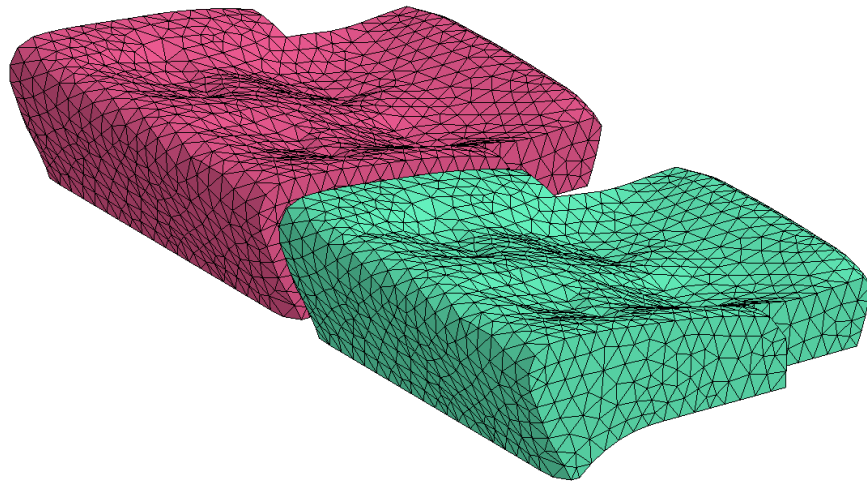
a)



b)

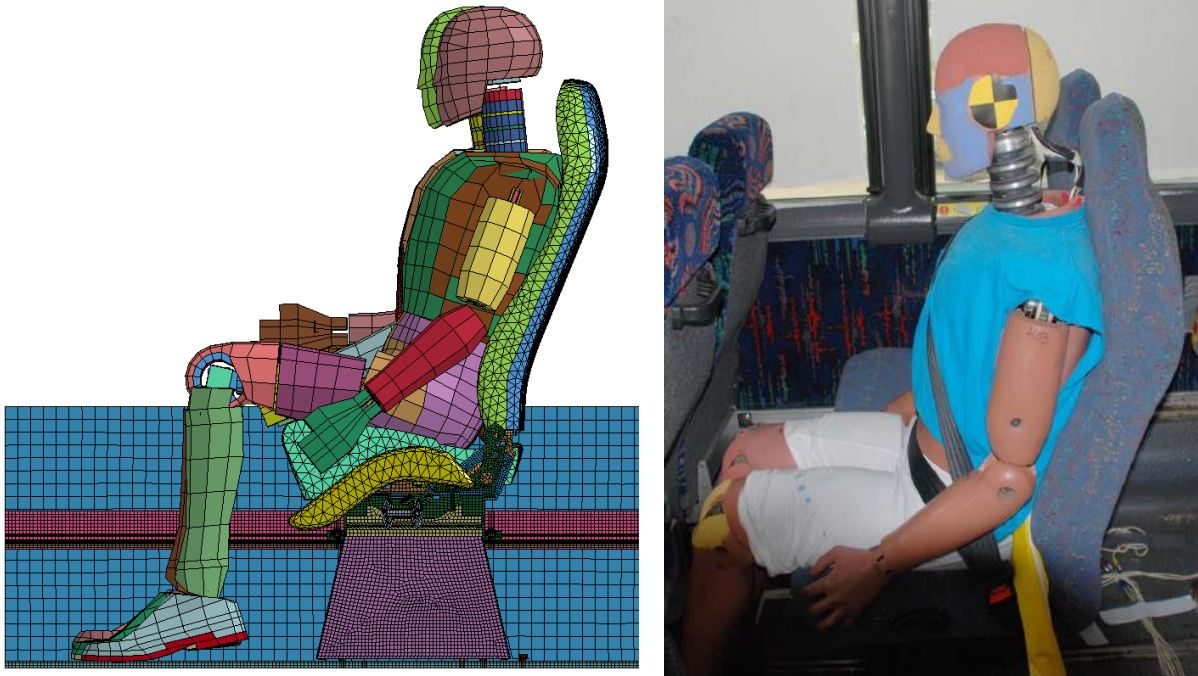


*Figure 4-26 a) Before the application of gravity b) After the application of gravity*



*Figure 4-27 Compressed cushions*

Afterward, the limb, lumbar, and neck are positioned in a way to better match the initial position of the implemented ATD in the physical test. Figure 4-28 compares the initial position of the ATD in the simulation with the implemented ATD in the physical test.



*Figure 4-28 Implemented ATD in the simulation vs. the test*

## 4.8 SEAT BELT

### 4.8.1 Overview

The 3-point seat belt is rooted over the ATDs. All the details of the seat belt assembly, slip-rings, retractors, and buckles, are also added to the seat belt model. As shown in Figure 4-29 a combination of 1d beam and 2d shell elements are used. 1d elements are used to simply model the webbing retraction toward retractor and also slipping of the belt through the slip-rings. A retractor is modeled in “point a” shown in Figure 4-29. 1d and 2d elements connect the retractor to the first slip-ring (point b) near the shoulder of the ATD. 1d elements can pass through the slip-ring if it is needed. The seat belt is rooted over the chest of the ATD and after passing the buckle, ends up with a fixed point (point d). The buckle is also modeled as a slip-ring (point c).

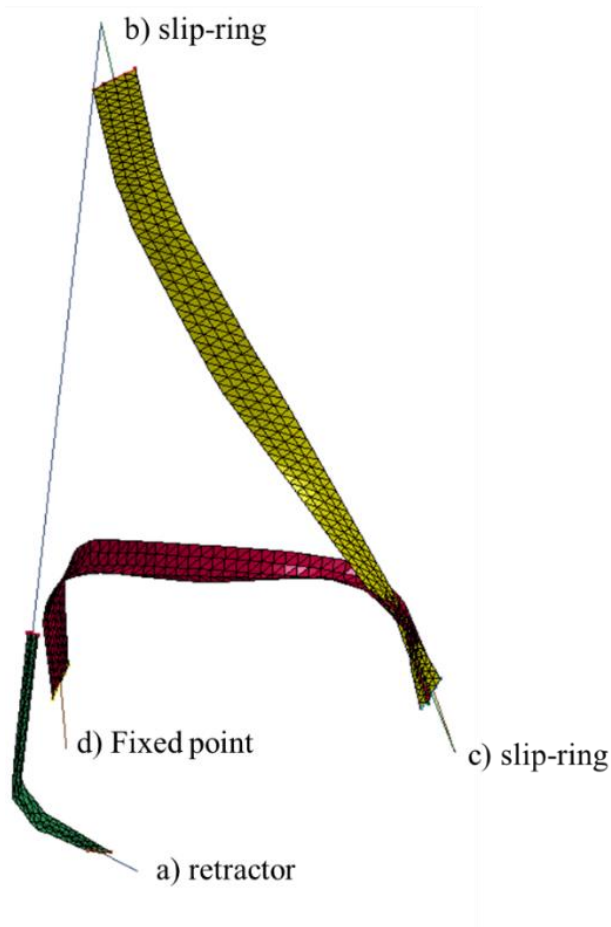


Figure 4-29 Seat belt

## 4.8.2 Seat Belt Material Property

### 4.8.2.1 Fabric Belt

The non-orthogonal fabric material data is extracted from the literature and used for the 2d shell elements. Its material property can be found in Table 4-13. A non-orthogonal material model is used since physical test results show that strength of the belt in the lateral direction is half of that in the longitudinal direction [38]. Figure 4-30 shows the stress versus strain curve for longitudinal and lateral directions.

Compressive stress is not eliminated in the fabric material modeling. Thin fabrics, like airbags, buckle in small wrinkles under compression. To catch this buckling behavior, a fine mesh is required. If the mesh is coarse, fabric mistakenly carries compressive force. To avoid this problem, compressive stress can be ignored in the material modeling. However, this elimination can cause instability in the fabric model. In the case of seat belt material, since the fabric buckles in large wrinkles, the assigned mesh can capture this buckling behavior. As a result, the compressive stress is not ignored in the fabric material modeling which allows avoiding the instability in the seat belt. The damping coefficient also plays a meaningful role in the stability of 2d shell element. The damping coefficient should be found by trial. It is found that .01 is the optimum damping for the model.

*Table 4-13 Fabric belt material properties*

<i>Material type</i>	<i>Material</i>	<i>Mass density (tone/mm<sup>3</sup>)</i>	<i>Poisson's Ratio (All directions)</i>
Fabric 034	Fabric	1e-9	0.3
<i>Rayleigh Damping Coefficient</i>	<i>Compressive Stress</i>	<i>Membrane Formulation</i>	<i>Used for</i>
0.01	Not eliminated	4	2d seat belt

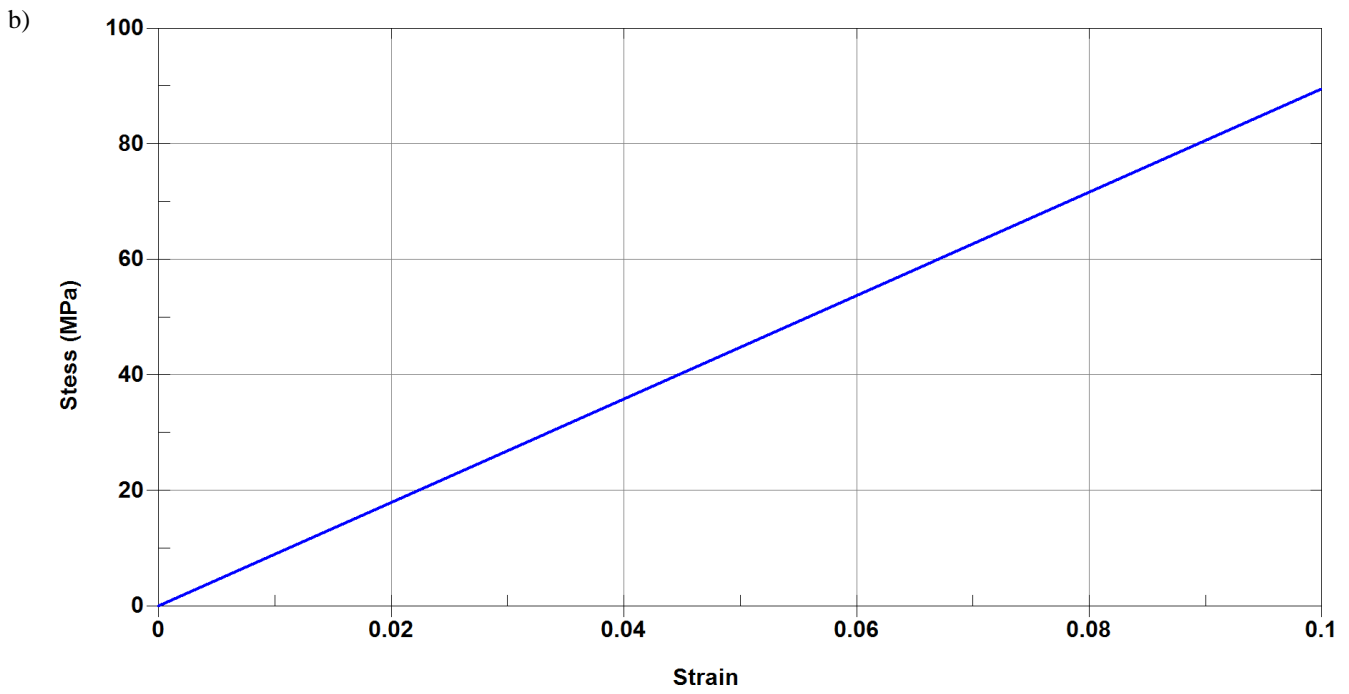
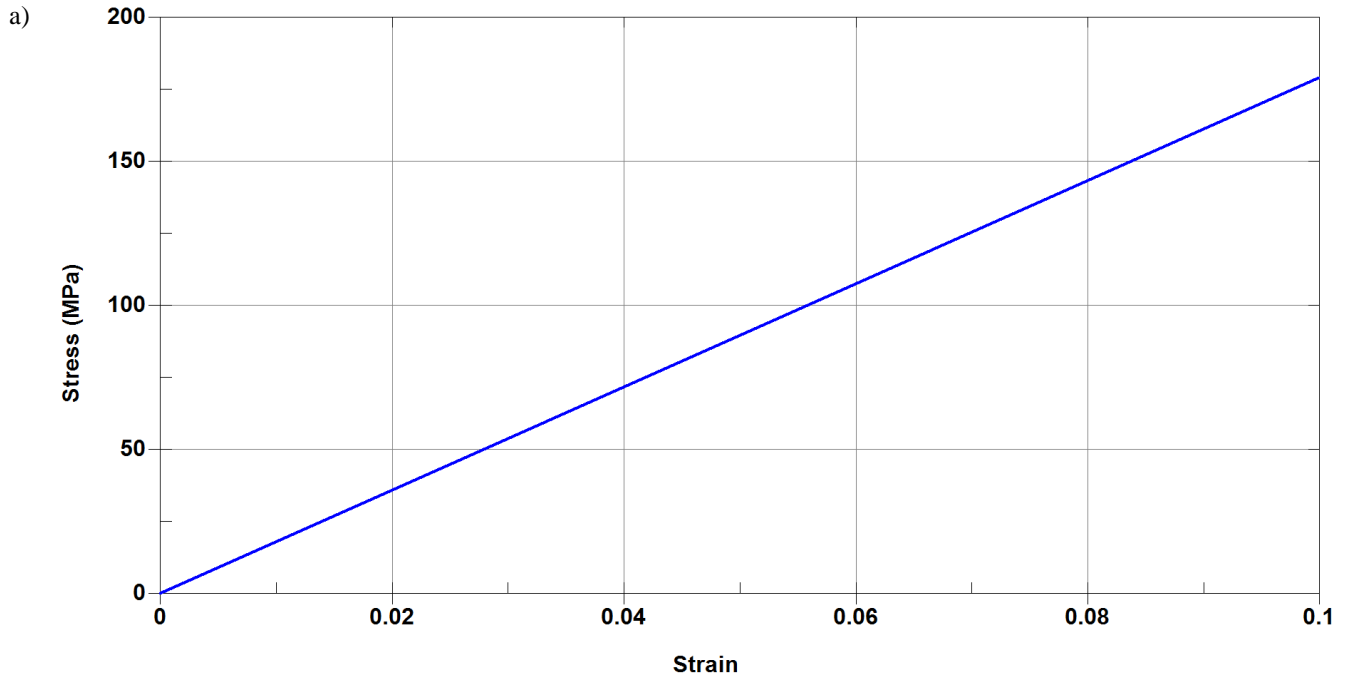


Figure 4-30 Stress versus strain curve for fabric belt a) longitudinal b) lateral

#### 4.8.2.2 Segment Belt

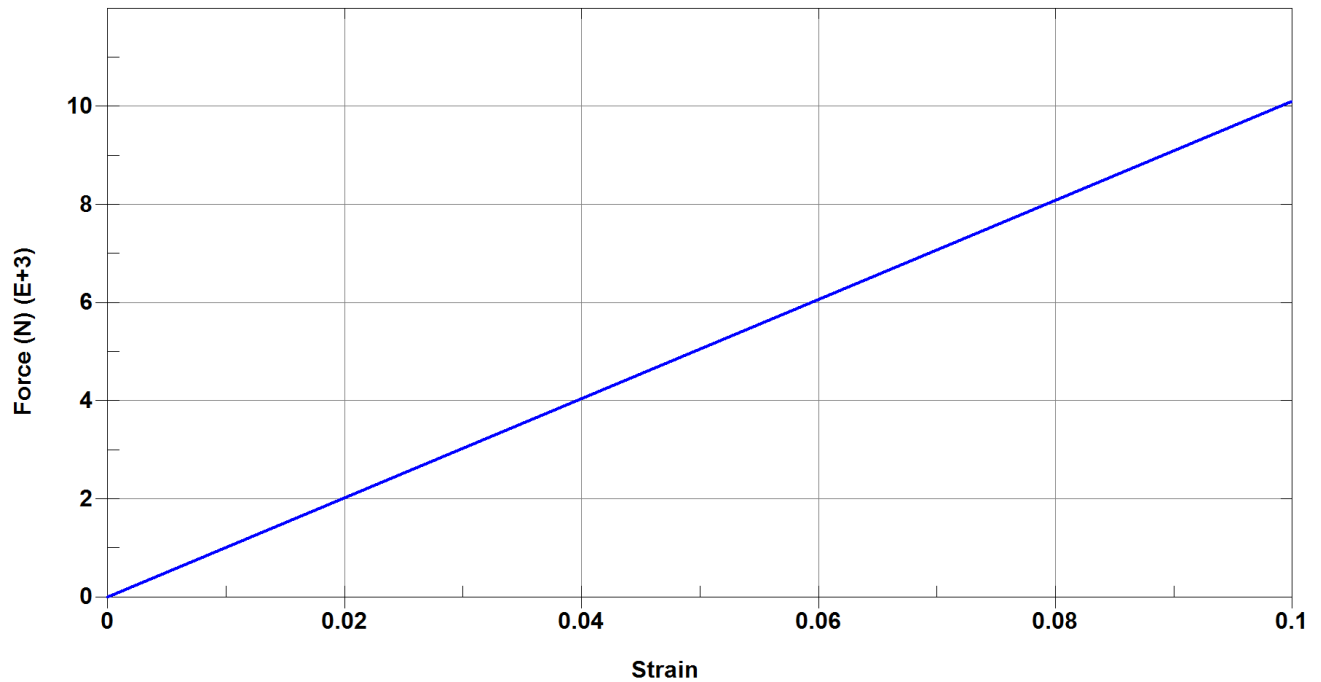
Table 4-14 shows the material property for 1d seat belt elements. For 1d beam elements of the seat belt, mass per unit length should be directly defined since there is no section property to calculate the volume. Moreover, a minimum allowable length must be defined. When the elements tend to pass through the slip ring, LS-DYNA needs to reduce the length of the elements. On the other hand, based on the Equation 3-3, the global time step is a function of the length of the elements. A minimum length of 1 mm is chosen for the elements to prevent them from becoming unnecessarily small and to control the time step.

In regards to compressive stress elimination, the element size of the 1d seat belt is small enough to capture the buckle of the belt; therefore, the compression is not eliminated.

The required force vs. strain curve for loading and unloading of the belt is extracted from literature [38] and is shown in Figure 4-31.

*Table 4-14 Segment belt material properties*

Material type	Mass per unit length (ton/mm)	Minimum Length (mm)	Compressive Stress
Seat Belt B01	8e-8	1	Not eliminated



*Figure 4-31 Force versus strain curve for segment belt*

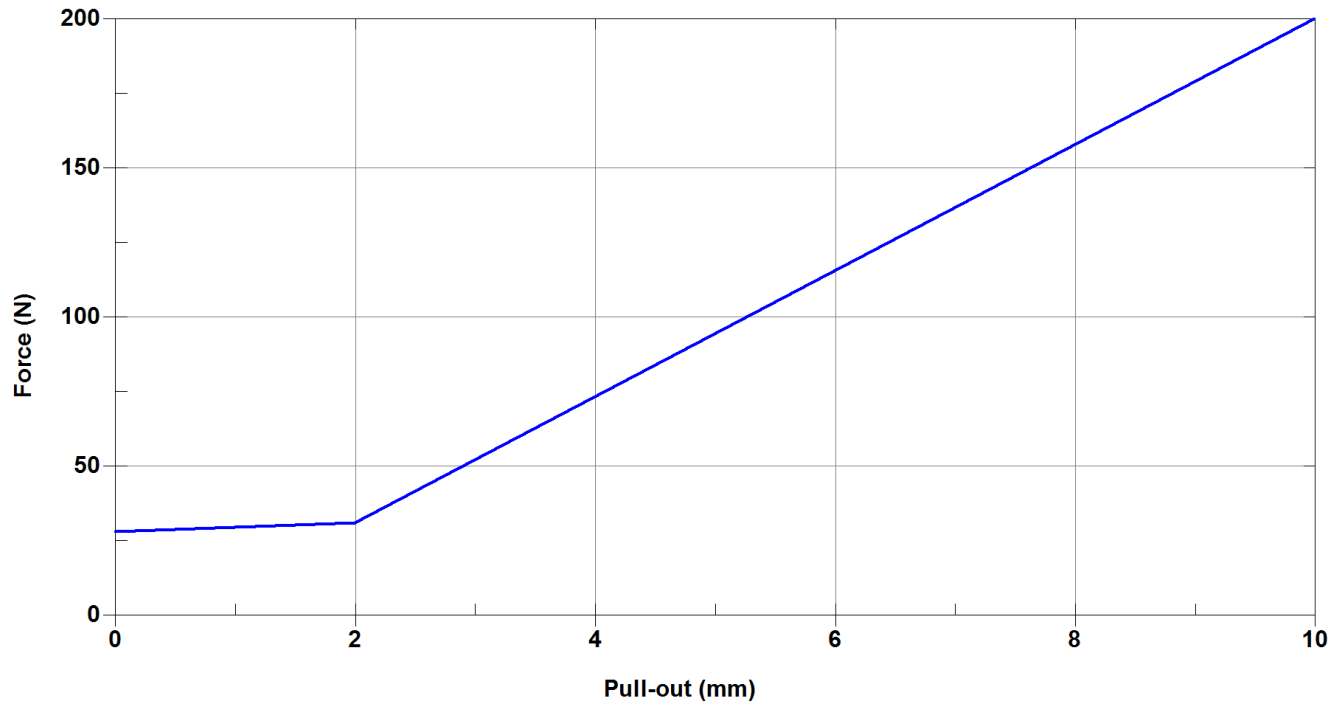
#### 4.8.3 Retractor

To investigate the effects of retractor performance, a detailed model of seat belt retractor is developed for the model. Hundreds of zero length elements are assigned to the retractor point (point “a” in Figure 4-29). When more webbing needs to be pulled out, the elements can emerge one by one as non-zero elements. The amount of pull out is controlled by a predefined force vs. pull out curve [38]. When the tension force in the seat belt drops, the webbing is retracted as zero-length elements back to the retractor. The maximum rate of pull out or pull in is controlled by a fed length that is 0.10 mm in this model.

The retractor locking mechanism is defined by force vs. pullout curve. When the required load for the extra pull out tend to infinity, no more webbing can be pulled out. Different force vs. pullout curve is used in this research to perform a parametric study on the performance of different



retractors. A sample of these curves can be seen in Figure 4-32. Different curves and their effects on the injury risk of passengers are presented in “Result and Discussion” section.



*Figure 4-32 Force vs. pull out for retractor*

#### 4.9 LOADING CONDITION

The applied load to the model is the acceleration history of an NHTSA’s physical rollover test. During a complete vehicle rollover test of a coach done by NHTSA, six accelerometers were installed in the coach. Figure 4-33 indicates the location of the accelerometers. Mid floor accelerometer data is considered as the acceleration that passengers undergo and used as an input loading for the model.

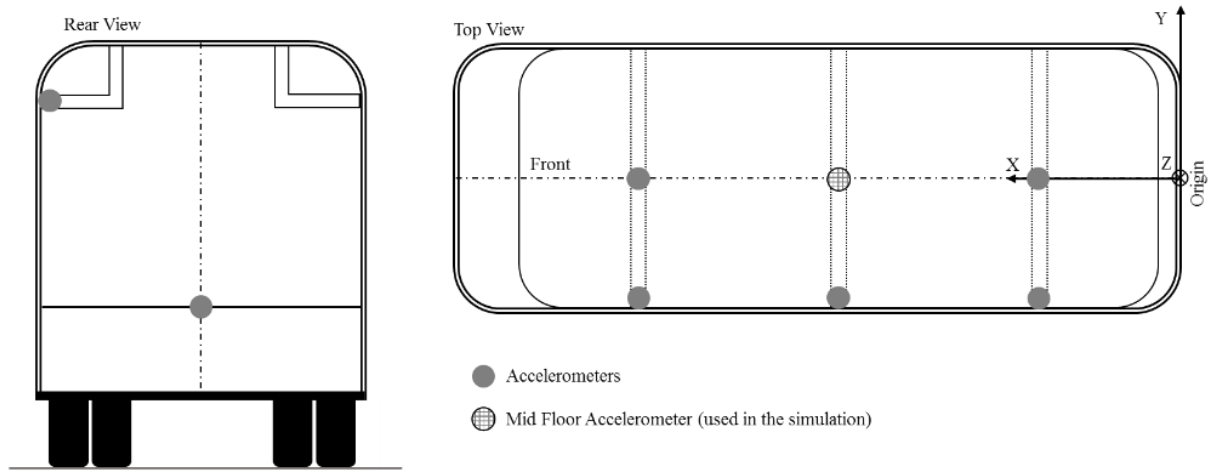


Figure 4-33 Accelerometers' locations

Mid floor Accelerometer's data which is shown in Figure 4-34 is applied to the model up to  $t = 0.8$  s when the acceleration values drop to almost zero. The acceleration in both Y and Z direction have two positive peak values with a negative value in between. The first peak acceleration comes from roof-to-ground impact and the second one is for floor impact. The negative acceleration value between two peaks corresponds to the coach structure rebound after the first impact.

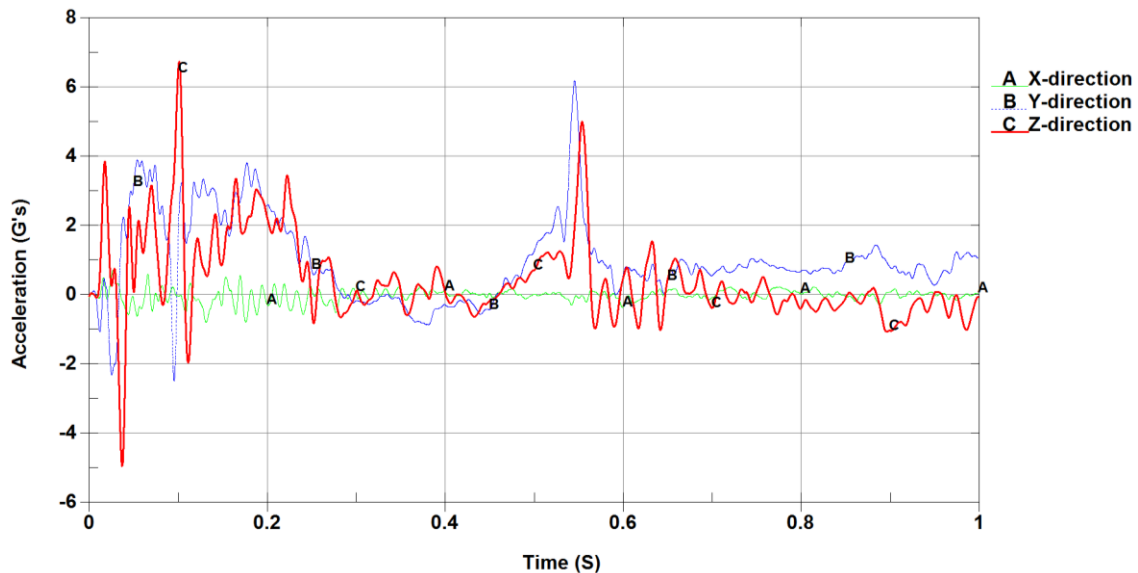


Figure 4-34 Mid-floor accelerometer data

## 4.10 SUB-MODEL

To capture accurate stress concentration at critical locations, sub-model techniques should be implemented. To have an accurate stress distribution in the desired part, fine mesh at the region of interest is required. If the whole model is used to capture stress concentration at the critical location, the small elements at the critical location cause the governing time step of the simulation to become unreasonably small.

For a sub-model analysis, the components in which accurate stress distribution is required have to be selected and cut from the whole model. The cutting faces are called cut boundary faces. The displacement or load field should be read from the cut boundary nodes. These fields are applied to the sub-model as a boundary condition.

In order to perform the integrity analysis of a coach seat, a highly-accurate stress distribution in the anchorage system is required. To achieve that, a sub-model of the anchorage system is necessary.

There are several reasons that the whole model cannot be used to read the stress at the critical location:

The first one is that although the mesh size and mesh quality in the whole model are fine enough to capture the total deformation of the structure, they are too coarse to be used for capturing stress. Secondly, the majority of the seat structure including anchorage system are modeled using shell elements. During solid to shell conversion, the corners and chamfers are simplified. As a result, stress concentration around these features cannot be captured in the whole model. Furthermore, the bolts and their contacts are simplified. Both bolt's shank and head are modeled as simple

cylindrical parts. The type of contact between bolt and rail is a “non-failure tied contact” which keeps bolt and rail attached together regardless of the load. From the performed analysis, it can be seen that carrying out a sub-model simulation with a finer mesh, no geometry simplification, accurate contact modeling and considering bolt pre-stress as an alternative to tied contact, is necessary. Figure 4-35 compares the anchorage system in the whole model and the developed sub-model.

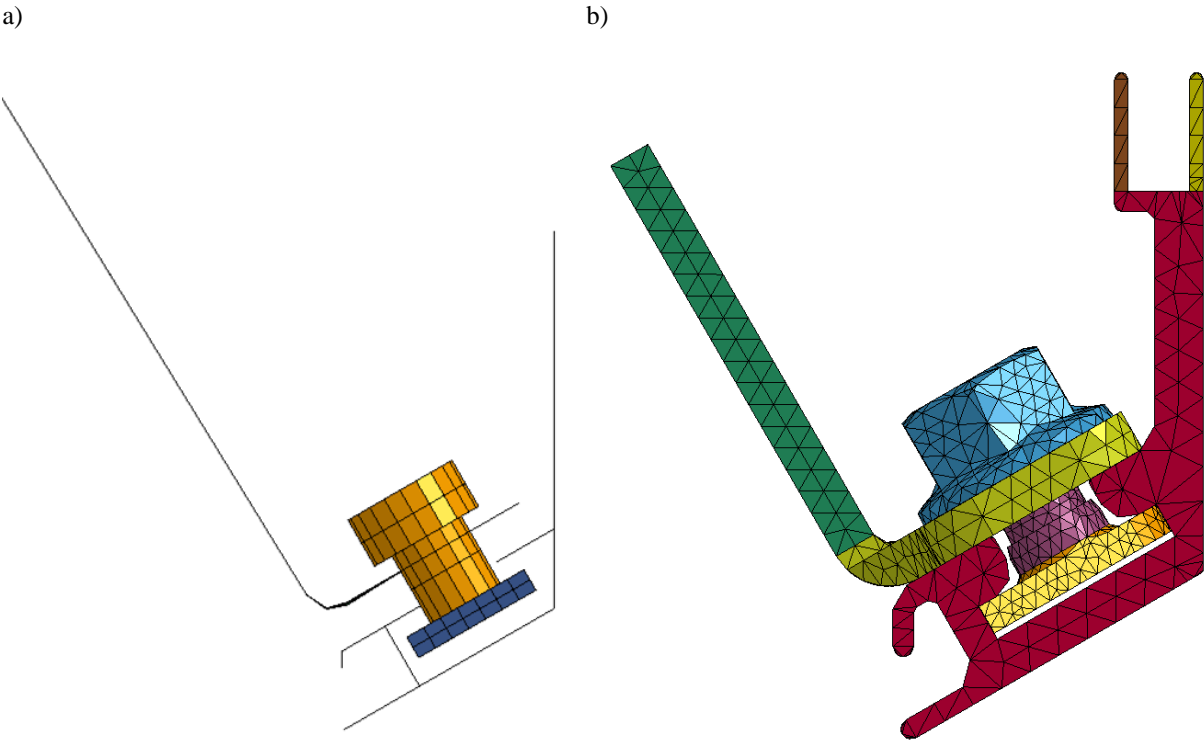
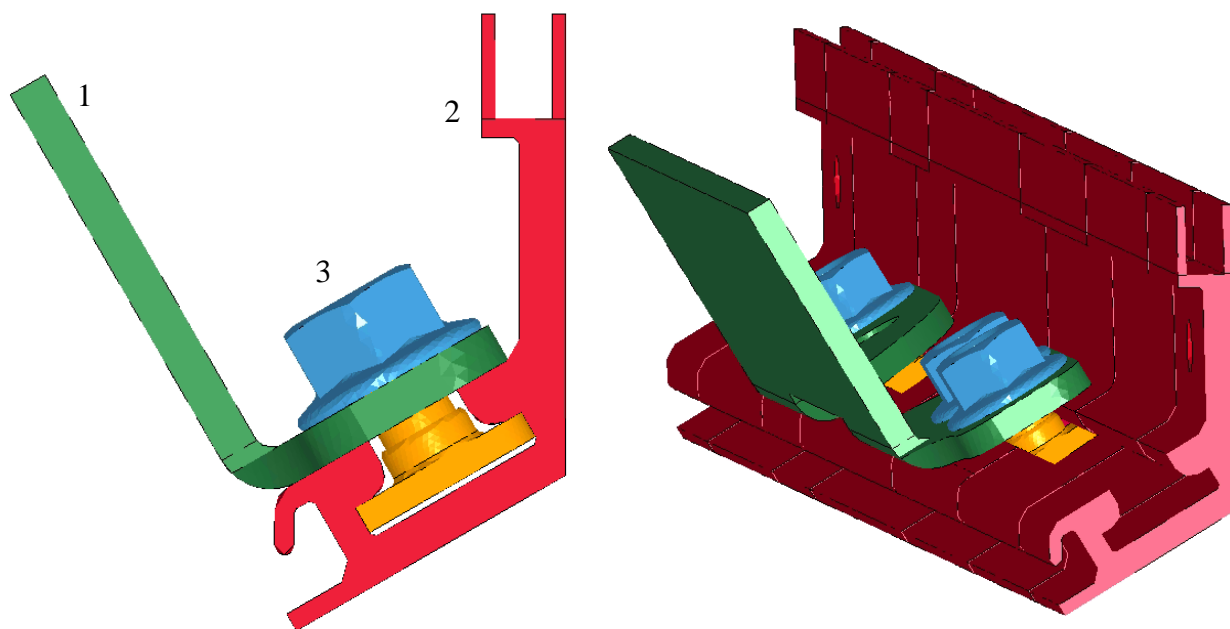


Figure 4-35 a) Anchorage system in the whole model b) Sub-model

4.10.1 Geometry

The cut boundary face is in the middle of seat bracket in the whole model. Therefore, the sub-model consists of three main parts. Bracket (part number 1 in Figure 4-36) is a part of the seat structure which connects seat’s transversal beam to the side rail. This part transfers the imposed

load from the weight of seat structure and the occupant to the side rail. Part number 2 in Figure 4-36 is the rail that is connected to the bus sidewall. Finally, six bolts and nuts which are labeled as part number 3 in Figure 4-36. No geometry simplification is made, and all parts are assembled precisely. A small gap between parts is considered to avoid any initial penetration.



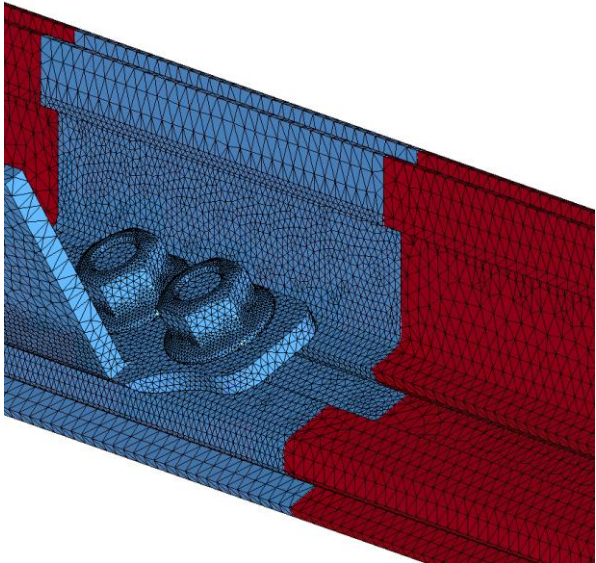
*Figure 4-36 Sub-model geometry*

#### 4.10.2 Mesh & Element Formulation

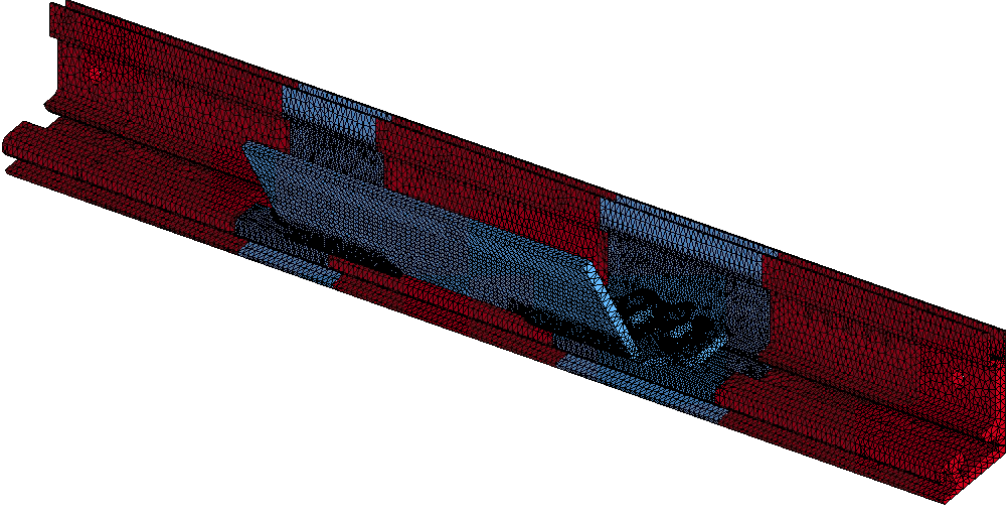
Sub-model parts are all solid. Solid parts should be exclusively discretized by either hexahedron or tetrahedron elements since pyramid elements are not acceptable in the explicit simulation. Due to the geometric complexity of parts, tetrahedron elements are assigned for the sub-model. The assigned element formulation is one-point tetrahedron.

Accurate stress distribution in the bolts, nuts and around the bolt-rail connection in the rail is desired. To capture this accurate stress distribution, higher mesh quality and density are assigned

to the desired areas. Mesh quality here is defined as aspect ratio, skewness, orthogonality, and smoothness of solid elements; however, mesh density refers to the number of elements in a unit volume. In Figure 4-37 fine mesh for the bolts, nuts and around the bolt-rail connection can be seen. Figure 4-38 demonstrates the final meshed model.



*Figure 4-37 Fine mesh*



*Figure 4-38 Final meshed model*

#### 4.10.3 Assembly and Connection

Two different kinds of contacts exist in the sub-model. The contacts between bolts and nuts are modeled as tied contacts. Tied contact constrains the relative sliding of the nut and the bolt. Sliding can happen when thread stripping would be the mode of failure in either nuts or bolts. However, in thread design process, bolts and nuts are always designed in a way that the fasteners should break first in tension prior to the threads stripping [39]. The aforementioned design constraint leads to the consideration that the bolts and nuts can be connected using tied contact. Contacts between “nuts and bracket,” “bracket and rail” and “rail to bolt” are considered to be frictional with a static coefficient of friction of 0.6. This value is the static coefficient of friction between the steel and aluminum surfaces when the surfaces are dry [40]. This type of contact allows parts separation which means that if severe deformation happens for rail, bolts can be pulled out from it.

#### 4.10.4 Bolt Pre-stress

One of the key advantages of the sub-model is that bolt pre-stress is considered in the simulation. Bolt pre-stress applies a compression force between the bracket and the rail keeping the assembly together.

Bolt pre-stress is added to the model by defining stress section in the shank of the bolts. Stress section preloads the cross-section of the solid shank to a prescribed stress value [41]. The preload is defined by a stress vs. time curve in which stress ramps from zero to the desired value (Figure 4-39). When the desired stress in the bolts is achieved, the preloading procedure must stop. For the solver to understand that the preloading procedure is completed, the stress value in the bolt pre-stress vs. time curve must drop to zero. This sudden drop in the curve is treated as the

termination of the preloading procedure, and the resultant stress in the structure would be considered as a pre-stress initial condition for the following simulations [41].

Application of bolt pre-stress imposes an undesired kinetic energy to the system. To attain convergence after application of the bolt pre-stress, a global damping is considered for the model. Figure 4-40 shows the damping coefficient vs. time. After the undesired kinetic energy is damped, the damping coefficient is ramped to zero.

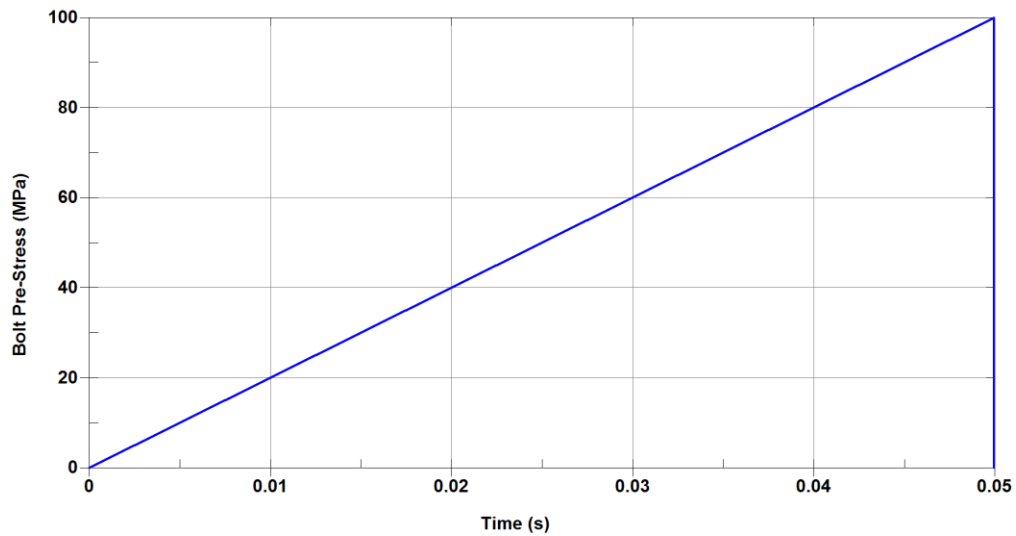


Figure 4-39 Bolt pre-stress vs. time curve

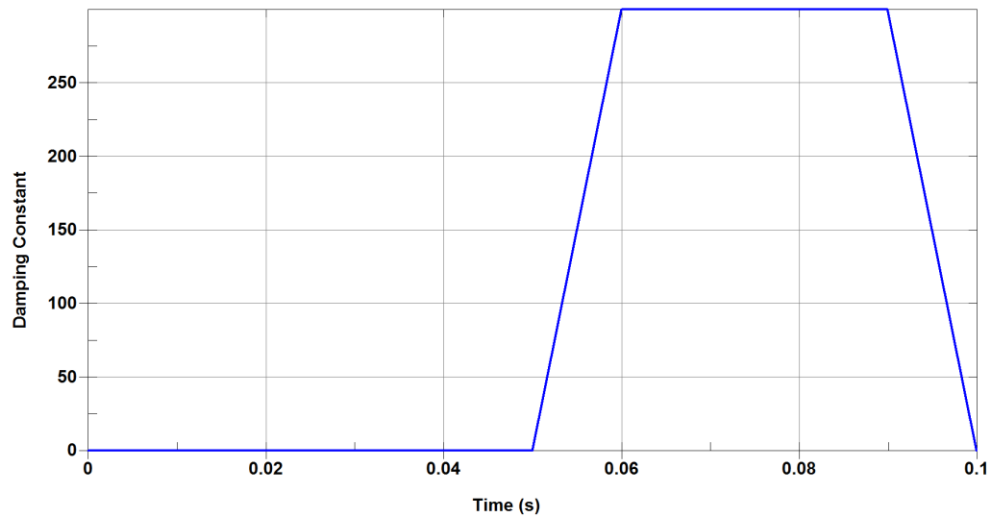
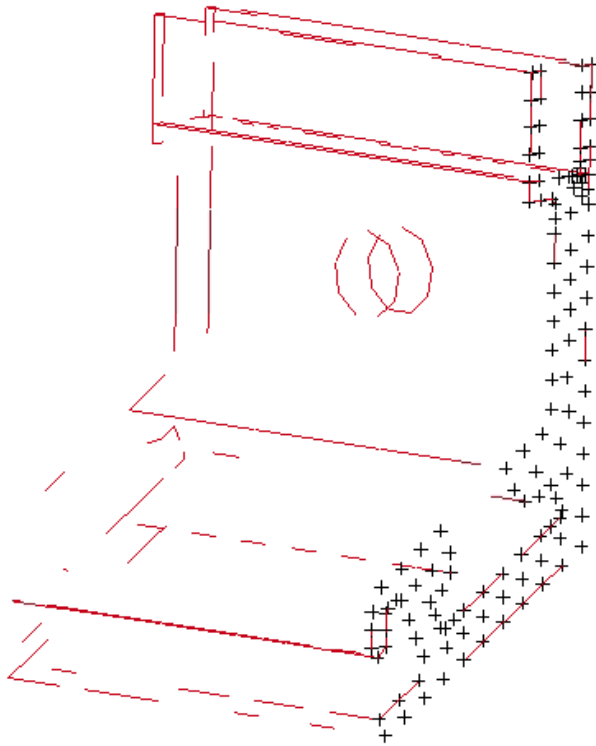


Figure 4-40 Damping coefficient vs. time curve

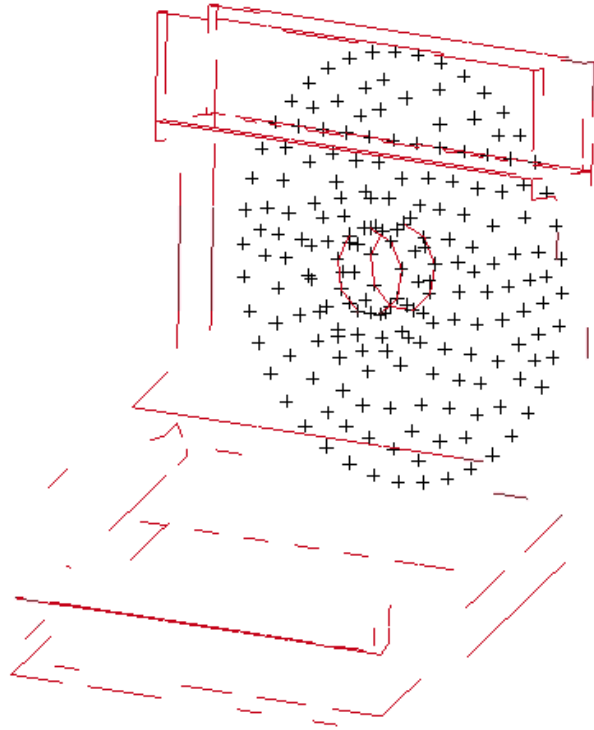


#### 4.10.5 Boundary Condition

The side rail is extended along the bus, and all seats are attached to it. In the sub-model, a section of it, which is beside a row of two seats, is modeled. To consider the effects of the continuation of the rail, symmetry condition is added to two ends of the rail (Figure 4-41). The rail is bolted to a cylindrical shape structure which is welded to the sidewall. The areas under the cylindrical shape structure and the bolt head are fixed in the perpendicular direction (Figure 4-42). The nodes in the bolt hollow are free to rotate in the perpendicular direction. The explained boundary conditions accurately simulate the connection of the rail to the sidewall.



*Figure 4-41 Symmetry condition*



*Figure 4-42 Fixed points in the perpendicular direction*

#### 4.10.6 Material Properties

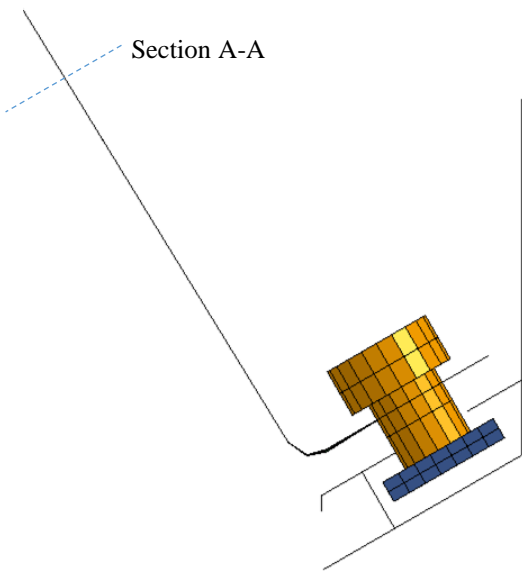
Material properties for the rail and the bracket in the sub-model are the same as in the whole model. The bracket is made of Steel\_S355, and the rail uses Aluminum AA6060T4. The material property for the bolts and nuts are “bilinear isotropic elastic plastic steel” with the properties reported in Table 4-15.

*Table 4-15 Bolt and nut material properties*

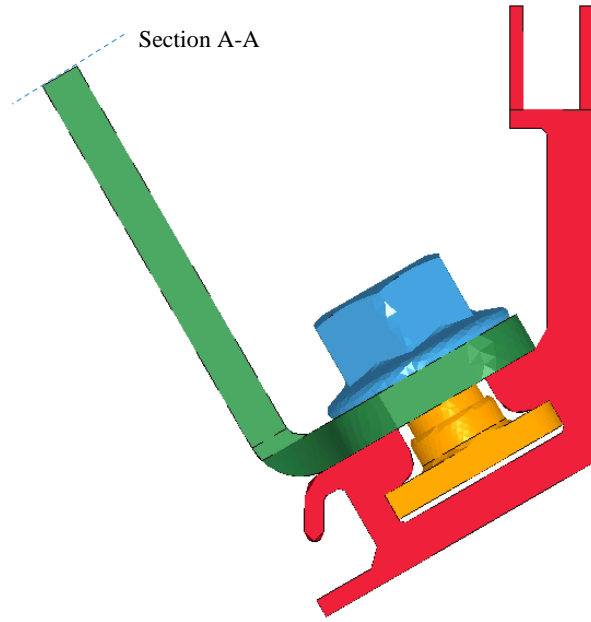
Material type	Material	Mass density (tone/mm <sup>3</sup> )	Young's modulus (N/mm <sup>2</sup> )	Poisson's Ratio	Yield Stress (N/mm <sup>2</sup> )	Tangent Modulus (N/mm <sup>2</sup> )
Bilinear elastic plastic	Steel-SAE J429	7.85e-9	2.1e5	0.3	634.32	1378.93

#### 4.10.7 Loading Condition

The cut boundary face in the whole model is section A-A shown in Figure 4-43. The load will be extracted from this section of the bracket in the simulation of the kinematics and will be applied to the same section in the sub-model. Figure 4-44 shows where force and moment should be applied to the sub-model.



*Figure 4-43 Section A-A in the whole model*



*Figure 4-44 Section A-A in the sub-model*

## 5 MODEL VERIFICATION AND VALIDATION

The model is verified and validated in two stages. Firstly, the seat structure is validated against the results of a quasi-static FMVSS 210 [42] test. Secondly, the kinematics of an occupant under rollover is verified and validated. In order to do that, the injury criteria values are extracted from the ATDs in the simulation and compared to the experimental results of a physical whole coach rollover test. The obtained correlation not only validates the model but also shows the reliability of the proposed modeling approach.

### 5.1 SEAT STRUCTURE VALIDATION

Regulation FMVSS 210 [42] specifies the static test procedure to verify the strength of the seat belt anchorages. In the test, two loading blocks are constrained to the seat by 3-point seat belts. The seat belts are then pulled to 3000 lbf (1.33 kN) quasi-statically. Although the test is targeted toward seat belt anchorage, the results can serve as a good benchmark for the verification of the total stiffness of the seat structure. The results of the physical test for the seat under consideration are provided by the seat manufacturer. Figure 5-1 shows the test setup and Figure 5-2 illustrates the applied loads measured in the experiment.

To validate the developed seat structure, shoulder and lap block are introduced to the model instead of ATDs. The simulation incorporates two stages. Firstly, the blocks are placed in the designated positions, and the gravity load is applied to obtain the equilibrium position. The resultant kinetic energy is damped using an internal damping coefficient in the foam material. Afterward, the 3-

point seat belts are fitted to the blocks. Blocks are connected to the loading point by the chains modeled as beam elements. Chains are pulled to the same peak force value as in the physical test, following the same time history. Figure 5-3 and Figure 5-4 show the comparison of the test and the simulation results.



Figure 5-1 Test setup

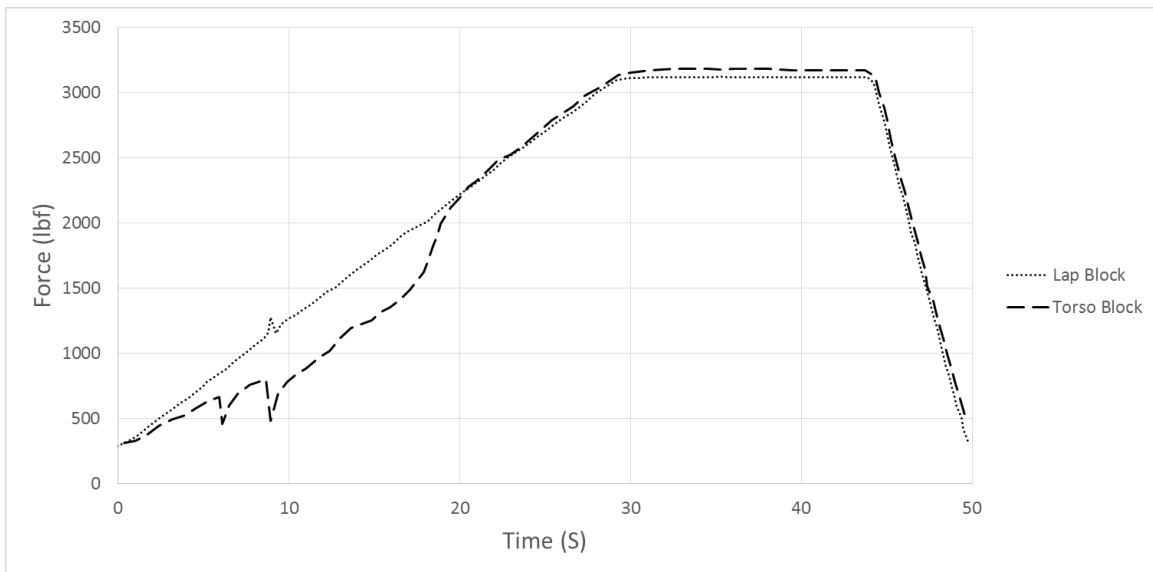


Figure 5-2 Applied load measured from the test


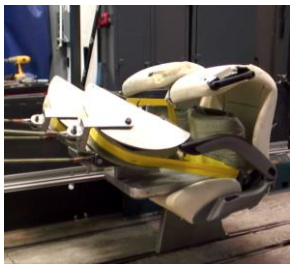

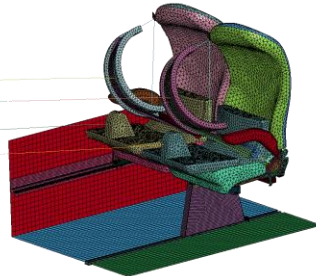
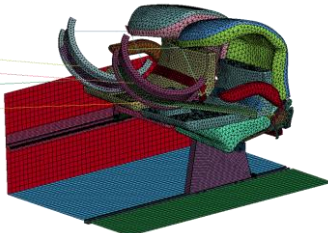
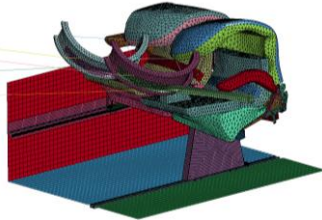
Load	1250 lb.	2000 lb.	3100 lb.
Experiment			
Simulation			

Figure 5-3 Experiment vs. simulation front view







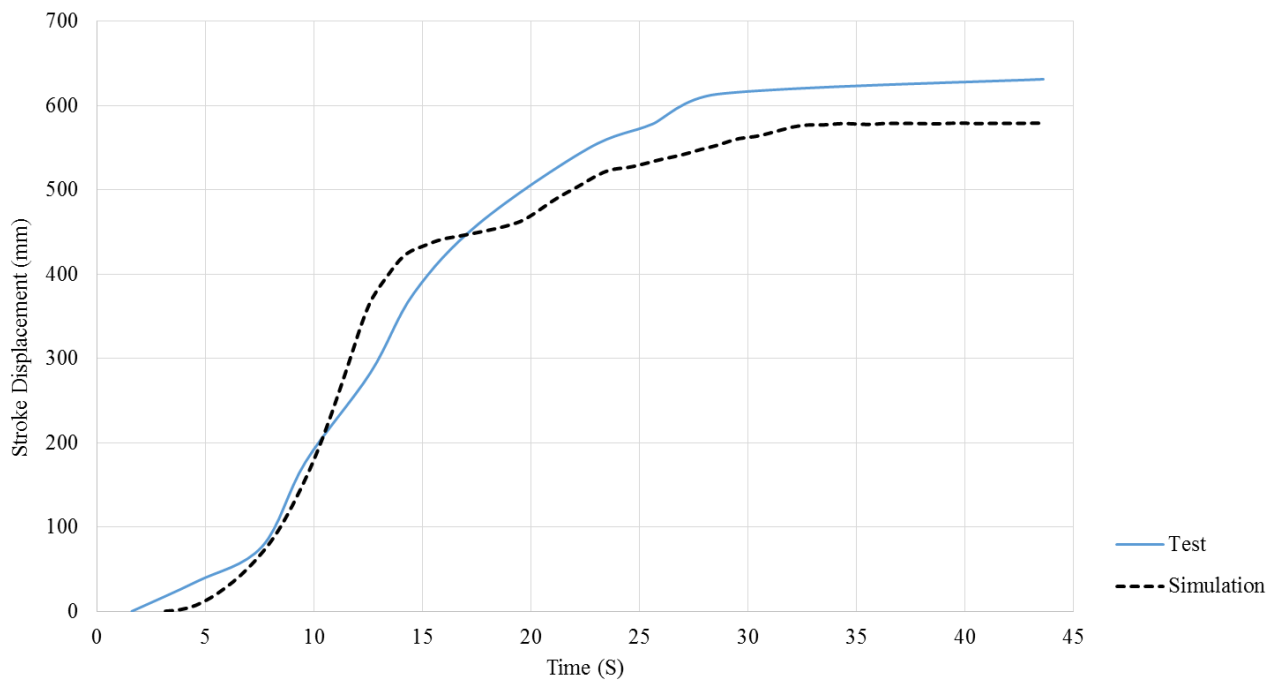
Load	1250 lb.	2000 lb.	3100 lb.
Experiment			
Simulation			

Figure 5-4 Experiment vs. simulation rear view

The mode of failure in the simulation results, folded seat back, is the same as the physical test. The deformation of the seat frame also correlates well with the experimental results.

Since the experimental loading is force-controlled, the displacement time history reflects the response of the structure to the loading. Thus this curve is used to validate the simulation results.

Figure 5-5 compares torso stroke displacement vs. time curve obtained experimentally and in the simulation. A good level of agreement between the simulation and the test results can be seen. For Figure 5-5, the total time of the simulation which is one second is scaled by a factor of 43 to match the total time of the test.



*Figure 5-5 Stroke displacement vs. time*

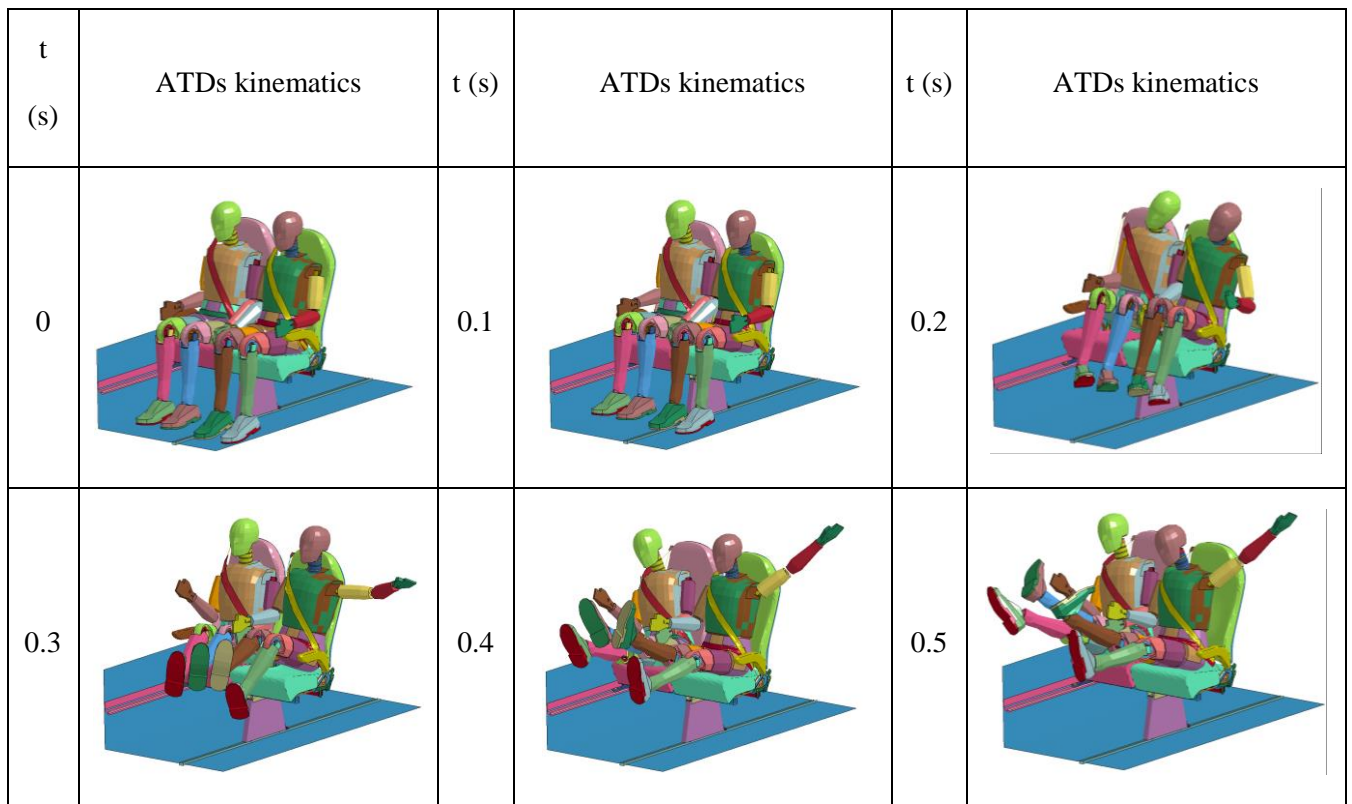
The Sprague & Geers and ANOVA metrics are calculated for stroke displacement time history and are reported in Figure 5-6. As all acceptance criteria are fulfilled, the model of the seat structure is considered to be validated.

Sprague & Geers		Status
Magnitude	-5.7%	Pass ✓
Phase	2.1%	Pass ✓
Comprehensive	6.1%	Pass ✓
ANOVA		
Average Residual	-3.8%	Pass ✓
Standard Deviation	5.6%	Pass ✓

Figure 5-6 Metrics results for seat structure validation

## 5.2 ATDs' KINEMATICS, VERIFICATION, AND VALIDATION

The simulation of the ATD kinematics under the applied acceleration had been running for one second, and the results are shown in Figure 5-7. The back and forth motion of ATDs comes from the presence of two peak accelerations with the negative value in between.







*Figure 5-7 ATDs kinematics*

The verification of the simulation is performed by analysis of the energy balance through the simulation (Figure 5-8). For complex simulations in which finding an analytical solution is impossible, some checking features are developed within the software to verify the results of the analysis. In LS-DYNA explicit simulation, the energy data forms a useful check for the verification of the results [32]. In the energy balance graph, negative contact (sliding) or internal energy is not acceptable and total energy must be conserved through the simulation. Existence of any negative energy in the energy balance curve is the sign of a numerical issue in the model. Throughout the simulation, the initial energy, which can be kinetic energy or external work, must be converted to secondary energies meanwhile the total energy should be kept constant. Dissipation of total energy in the system is another sign of a numerical issue.

In this model, the external work done by the applied acceleration is converted to internal energy and contact energy. No negative or dissipated energy can be seen in the model which verify the analysis results. The contact energy mainly comes from the friction between ATDs, seats, and seat belts. The fact that contact energy takes a considerable part in comparison to internal energy can be explained by the small deformation in the seat structure. The artificial hourglass energy is kept less than 10% of the total energy. Hourglass energy comes from the computational mechanism

preventing the unphysical deformation modes of under-integrated element used in the model. To achieve a larger explicit time step, nonphysical mass (mass scaling) is added to unreasonably small elements that cause the total energy to increase through the simulation; however, the added mass is kept less than 5%.

To provide the quantitative comparison of the simulation results with the physical test, the ATD injury data is used. The injury criteria values are compared in Table 5-1 to Table 5-4.

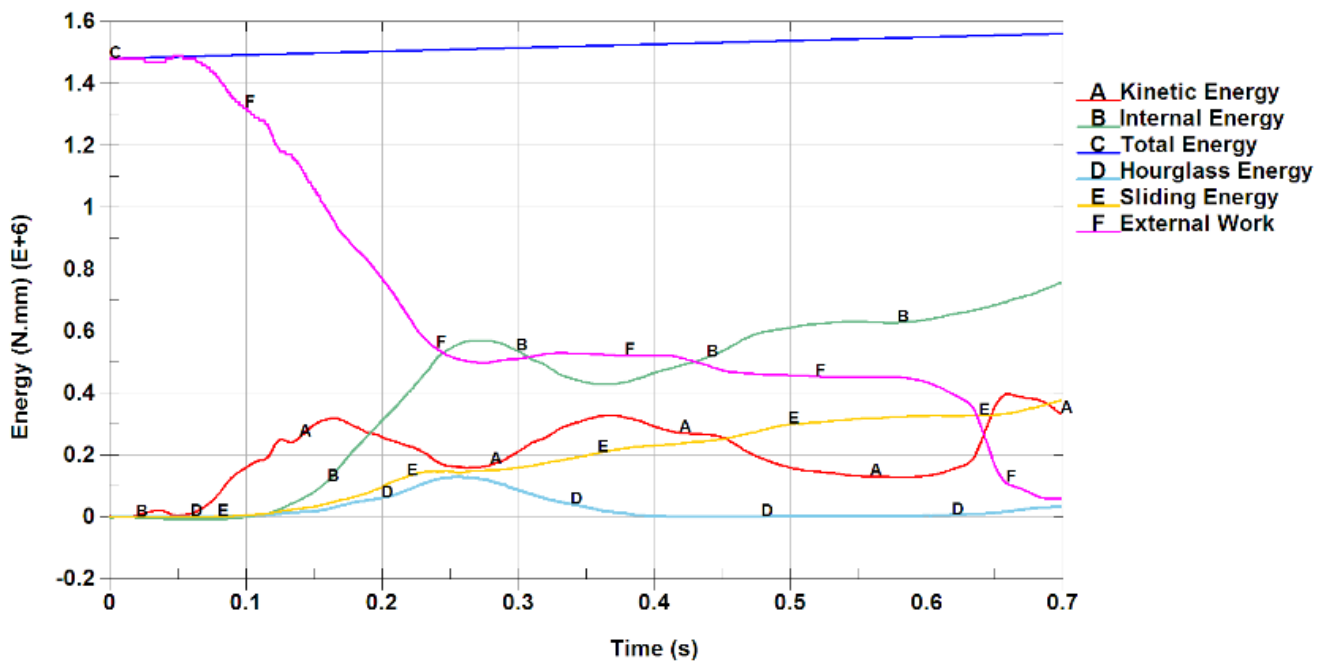


Figure 5-8 Energy balance

Table 5-1 Head acceleration\*

Injury	Experiment		Simulation	
	Max: 4.5 G's Tmax: 387 ms	Min: -4.5 G's Tmin : 239 ms	Max: 4.32 G's Tmax: 349 ms	Min: -3.48 G's Tmin: 354 ms
Head X acceleration in local CS of head accelerometer	Max: 5.48 G's Tmax: 312 ms	Min: -1.76 G's Tmin : 457 ms	Max: 7.97 G's Tmax: 200 ms	Min: -3.81 G's Tmin: 324 ms

Head Z acceleration in local CS of head accelerometer	Max: 7.64 G's	Min: -1.82 G's	Max: 7.52 G's	Min: -1.74 G's
	Tmax: 212 ms	Tmin : 304 ms	Tmax: 216 ms	Tmin: 404 ms

\*Data are filtered to 60 Hz by SAE filtering

*Table 5-2 Chest acceleration\**

Injury	Experiment		Simulation	
Chest X acceleration in local CS of chest accelerometer	Max: 2.1 G's	Min: -2.8 G's	Max: 2.7 G's	Min: -2.3 G's
	Tmax: 163 ms	Tmin : 229 ms	Tmax: 174 ms	Tmin: 214 ms
Chest Y acceleration in local CS of chest accelerometer	Max: 3.84 G's	Min: -0.54 G's	Max: 5.65 G's	Min: -4.97 G's
	Tmax: 232 ms	Tmin : 417 ms	Tmax: 171 ms	Tmin: 402 ms
Chest Z acceleration in local CS of chest accelerometer	Max: 6.01 G's	Min: -1.74 G's	Max: 5.24 G's	Min: -2.39 G's
	Tmax: 212 ms	Tmin : 629 ms	Tmax: 216 ms	Tmin: 661 ms

\*Data are filtered to 60 Hz by SAE filtering

*Table 5-3 Pelvis acceleration\**

Injury	Experiment		Simulation	
Pelvis X acceleration in local CS of pelvis accelerometer	Max: 1.8 G's	Min: -4.6 G's	Max: 3.9 G's	Min: -4.6 G's
	Tmax: 267 ms	Tmin : 180 ms	Tmax: 150 ms	Tmin: 185 ms
Pelvis Y acceleration in local CS of pelvis accelerometer	Max: 5.23 G's	Min: -3.77 G's	Max: 6.60 G's	Min: -2.25 G's
	Tmax: 176 ms	Tmin : 160 ms	Tmax: 211 ms	Tmin: 408 ms
Pelvis Z acceleration in local CS of pelvis accelerometer	Max: 4.64 G's	Min: -1.48 G's	Max: 3.43 G's	Min: -2.12 G's
	Tmax: 214 ms	Tmin : 303 ms	Tmax: 211 ms	Tmin: 651 ms

\*Data are filtered to 60 Hz by SAE filtering

Table 5-4 Upper neck forces in local CS\*

Injury	Experiment		Simulation	
Upper X neck forces in local CS	Max: 95.4 N Tmax: 382 ms	Min: -125.4 N Tmin : 284 ms	Max: 104 N Tmax: 750 ms	Min: -121 N Tmin: 620 ms
Upper Y neck forces in local CS	Max: 230 N Tmax: 304 ms	Min: -72 N Tmin : 453 ms	Max: 352 N Tmax: 200 ms	Min: -170 N Tmin: 324 ms
Upper Z neck forces in local CS	Max: 321 N Tmax: 211 ms	Min: -69 N Tmin : 297 ms	Max: 326 N Tmax: 215 ms	Min: -76 N Tmin: 662 ms

\*Data are filtered to 60 Hz by SAE filtering

The acceleration and force histories of the test and the simulation are compared in Figure 5-9 to Figure 5-17. Since the motion in a rollover is mostly planar, the data is compared in Y and Z directions only. The good level of correlation can be observed for the Z-direction in which the highest peak values occur. Table 5-5 summarizes the comparison metrics for Y and Z directions. As can be seen, the validation requirements are met for the majority of the metrics.

The unknown initial position of ATD and any possible impact of ATD with interior objects in the rollover test introduce some uncertainties in the physical test results. Moreover, due to the cost issues, several physical tests are not feasible; therefore, the level of the uncertainty for the results of the physical test cannot be evaluated. Since the Finite Element model is shown to be robust to artificial parameters in a preliminary sensitivity analysis, and taking into the account the uncertainties of the physical test, the results of the validation study is considered acceptable. In the next section, the developed and validated model is used to study the influences of certain physical parameters of the seat belt on the passenger's safety.

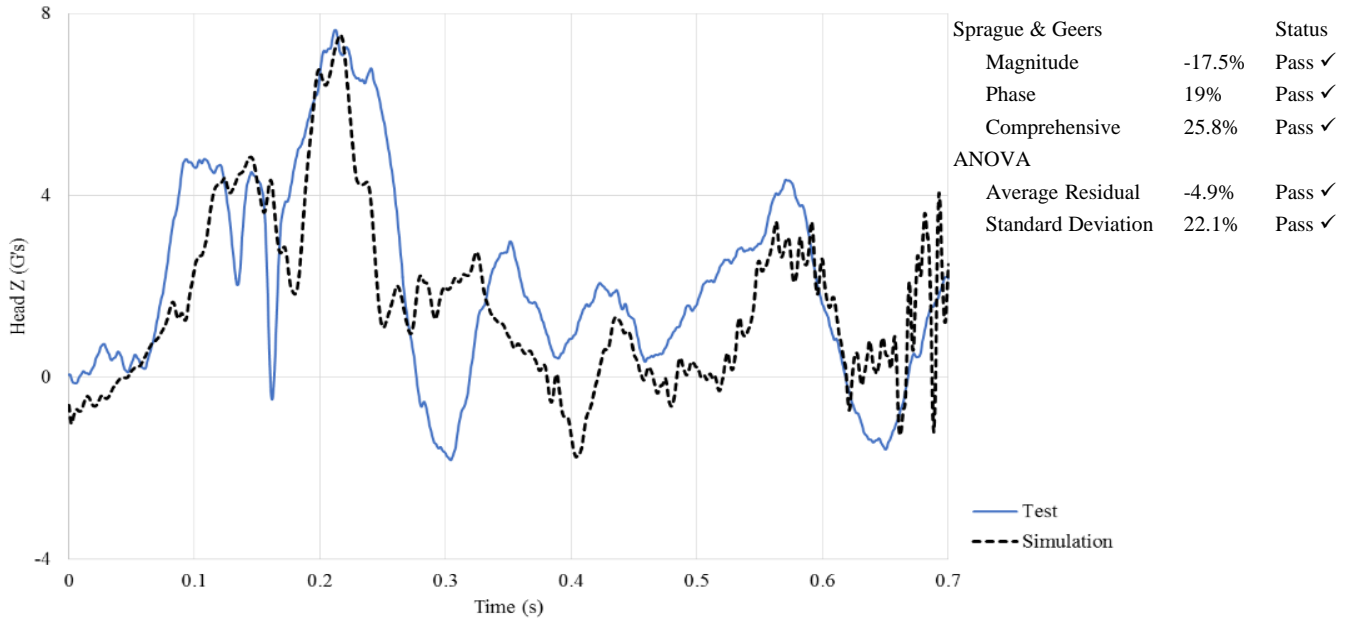


Figure 5-9 Head Z (G's) vs. time (s)

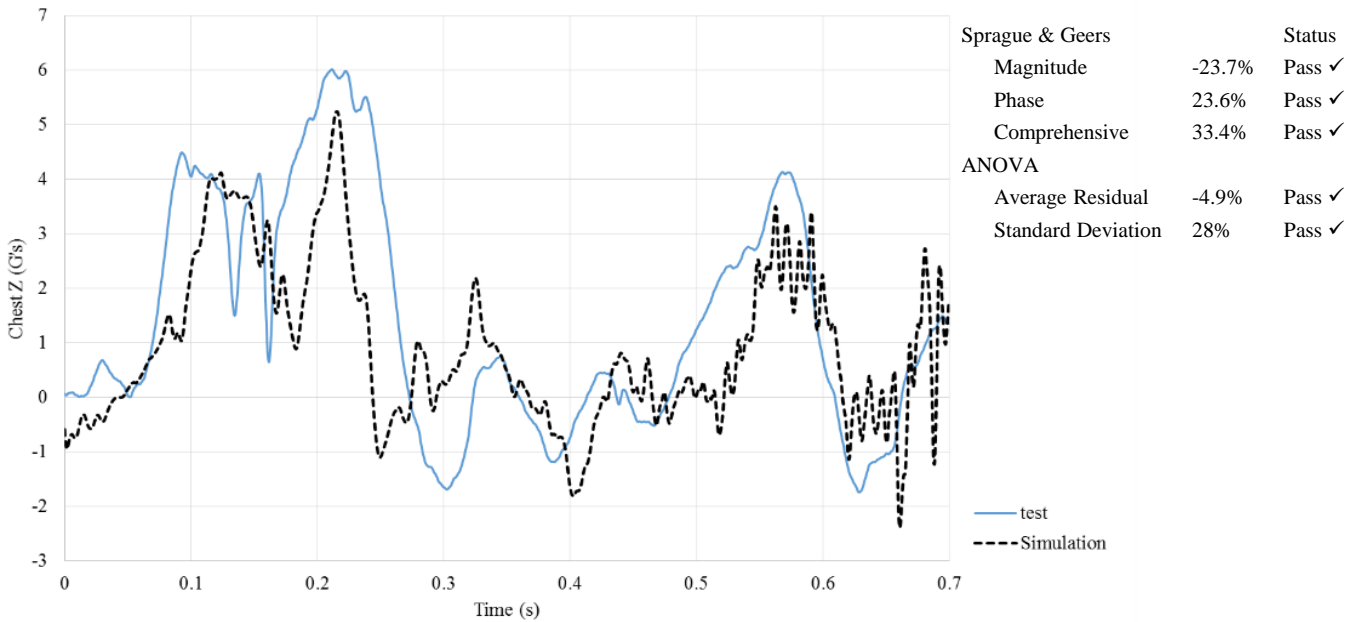


Figure 5-10 Chest Z (G's) vs. time (s)

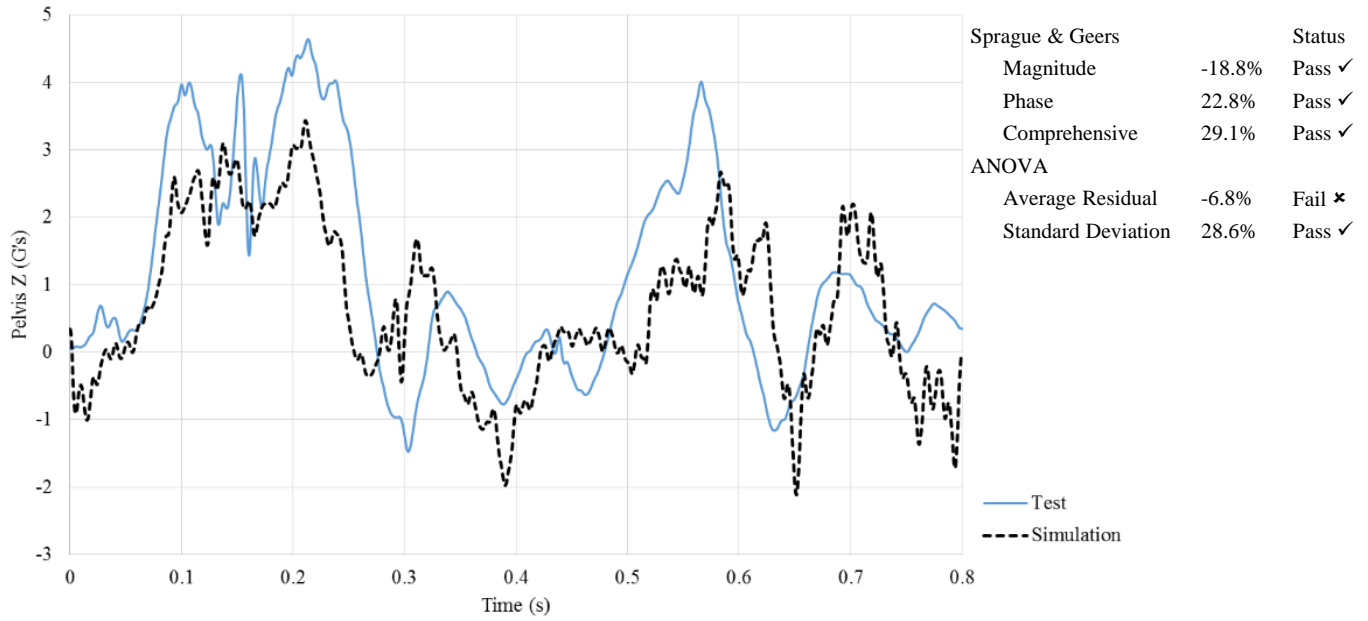


Figure 5-11 Pelvis Z (G's) vs. time (s)

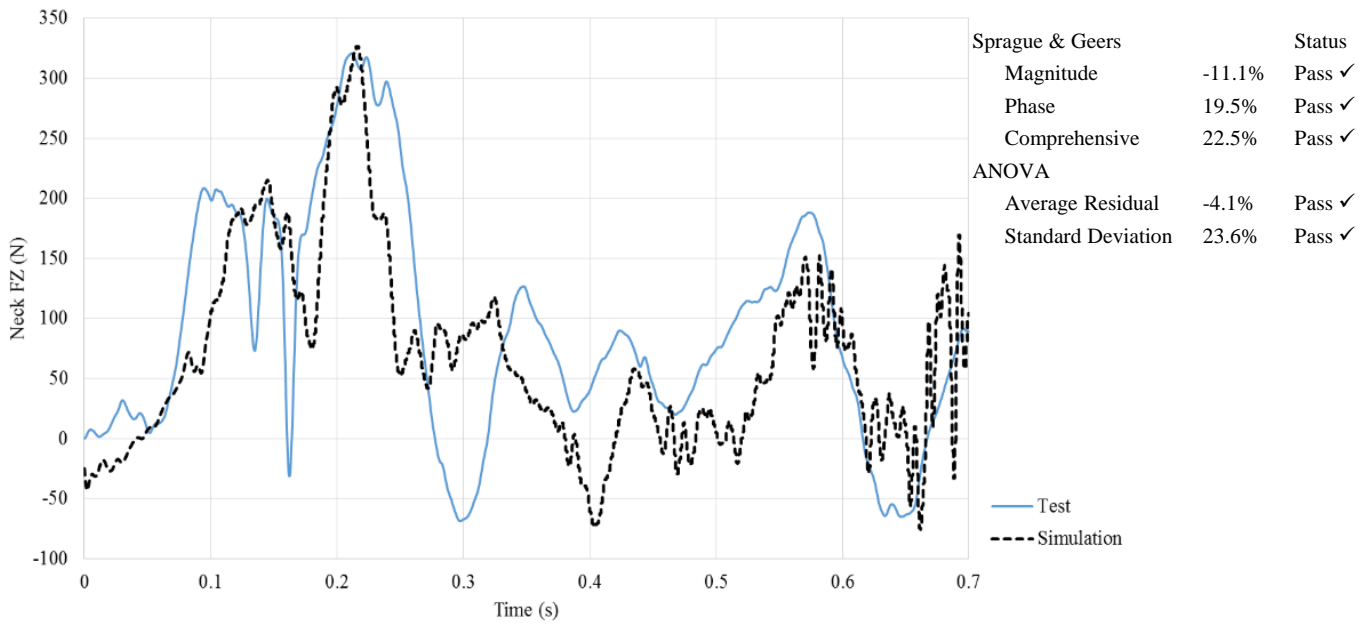


Figure 5-12 Neck FZ (N) vs. time (s)

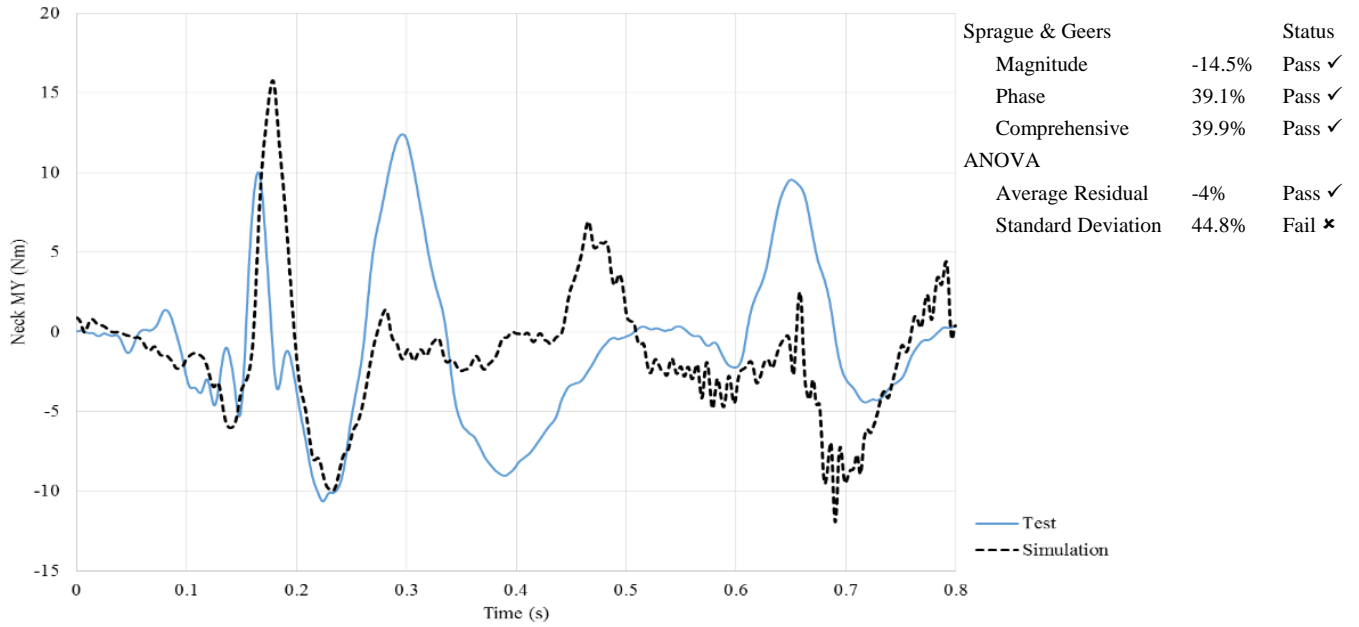


Figure 5-13 Neck MY (Nm) vs. time (s)

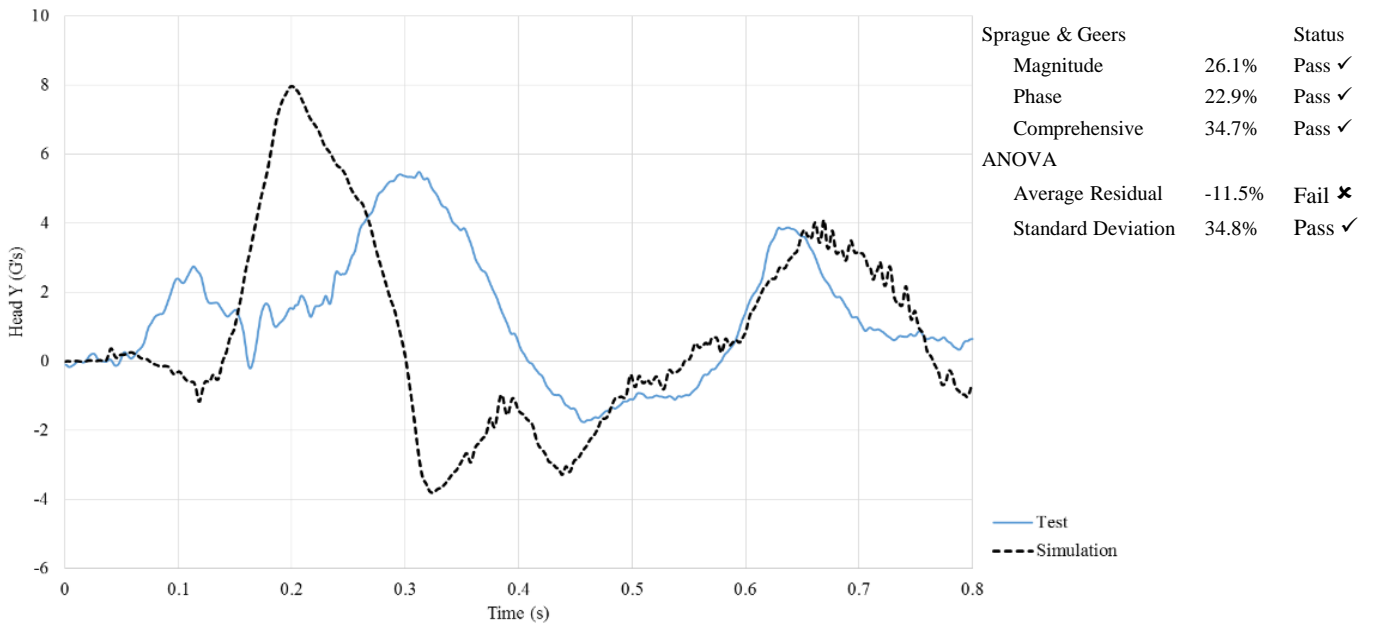


Figure 5-14 Head Y (G's) vs. time (s)

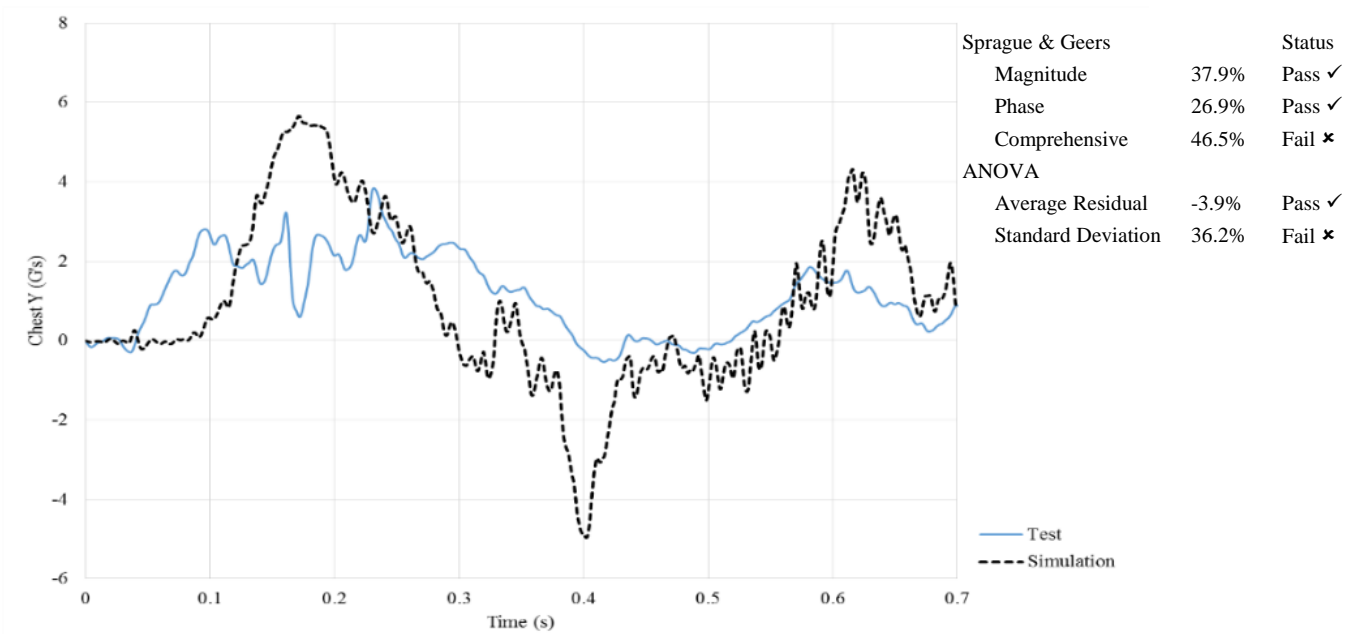


Figure 5-15 Chest Y (G's) vs. time (s)

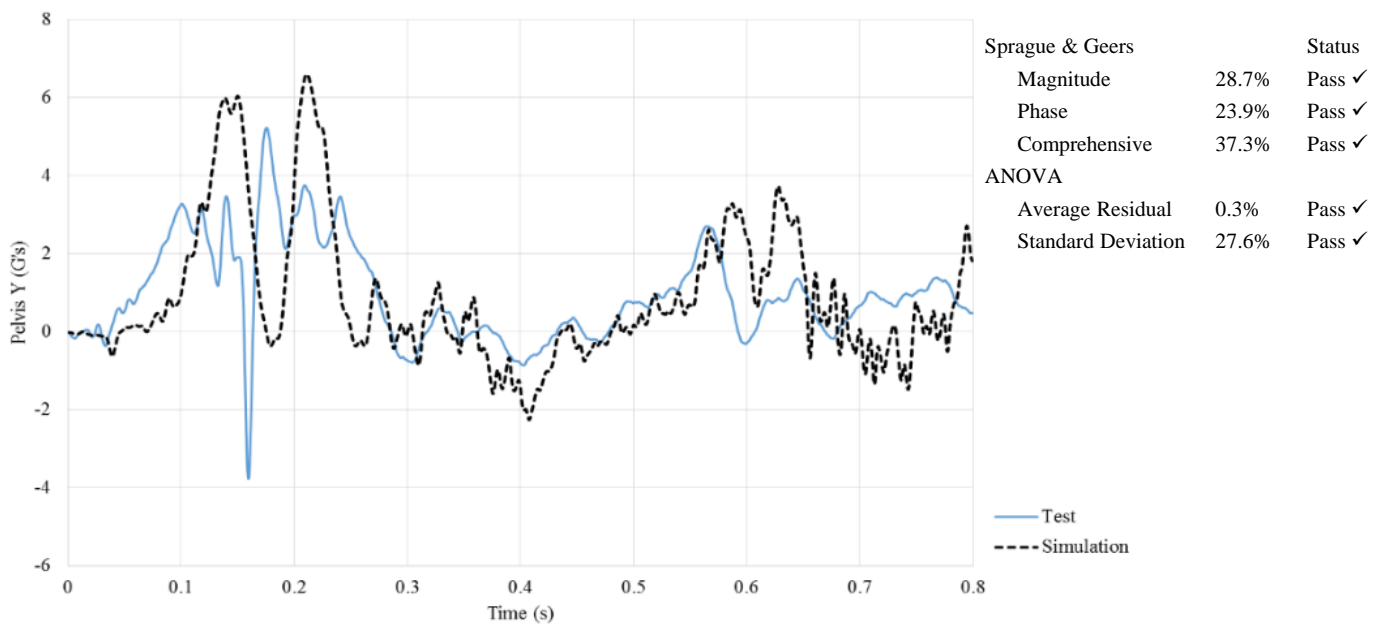


Figure 5-16 Pelvis Y (G's) vs. time (s)



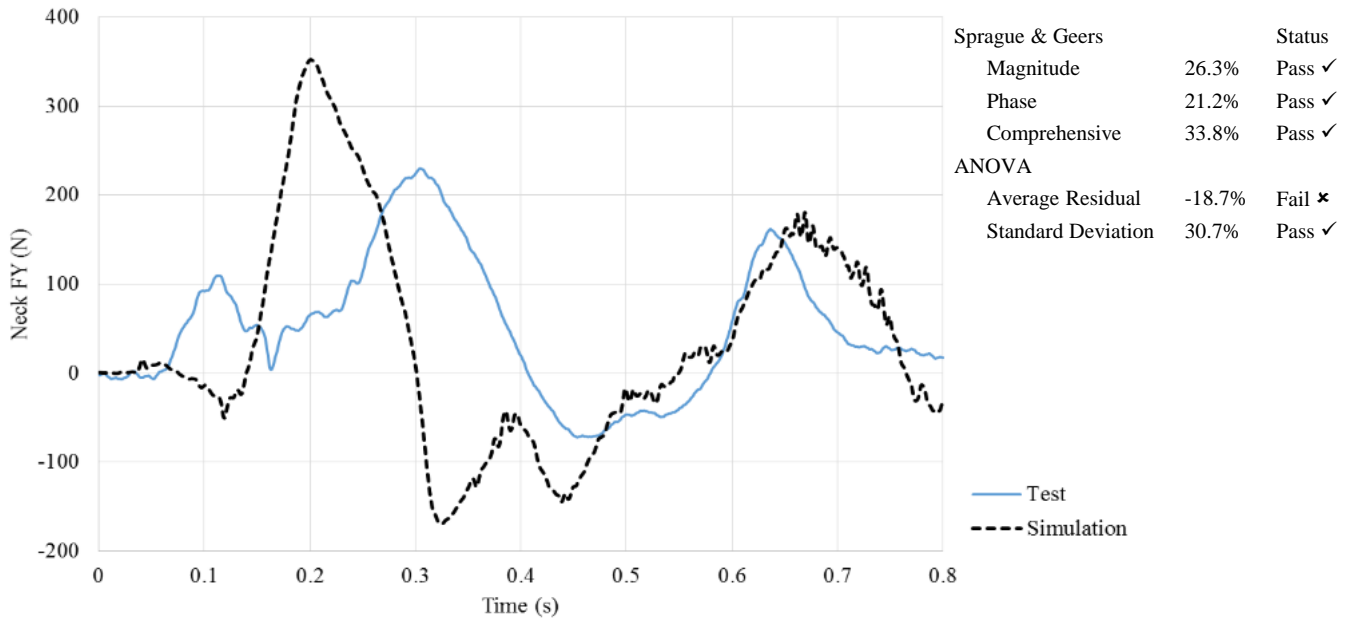


Figure 5-17 Neck FY (N) vs. time (s)

Table 5-5 Summarized metrics' results

Metrics →	Sprague & Geers						ANOVA			
	Magnitude		Phase		Comprehensive		Average Residual		Standard	
Head A <sup>1</sup> Z	-17.5%	✓ <sup>4</sup>	19%	✓	25.8%	✓	-4.9%	✓	22.1	✓
Head AY	26.1%	✓	22.9%	✓	34.7%	✓	-11.5%	✗ <sup>5</sup>	34.8%	✓
Chest AZ	-23.7%	✓	23.6%	✓	33.4%	✓	-4.9%	✓	28%	✓
Chest AY	37.9%	✓	26.9%	✓	46.5%	✗	-3.9%	✓	36.2%	✗
Pelvis AZ	-18.8%	✓	22.8%	✓	29.1%	✓	-6.8%	✗	28.6%	✓
Pelvis AY	28.7%	✓	23.9%	✓	37.3%	✓	0.3%	✓	27.6%	✓
Neck F <sup>2</sup> Z	-11.1%	✓	19.5%	✓	22.5%	✓	-4.1%	✓	23.6%	✓
Neck FY	26.3%	✓	21.2%	✓	33.8%	✓	-18.7%	✗	30.7%	✓
Neck M <sup>3</sup> Y	-14.5%	✓	39.1%	✓	39.9%	✓	-4%	✓	44.8%	✗

1 Acceleration      4 Passed the criteria  
 2 Force                5 Does not meet the criteria  
 3 Moment

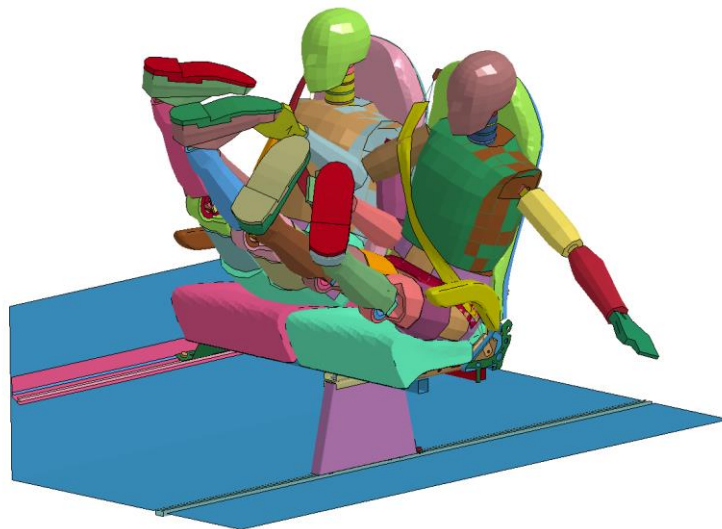
## 6 RESULTS AND DISCUSSION

The results of this study are targeted toward two main objectives; namely, seat structural integrity analysis and sensitivity analysis to the restraint properties. These two objectives are explained individually in this chapter.

### 6.1 SEAT STRUCTURAL INTEGRITY

#### 6.1.1 Kinematics of Occupants

The simulation of the kinematics of occupants in a rollover is conducted, and the results are shown in Section 5.2. Figure 6-1 demonstrate the moment when the imposed inertial force on the structure due to the occupants mass is maximal.



*Figure 6-1 the moment with the highest imposed load*

The distribution of plastic strain in the load bearing parts for the moment with the highest imposed load is shown in Figure 6-2. As it can be seen, the sidewall anchorage undergoes approximately

3% plastic strain. The plastic strain may lead to the failure of anchorage system during a rollover. Therefore, to obtain an accurate stress distribution for this critical anchorage, the sidewall mounting structures is sub-modeled.

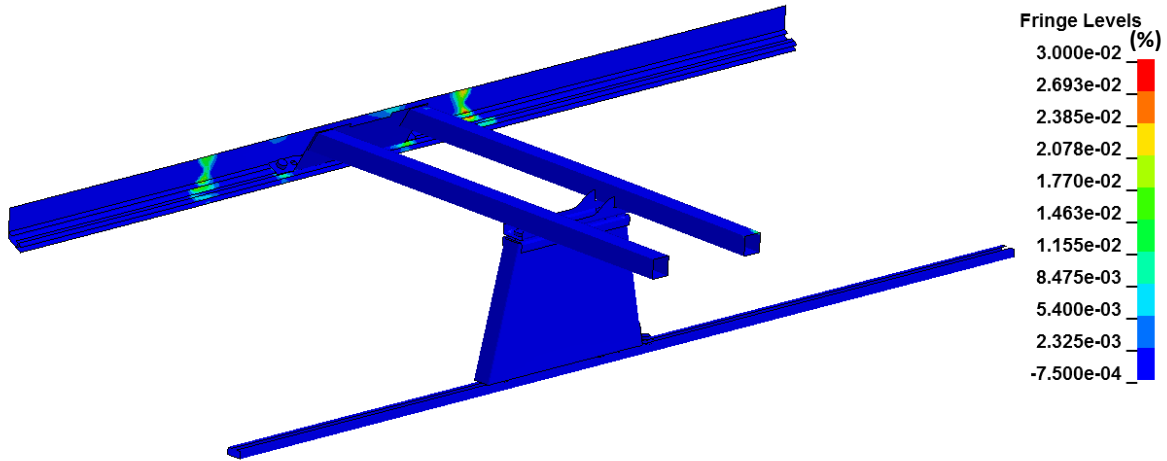
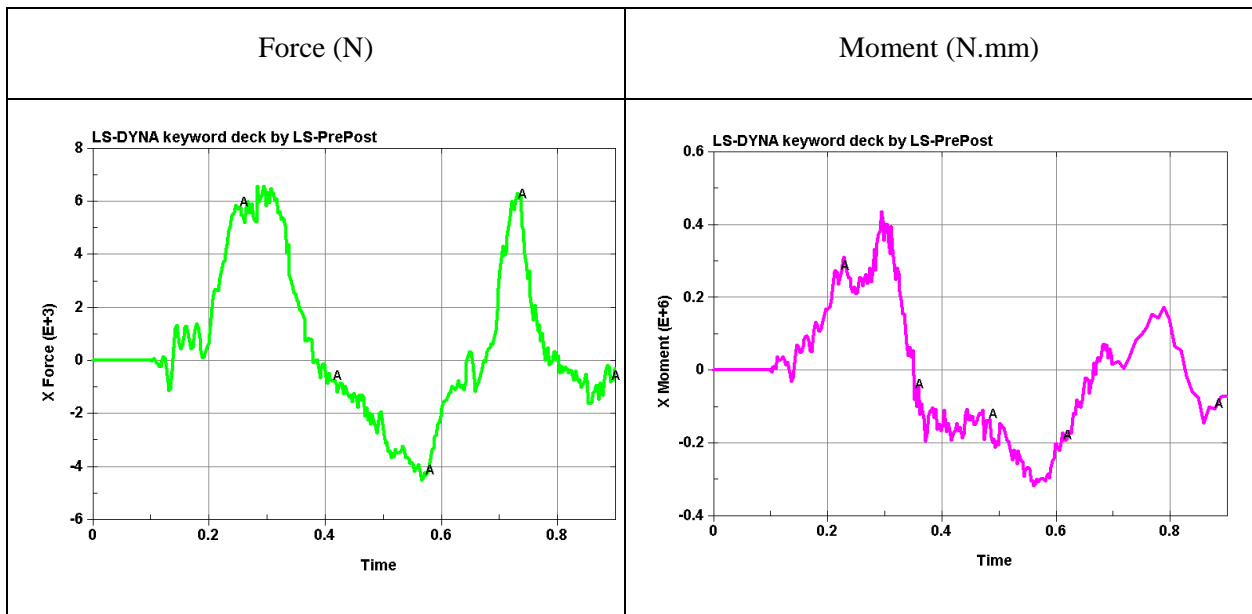


Figure 6-2 Plastic strain distribution

The transferred load to the anchorage system is obtained from the simulation of kinematics and is applied to the sub-model simulation. The loads are extracted from a cut boundary that is shown in Section 4.10.7. Figure 6-3 shows the extracted forces and moments in three directions.



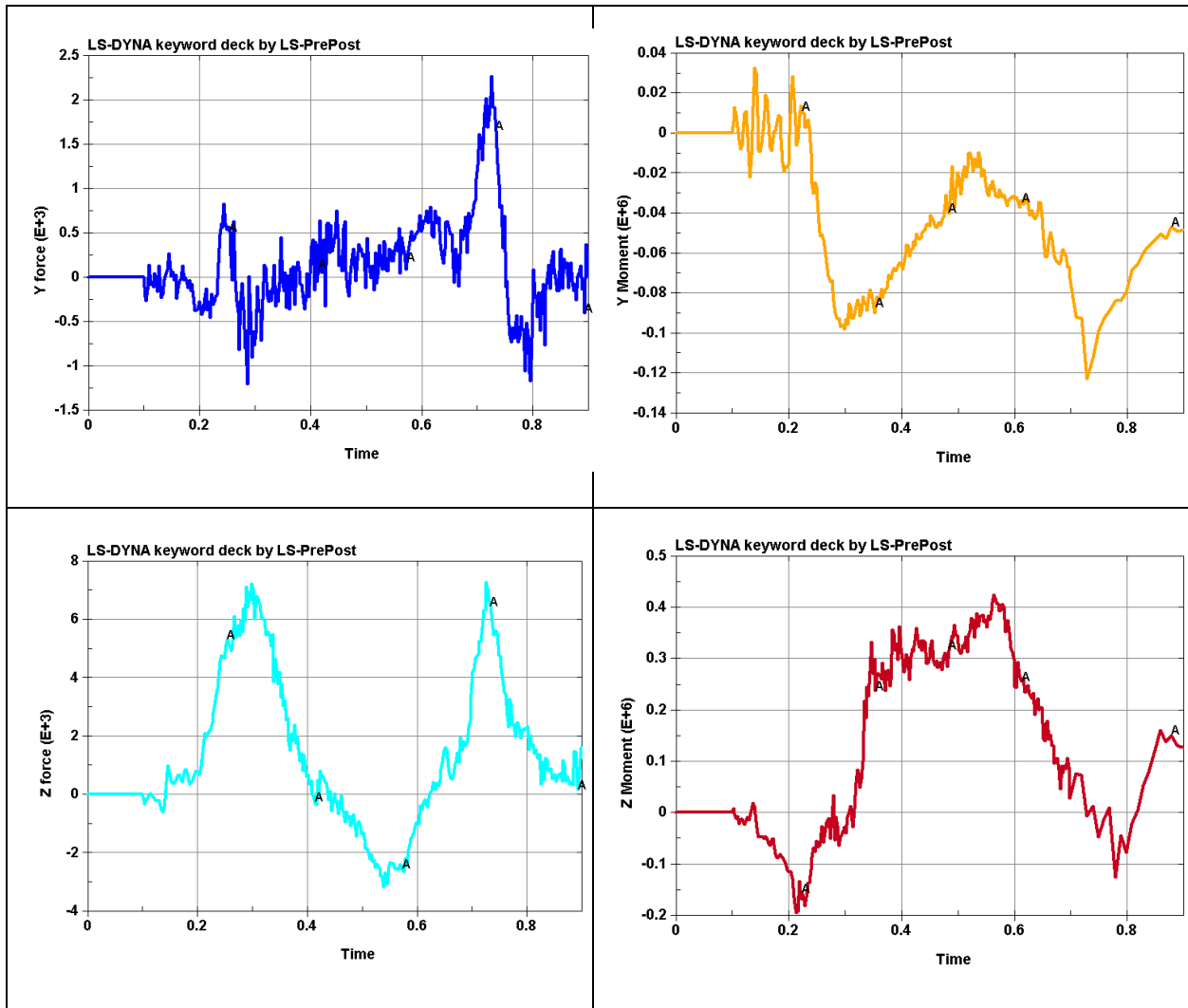


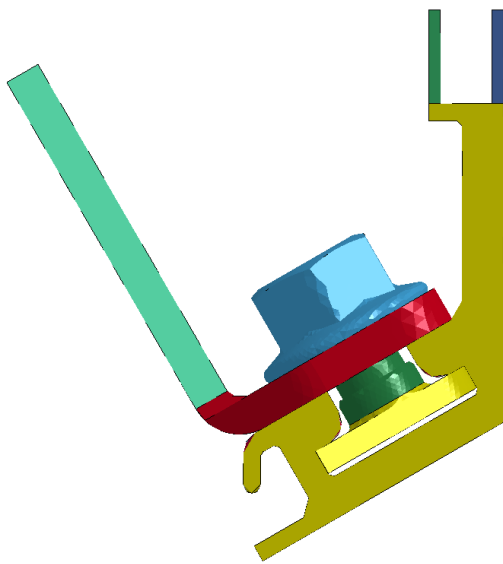
Figure 6-3 Extracted load from the cut boundary

### 6.1.2 Sub-model

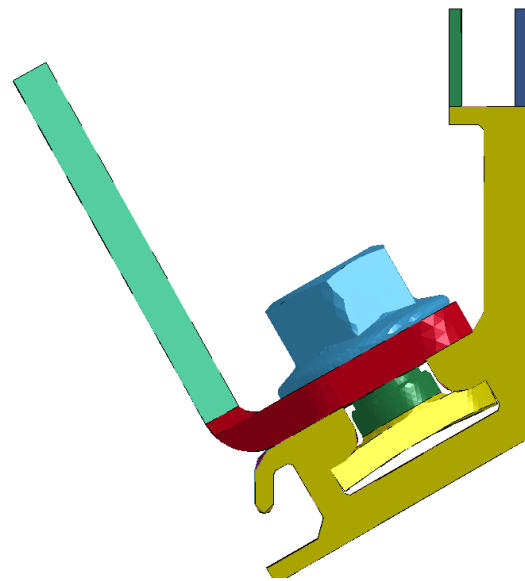
Sub-model simulation has two sub-steps. Firstly, the pre-stress is applied to the bolt shanks and afterward, the external load is imposed on the model. The results of each sub-steps are reported individually.

### 6.1.2.1 Bolt Pre-stress

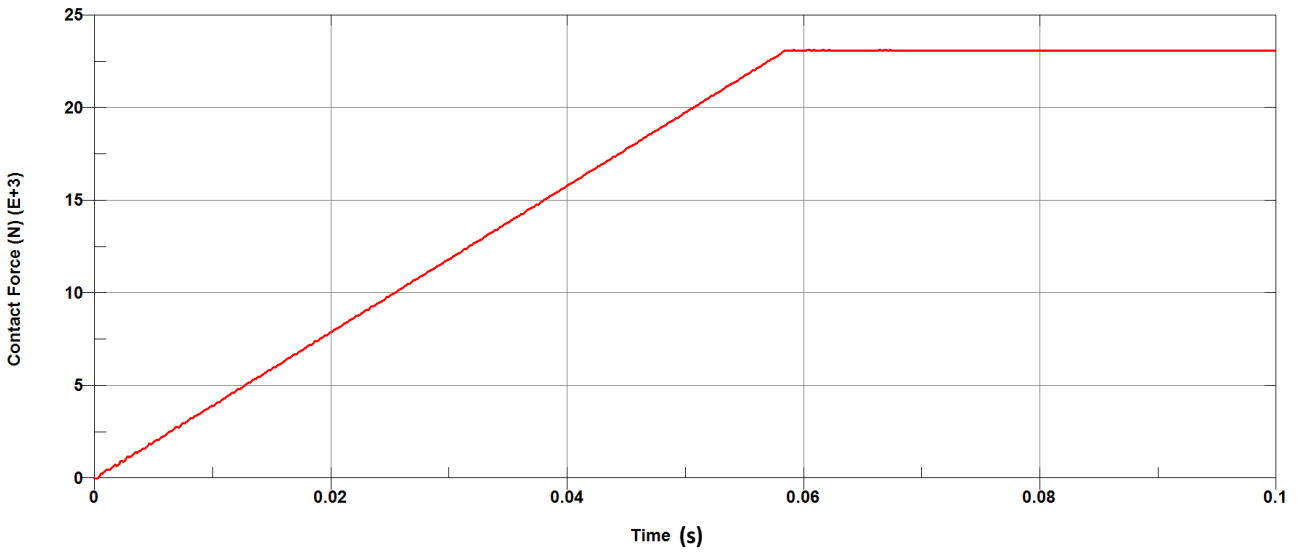
The bolts pretension plays an important role in the structural response of an assembly. In the whole model simulation, the bolt pretension is not considered, and the parts are tied together. However, in the sub-model simulation, bolt pretension is accurately modeled. In the first part of the sub-model simulation, from  $t = 0$  to  $t = 0.1s$ , a pre-stress is applied to the bolts to represent the bolt pretension. Figure 6-4 and Figure 6-5 compares the model before and after the application of the bolt pre-stress. As it can be seen, the bolts head after the application of the pre-stress is deformed. Bolt pre-stress forms a compressive stress between the bracket and the rail which bonds the parts together. The compressive stress creates a contact force between the bracket and the rail which ramps from zero (Figure 6-6). The presence of contact force confirms that parts are in touch and compressed together.



*Figure 6-4 Sub-model before bolt pre-stress*

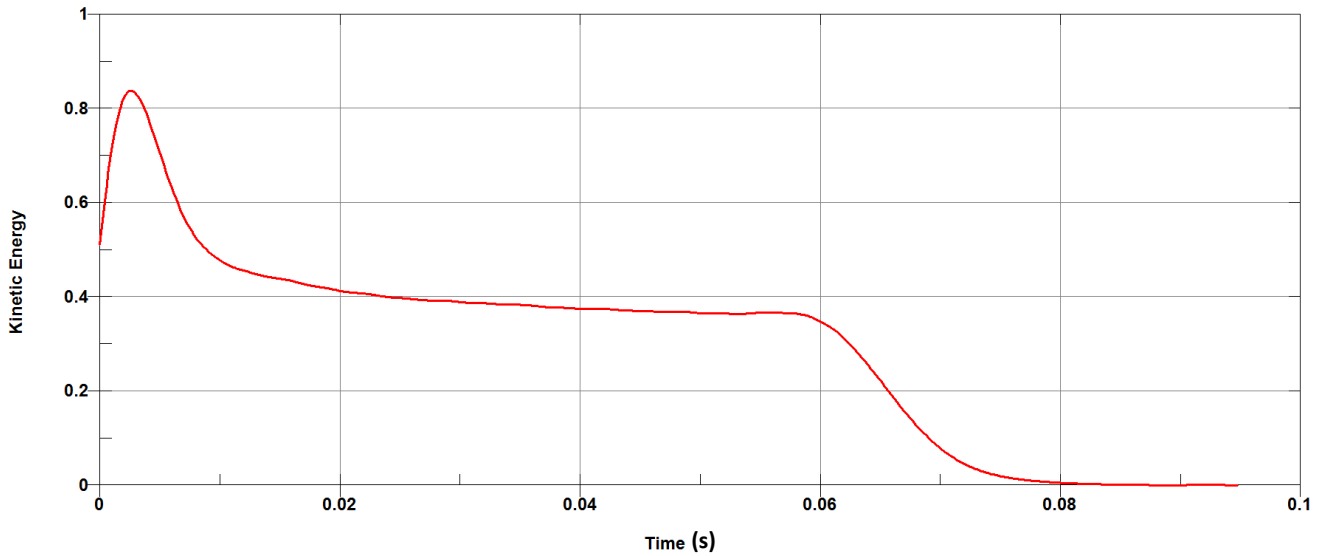


*Figure 6-5 Sub-model after bolt pre-stress,  
Displacement scale factor: 10*



*Figure 6-6 Contact force*

Application of the bolt pre-stress creates an undesired kinetic energy in the model. It can be described by the presence of primary gaps between the parts that must be omitted by the bolt pre-stress. Figure 6-7 shows how the kinetic energy increases at the beginning of the simulation and how it is damped later.



*Figure 6-7 Damped kinetic energy*

The bolt pre-stress creates the predefined stress in the shank; however stress in the bolt head goes beyond yield strength (Figure 6-8) what can be described by the specific geometry of this assembly. As it can be seen in Figure 6-9, the bolt head does not have a complete support in the head area. Thus, the application of the bolt pre-stress causes a stress concentration at the corner of the bolt head.

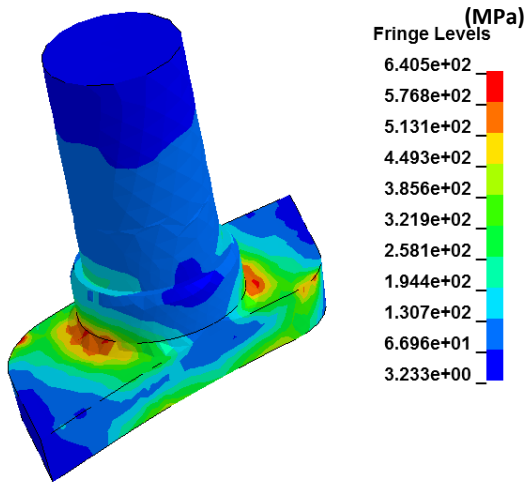


Figure 6-8 Stress distribution in bolts

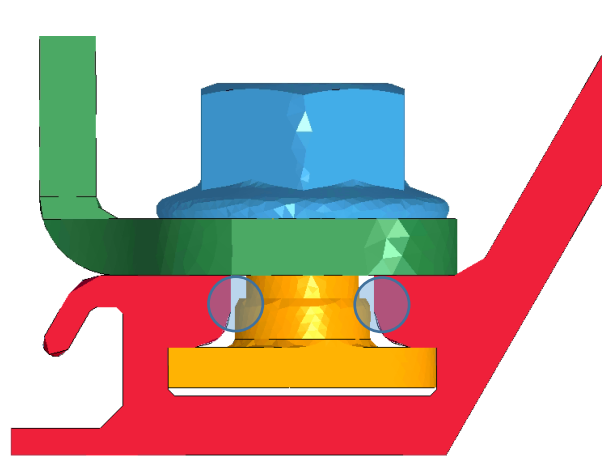


Figure 6-9 Stress concentration locations

There are handbooks which recommend an optimum fastening torque for bolts [43]. However, the recommended torque results in an unreasonable stress distribution in the bolts head for this assembly. The reason, as described in the previous paragraph, is the lack of support in the bolt head area. Consequently, a parametric study is carried out to find an optimum value for the bolt pre-stress for this specific assembly.

#### 6.1.2.2 Parametric Study on Bolt Pre-load

In this parametric study, the variable is the bolt preload. To conduct the parametric study, different bolt preloads is applied to the assembly, and the model is solved in ANSYS mechanical. The resultant stress in the shank and the bolt's head are extracted from the simulation. Although the

recommended preload for the present bolt is of the order of 33.0 kN [43], the simulation results show that preload cannot exceed 11.0 kN. If preload exceeds 11.0 kN, the resultant stress in the bolt's head goes beyond the yield strength of the bolts which is not acceptable (Figure 6-12). Figure 6-10 shows the configuration of the model and Figure 6-11 illustrates the feature which applies the preload to the model.

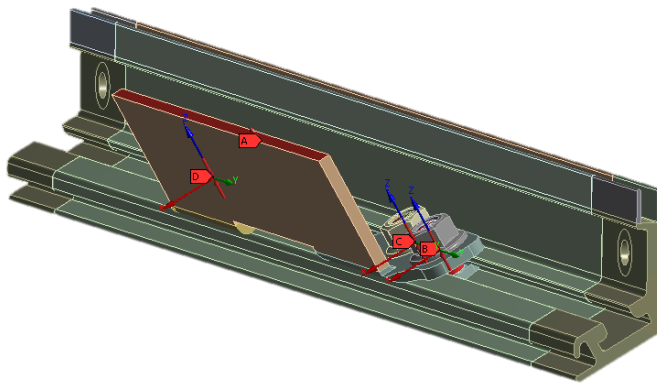
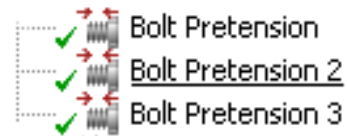


Figure 6-10 Bolts pre-load application



Tabular Data			
	Steps	<input checked="" type="checkbox"/> Define By	<input checked="" type="checkbox"/> Preload [N]
1	1.	Load	11000
2	2.	Lock	N/A
*			

Figure 6-11 Load and lock steps

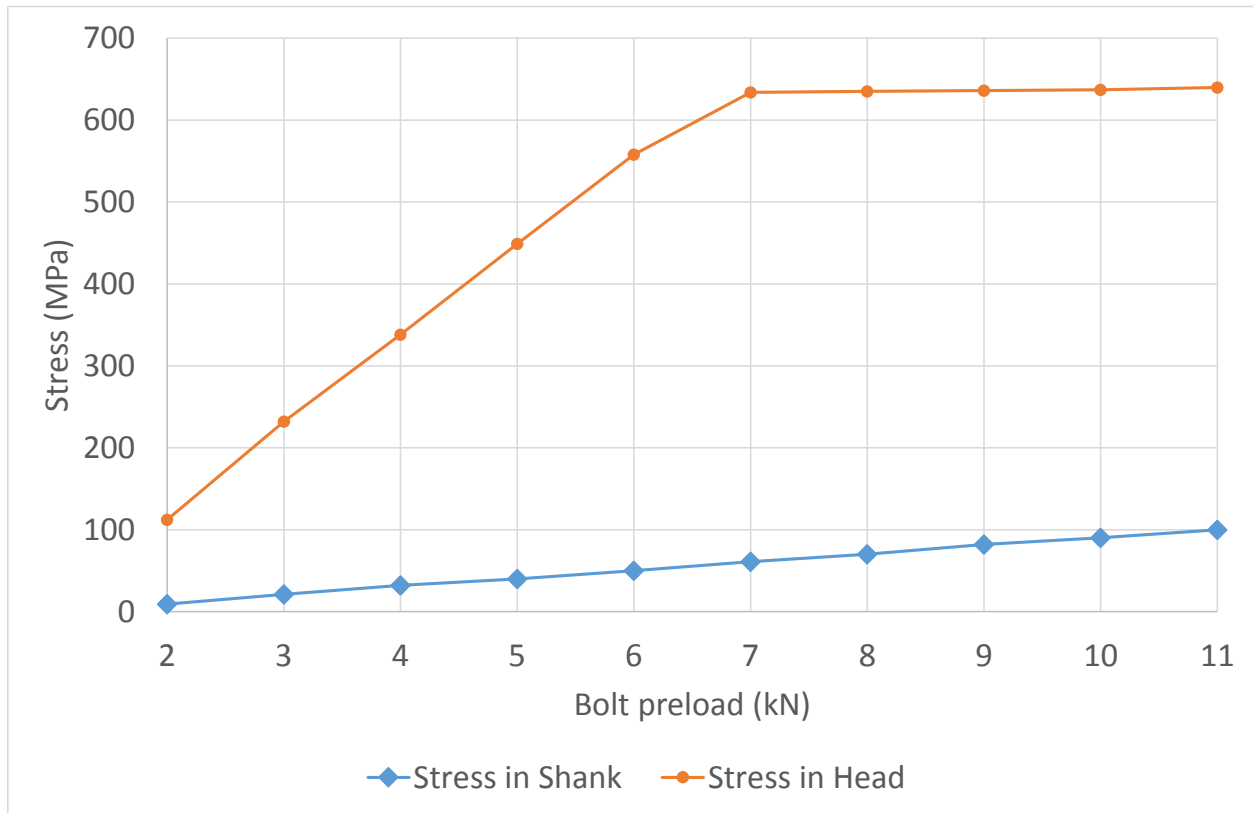
A range of preload from 1.0 kN to 11.0 kN with 1.0 kN step size is studied. Table 6-1 shows the resultant stress in the shank and the head of the bolts for different pre-loads. Figure 6-12 illustrate the results in a graph. As it can be seen, the stress in the bolts reaches a critical value close to the yielding strength by 7.0 kN bolt preload. To keep a factor of safety for the bolts, a preload of 5.0 kN is recommended for this specific assembly. This preload is used for the rest of simulations.

Table 6-1 Resultant stress for different bolt preload

Variable, Bolt Preload (kN)	Stress in Shank (MPa)	Stress in Head (MPa)
2	9	112
3	21	232
4	32	338
5	40	449



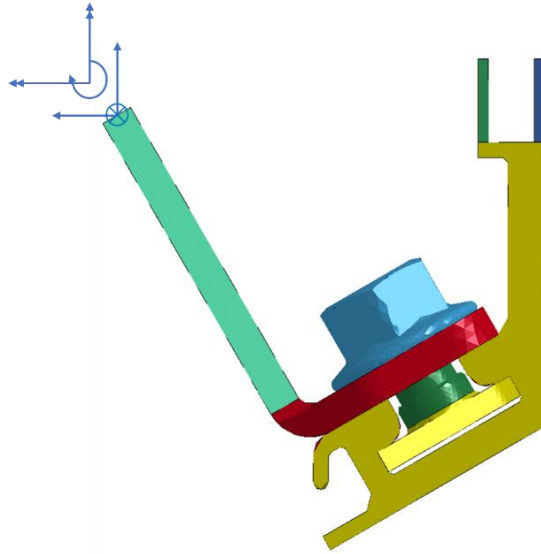
6	50	558
7	61	630
8	70	632
9	82	634
10	90	634
11	100	635



*Figure 6-12 Resultant stress for different bolt preload*

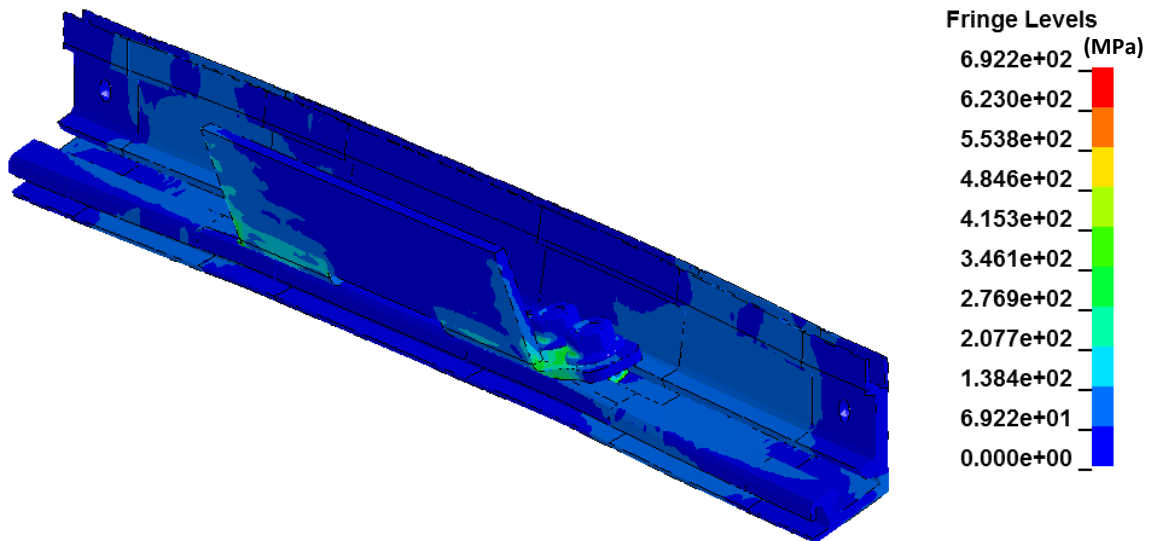
### 6.1.2.3 Load Application

After the application of bolt pretension, the external load shown in Figure 6-3 is applied to the model. The face which load is imposed on can be seen in Figure 6-13.



*Figure 6-13 Sub-model loading face*

The required outputs from the sub-model simulation are stress and plastic strain distributions, the location of the maximum stress and plastic strain and eventually, the probability of anchorage failure in a rollover. Figure 6-14 shows the distribution of the von misses stress at  $t = 0.775 \text{ sec}$  in which the stress reaches its peak value.



*Figure 6-14 Von misses stress distribution*

Since the material properties of the parts are different, the maximum stress and the Ultimate Tensile Strength (UTS) for different parts are reported in Figure 6-15. The factor of safety is calculated for each part as well. As it can be seen, stress in all the component is close to the UTS which makes the factor of safety to be small.

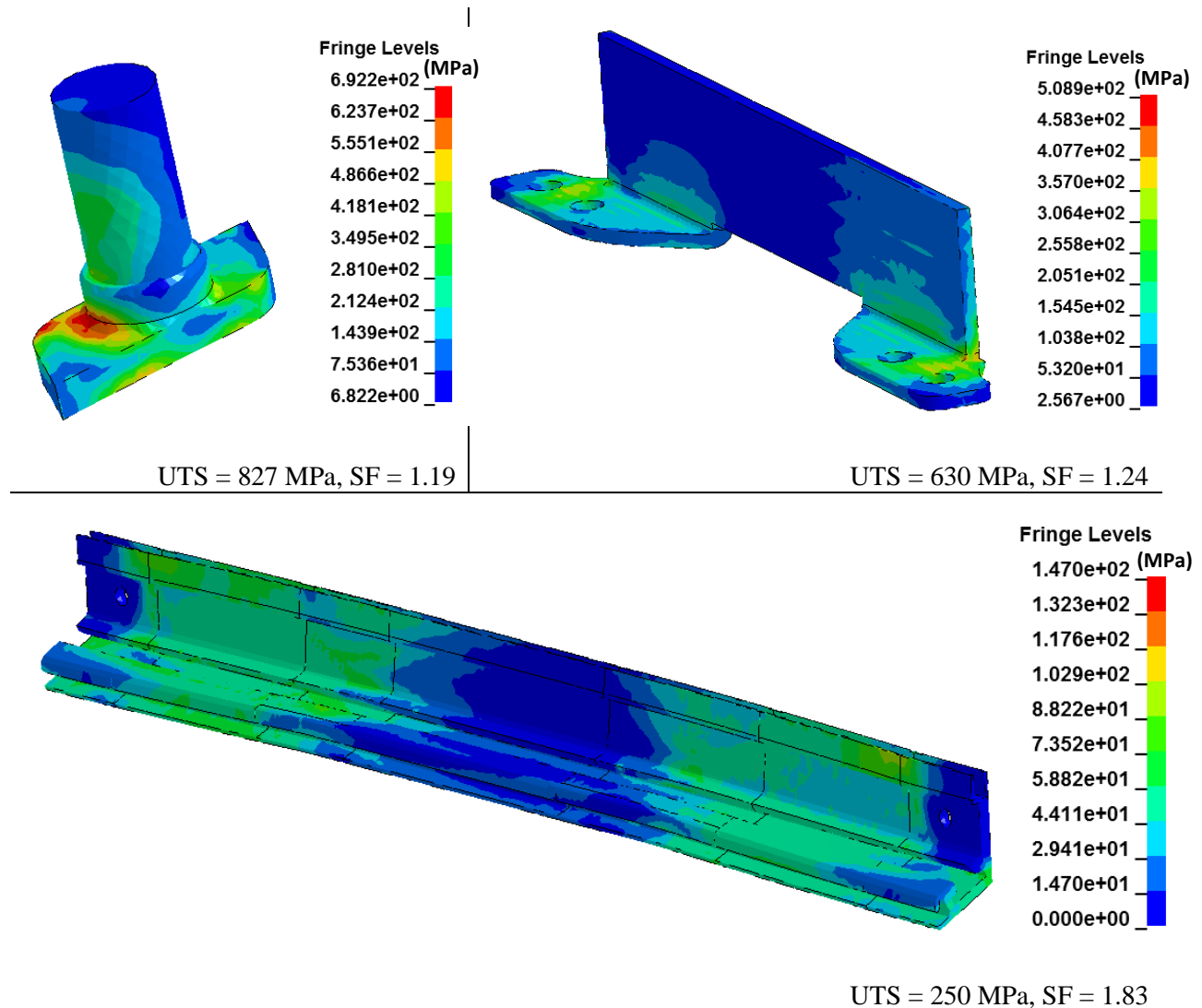
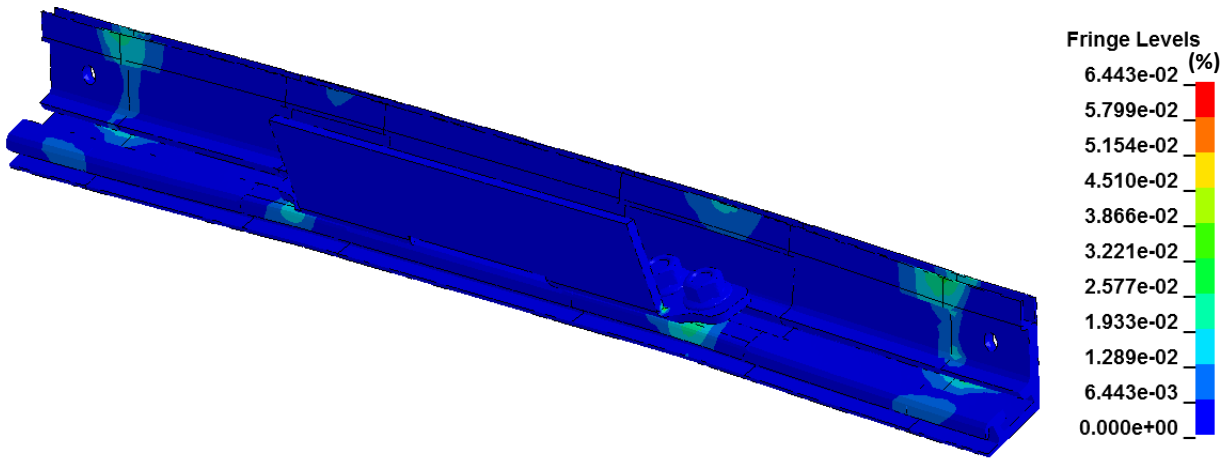


Figure 6-15 Stress distribution in each part

Figure 6-16 shows the distribution of the plastic strain in the sub-model. Approximately 6% plastic strain can be seen in the rail. The elongation at break for the type of the aluminum used in the rail is 16% [44] which makes the factor of safety to be around 2.5 based on plastic deformation.

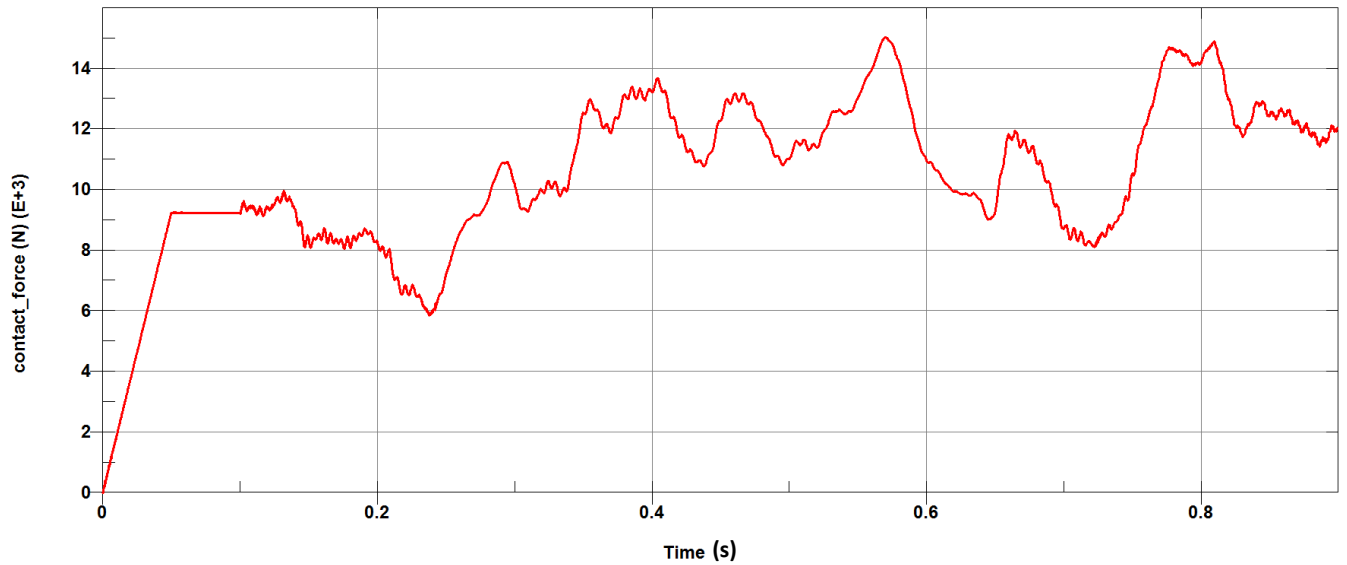


*Figure 6-16 Plastic strain distribution*

#### 6.1.2.4 Contacts Forces

Figure 6-17 shows the contact force between the bracket and the rail in the model. As it can be seen in the figure, the force between the bracket and the rail decreases after the application of the external force. If this contact force reaches zero, the bracket separates from the rail and the probability of anchorage failure increases. As a result of this discussion, the initial bolt pretension must be high enough to ensure that the contact force is kept larger than zero during the rollover. It can be concluded from Figure 6-17 that the proposed pre-stress is large enough to keep the bracket and the rail together during a rollover.

From above results and discussions, it can be concluded that although the assembly remains bonded together, the stress in components is close to their failure points. If even one seat anchorage fails during the rollover, the whole coach test must be repeated. To avoid this problem, a component test on the anchorage system seems necessary. A component test for the sub-model is designed and proposed to the manufacturer. This test can show the peak load that the assembly can resist before the failure. Comparing the imposed load on the anchorage in a rollover with the finding of the test ensures that no anchorage fails during a rollover.



*Figure 6-17 Contact Force between bracket and rail*

#### 6.1.2.5 Proposed Component Test

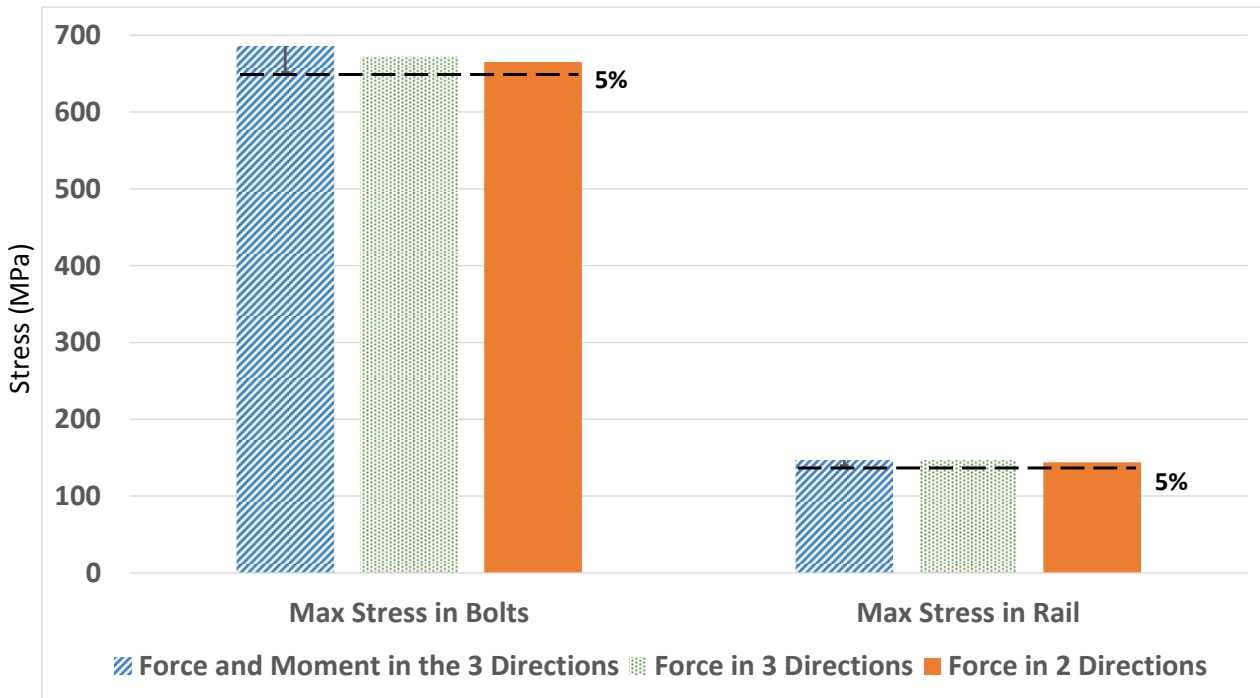
A component test on the assembly of the bracket, rail and bolts are proposed to the bus manufacturer. The geometries and boundary conditions in the test should be the same as sub-model simulation. The only difference between the test and the simulation is the external forces. In the sub-model simulation, force and moment are applied in three directions. However, applying both force and moment in three directions to a physical surface makes the test unreasonably complex. Consequently, the effects of the moments and Y direction force on the final results are investigated. As it can be seen in Figure 6-3 the force in Y direction is less than one-third of the force in the other two directions.

Three different scenarios are investigated. In the first one, force and moments in three directions are applied to the model (the original sub-model simulation). In the second one, the moment in all three directions is ignored, and just three-directional force is applied. Eventually, the load in Y

direction is omitted, and force in X and Z are the only external load on the model. Maximum stress in the bolts and rail and plastic strain are extracted for each scenario, and the results are shown in Table 6-2. The comparison of graphs (Figure 6-18 and Figure 6-19) illustrates that the difference in the maximum stress is less than 5%, and the difference in the plastic strain is less than 8%.

*Table 6-2 Maximum stress and strain for different load scenarios*

	Max Stress in Bolts (MPa)	Max Stress in Rail (MPa)	Plastic Strain in Rail (%)
Force and Moment in the 3-D	686	147	5.17
Force in 3 Directions	672	147	5.16
Force in 2 Directions	665	144	4.8



*Figure 6-18 Maximum stress*

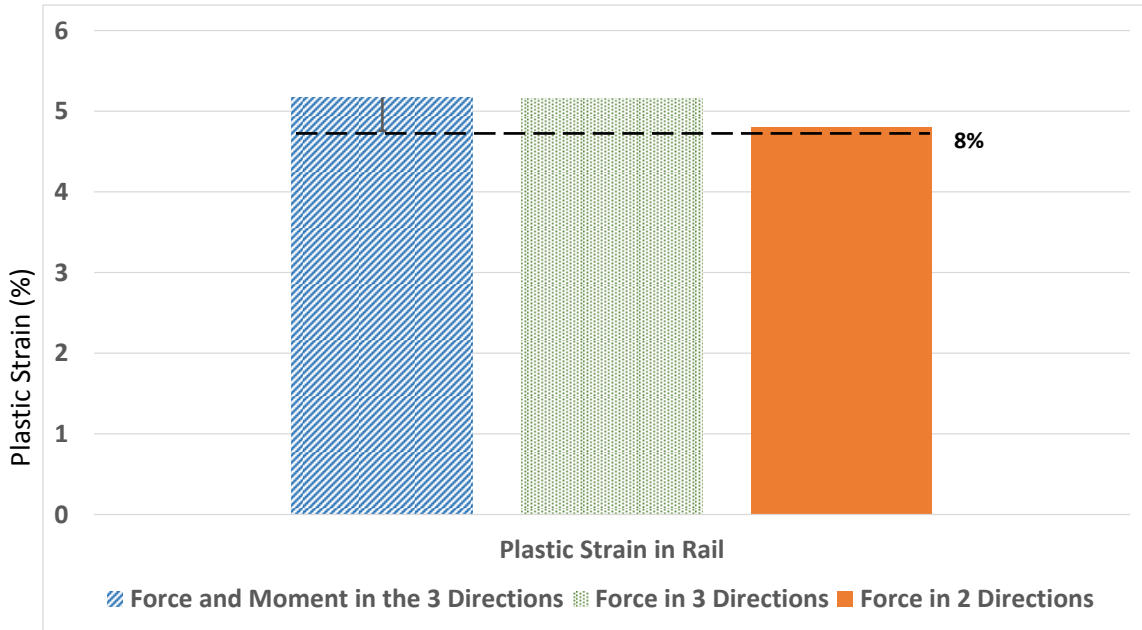


Figure 6-19 Plastic strain

From above results and discussions, it is concluded that the main imposed external load to seat anchorage system in a rollover acts in X and Y directions. Thus, an in-plane component test in which the bracket should be pulled is proposed to the bus manufacturer. Figure 6-20 shows the test setup. The test is approved by the bus manufacturer company to be performed before a complete rollover test of a coach. The direction of the load application is determined by adding the vectors of X and Z force at the moment of peak values.

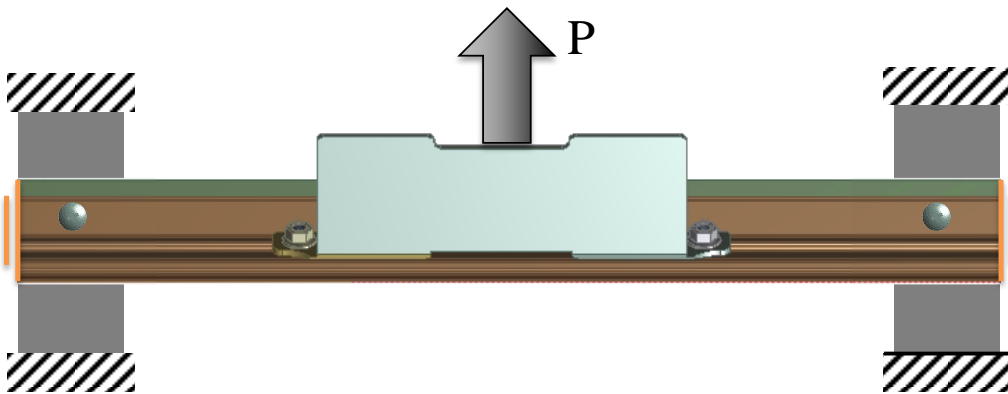


Figure 6-20 Component test setup

### 6.1.3 Mesh convergence

A mesh convergence study for the bolts is carried out to make sure that the results are not dependent on element size. Bolt is chosen for the convergence study since the maximum stress occurs in this part. Since this parts is most likely to fail first; therefore, it is considered as the main component in which highly accurate stress distribution is needed. Figure 6-21 shows stress distribution in bolts for different element sizes.

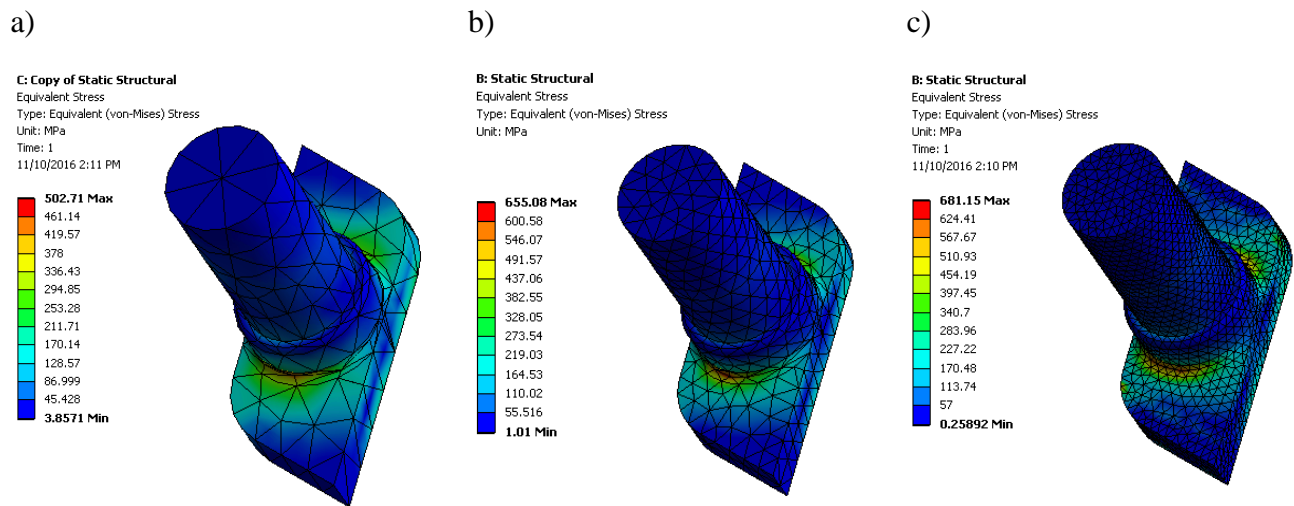


Figure 6-21 Stress distribution for different element sizes a) 4mm b) 2mm c) 1 mm

The result of convergence study shows less than 4% difference in the maximum stress from 2 to 1 mm in element size. This level of perturbation is considered acceptable, and 2 mm element size is chosen.

## 6.2 SENSITIVITY ANALYSIS OF RESTRAIN PROPERTIES

To understand the effects of retractor performance on the safety of passengers, four different configurations are studied. These configurations are summarized in Table 6-3.



Table 6-3 Retractor Configurations

Simulation #	Retractor Type	Brief Description
1	Unlocked Retractor	Webbing is free to be pulled out
2	Retractor with activated Emergency Locking Mechanism (ELM)	Retractor gets lock after 10.0 mm pull out
3	Retractor with pretensioner	Webbing is retracted back for 40 mm at the beginning of the simulation
4	Energy Management Retractor (EMR)	Does not get activated

In the first simulation, the retractor is assumed to remain unlocked during the whole rollover simulation. In order to model an unlocked retractor, the force vs. pull out curve, which is explained in Section 4.8.3, is modified. For an unlocked retractor, it is considered that the webbing can be pulled out up to one meter under low tension. Figure 6-22 shows the modified force vs. pullout curve for an unlocked retractor.

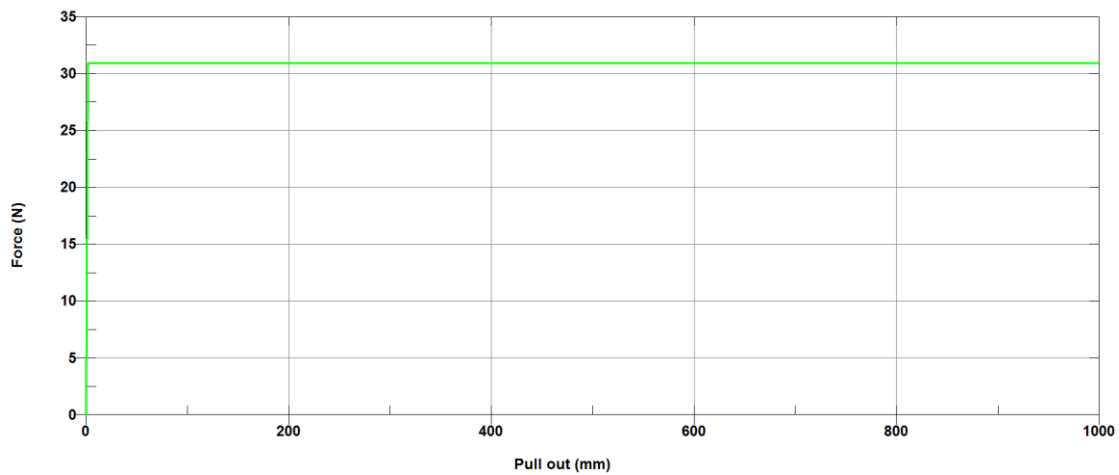
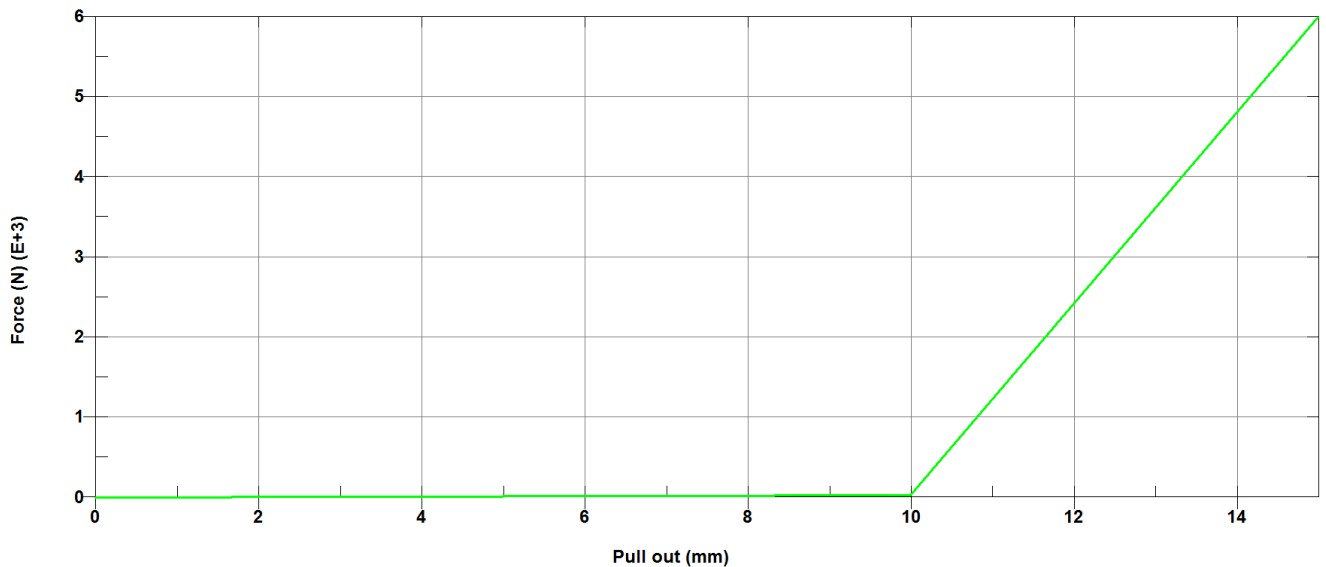


Figure 6-22 Force vs. pull out for unlocked retractor

In the second simulation, the retractor performs ideally. An ideal performance of a retractor is that the retractor locks up after a small amount of webbing is pulled out. The initial pull out is due to the belt slack within the retractor which should be eliminated before the retractor locks. Figure 6-23 shows the defined force vs. pull out for the ideal retractor. As the graph illustrates, 10 mm webbing can be pulled out under a low load. Afterward, the curve becomes very steep, and the pull out will be minimal.

Eventually, to investigate the effects of pretensioner in a rollover, one simulation with pretensioner deployment is performed. Although pretensioner is not designed to deploy in a rollover, it can be activated using new sensor technologies. Consequently, the possible positive effects are investigated in this thesis. The retractor deploys at  $t = 0.001s$  in the simulation and retracts 40 mm of the webbing. Afterward, due to the seat belt force, retractor locks and keeps the 40 mm retraction constant during the simulation.



*Figure 6-23 Force vs. pull out for unlocked retractor*

EMR is not studied since the maximum belt load reached in rollover simulations is of the order of 0.5 kN which is less than the required load to trigger a load limiter. The required load in a typical passenger car's EMR is of the order of 4 kN [45].

The results of the first simulation show that if the retractor does not lock properly, approximately 300 mm webbing is pulled out (Figure 6-24). This high webbing pullout in a rollover accident increases the chance of partial or complete ejection of the occupants. Ejection increases the injury risks of passengers up to 10 times [16]. Although it was concluded by other researchers [16], [6] that seat belt can improve the protection of passengers in a rollover, it can be seen from this research that introduction of the seat belt itself is not sufficient. Retractors used in coaches should be designed in a way, to guarantee that they remain locked under imposed acceleration of coaches' rollover to prevent the ejection.

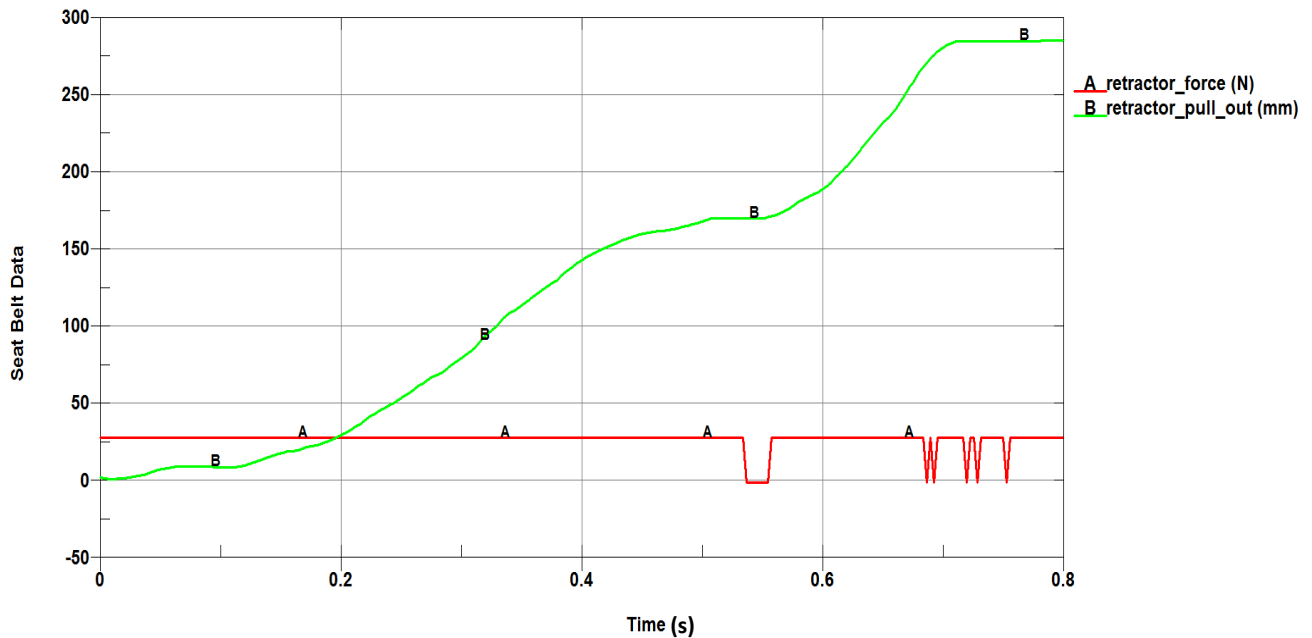
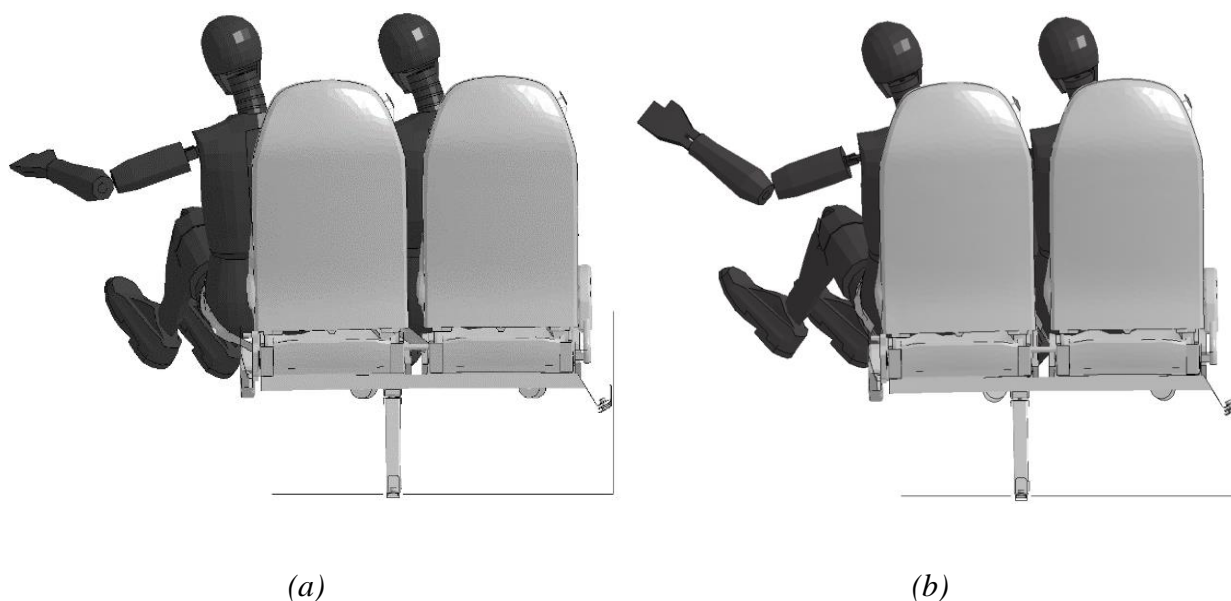


Figure 6-24 Unlocked retractor performance

Figure 6-25 compares ATDs' position with unlocked and locked retractor at the same moment. As it can be seen in Figure 6-25a (with unlocked retractor) ATD is partially ejected from the seat, and its hip is not in touch with the seat cushion. However, in the simulation with locked retractor (Figure 6-25b) ATD is kept safely on the seat.

In Figure 6-26 the performance of the locked retractor in the rollover simulation is shown. When the belt force reaches a threshold, at around  $t = .08$  s, the locking mechanism in retractor becomes activated, and no more webbing can be pulled out. The initial 10 mm pull out can be seen before  $t = .08$  s.



*Figure 6-25 a) Unlocked retractor b) Locked retractor*

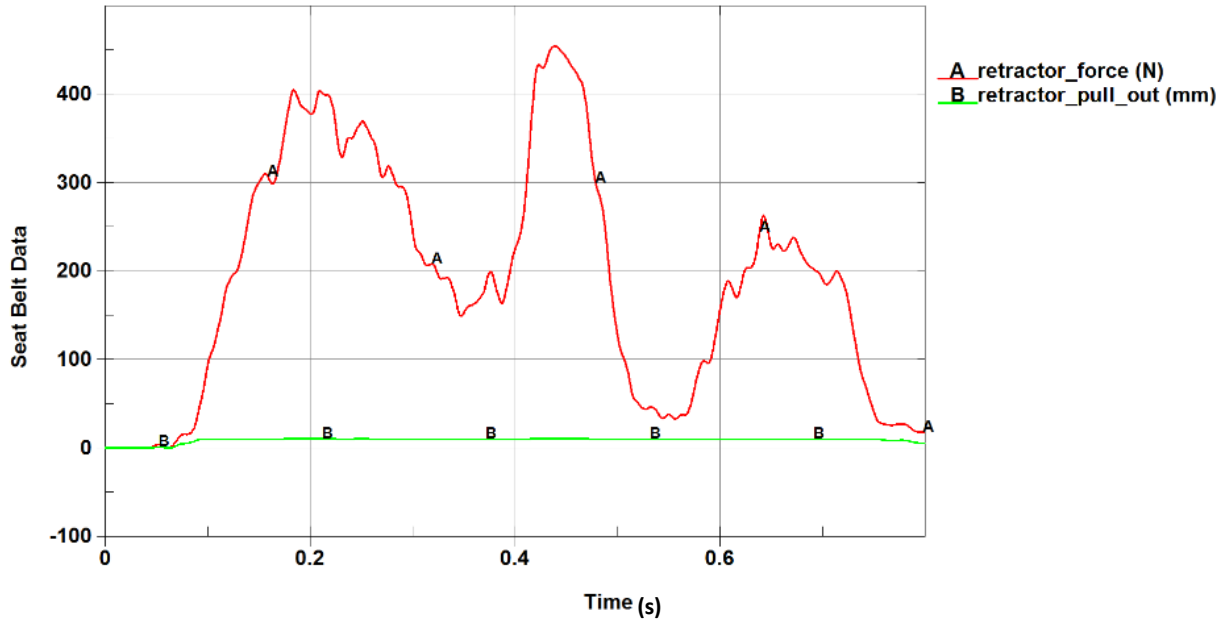


Figure 6-26 Locked retractor performance

The performance of the retractor pretensioner is shown in Figure 6-27. As it can be seen, 40 mm webbing is retracted at the beginning of the simulation. Afterward, the belt tension activates the retractor locking mechanism, and no webbing can be pulled out.

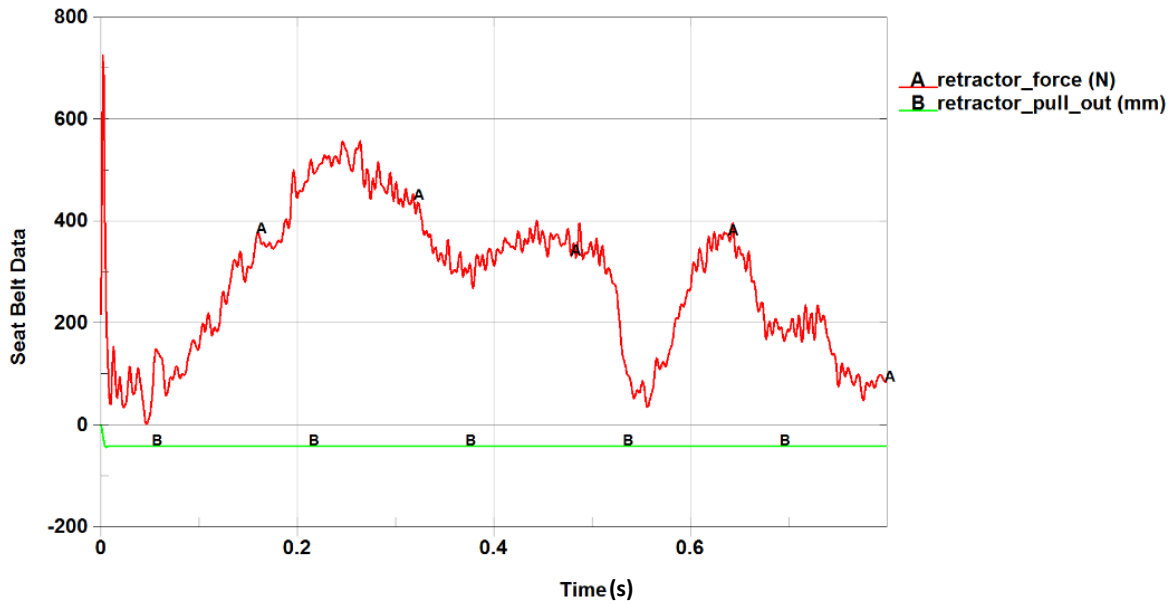


Figure 6-27 Pretensioner performance

Table 6-4 summarizes the obtained results. Use of the pretensioner can reduce the HIC36, chest deflection, and 3 ms-clip thorax acceleration by 11%, 20%, and 60% respectively. Although pretensioner increases the chest deflection at the beginning of the simulation, the maximum chest deflection which comes from the peak acceleration is reduced (Figure 6-28).

It was shown in [16] and [6] that the impact of the occupant's head to the sidewall is the primary reason of injury. To investigate the effect of the pretension on the risk of the impact to the sidewall, the maximum head displacement of the window seat's ATD is also reported. As can be seen, use of pretensioner decreases the chance of this hard impact by decreasing the displacement of the head. All the injury criteria not listed in Table 9 show no dependency on the use of pretensioner.

*Table 6-4 Injury risk comparison*

Injury risk	No Pretensioner	With Pretensioner	Percentage of Improvement
Peak head acceleration Z (G's)	8.1	7.48	8%
HIC36	12.85	11.46	11%
Head displacement (mm)	315	275	14%
Chest deflection (mm)	5	4.2	20%
3 ms-clip thorax peak acceleration (G's)	17.10	7.16	60%

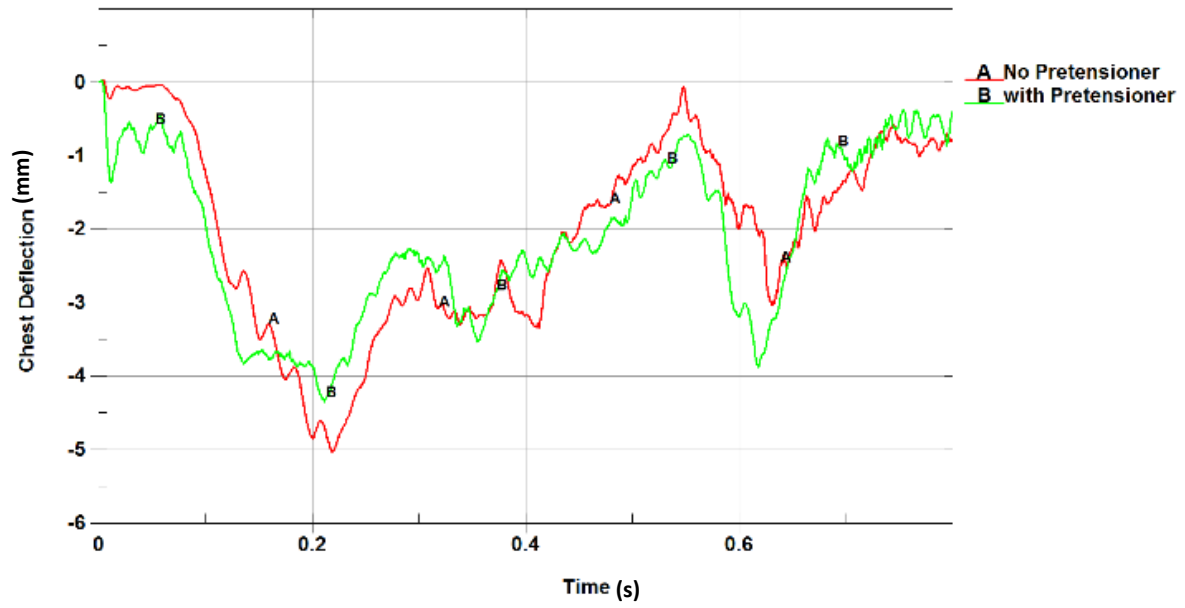


Figure 6-28 Chest deflection comparison

## 7 SUMMARY AND FUTURE WORK

### 7.1 OVERVIEW

In this study, the integrity of a coach seat structure and the safety of restrained occupants in a rollover is investigated. To have a realistic loading for the seat, and to perform the study on the passenger safety, the kinematics of occupant in a rollover is simulated.

Firstly, a detailed model of the coach seat is constructed. The model is validated against the results of a quasi-static experiment (FMVSS 210), and a good level of agreement is demonstrated. Secondly, a new approach is proposed for the dynamic simulation of the occupant behavior in a rollover. Instead of simulating a whole coach or a bay section rollover test, the acceleration time history from a complete vehicle rollover test is imposed directly on the seat model occupied by the ATDs. The approach yields a highly computationally effective model, which is well suited for the parametric studies on the occupant safety. To validate both the model and the modeling approach, injury criteria values of the ATD are compared to the experimental results and an acceptable level of correlation is shown. In this study, the validation is performed by calculating the quantitative comparison metrics.

To investigate the seat structural integrity in a rollover, the total deformation of the seat under the imposed inertial load of occupants is inspected. The anchorage in which maximum stress occurs is found. To capture an accurate stress distribution in the anchorage system, a sub-model with the detailed features of anchorage assembly is developed. The imposed loading on the sub-model is extracted from the simulation of kinematics. The results show that although the anchorage system



performs ideally and no part separation is observed, the stress in bolts head and rail exceeds the yield strength. To ensure that anchorage system does not fail in the whole coach rollover test, a component test on the anchorage system is designed and proposed to the manufacturer to be performed prior to the whole coach rollover test. The component test procedures and loading direction are designed based on the results of this study to represent the anchorage performance in a rollover precisely.

The validated model is then used to evaluate the effects of seat belt retractor's performance on the safety of the occupant through a parametric study. In this parametric study, four different retractors (unlocked retractor, retractor with activated ELM, retractor with pretensioner, and EMR) are investigated. The result of a study with unlocked retractor shows a 300 mm pullout of the webbing during the rollover. This amount of pullout increase the chance of partial or complete ejection of the passengers even with a fastened seat belt. It can be concluded that the presence of the seat belt itself does not guarantee that passengers remain restrained during the rollover. It is of paramount importance for the safety of passengers to ensure that the retractor locks during a rollover.

The results of the study with a locked retractor confirms that if the retractor performs ideally, the passengers remain restrained to the seat during the rollover which decrease the risk of injury.

Afterward, the possible positive effects of pretensioner deployment in a rollover accident are investigated. It is concluded that pretensioner implementation in a rollover can improve the safety of passengers. The pretensioner can also decrease the chance of head impact with the sidewall which is the main reason for the injury of an occupant seated in a window seat.

The result of a simulation with EMR demonstrates that this retractor does not get activated during the rollover and has no effects on the safety of passengers.

## 7.2 CONCLUSIONS

The following points can be concluded from this thesis:

- The seat structure is likely to remain attached during the rollover test, however, performing a component test on anchorage system prior to the whole coach rollover test is highly recommended.
- Comparing the anchorage system test's results with the findings of this research can assure the integrity of the seat structure during the rollover test.
- The safety of the passengers in a rollover is not 100% guaranteed by just the presence of the seat belt. It is more important for the safety of passengers to ensure that the retractor remains locked during a rollover.
- The probability of the injury to the restrained passengers can be decreased by implementing retractor pretensioners in coaches.

## 7.3 ANSWERS TO THE RESEARCH QUESTIONS

The stated questions in Section 1.2.2 are answered through the thesis and summarized as bellow:

- This study shows that to simulate the kinematics of occupant in a rollover, instead of performing a complete vehicle simulation, the acceleration history of a physical rollover test can be applied to a system of seats and ATDs.
- This modeling approach can be validated against experimental results by comparing the injury criteria values of the implemented ATD in the simulation and a physical test.
- To have a quantitative validation, comparison metrics, i.e. Sprague & Geers MPC and ANOVA metrics, can be evaluated for each pair of the curve.

- Omitting the vehicle structure from modeling procedure yields a computationally effective model that is highly suitable for a parametric study on the passenger safety. The required run-time for a whole coach rollover test for obtaining kinematics is several days; however, the required run-time by the new modeling approach is less than six hours.
- A sensitivity analysis on effects of retractor performance on the occupant safety is performed in this thesis. The results show that how the performance of retractor affects the safety of passengers in a coach rollover.

#### 7.4 FUTURE WORK

Time, data, and sample constraints leave the following points-of-interests to be examined in any possible continuation of this study:

- Considering the sidewall deformation by simply modifying boundary condition in the model.
- Comparing the strength of the anchorage assembly, which will be the finding of the component test with the result of the sub-model simulation.
- Performing more parametric studies on effects of a variety of parameters on the safety of passengers; i.e. foam stiffness, seat belt material, the initial position of the seat and ATDS, etc.
- Improving the correlation of the simulation results with experimental results by tuning the initial position of ATDs and/or calibrating the model.

## REFERENCES

- [1] V. Belsare, C. Pathak, M. Kulkarni, "Rollover Analysis of Passenger Bus as per AIS-031," *International Journal of Engineering Research and Development*, vol. 4, no. 5, pp. 49-59, 2012.
- [2] National Highway Traffic Safety Administration, "Federal Motor Vehicle Safety Standards; Bus Rollover Structural Integrity," US Department of Transportation, 2014.
- [3] S. Bozzini, C. Shipp, D. Friedman, E. Dugay, "An Examination and Comparison of Passenger Transport Bus Occupant Protection Regulations Across 5 Continents," 23rd International Technical Conference on the Enhanced Safety of Vehicles (ESV), 2013.
- [4] National Highway Traffic Safety Administration, "Standard No. 208; Occupant crash protection," US Department of Transportation.
- [5] RONA Kinetics and Associates Ltd., "Evaluation of Occupant Protection in Buses," North Vancouver, British Columbia, 2002.
- [6] L. Martinez, F. Aparicio, A. Garcia, J. Paez, G. Ferichola, "Improving Occupant Safety in Coach Rollover," *International Journal of Crashworthiness*, vol. 8, no. 2, pp. 121-132, 2003.
- [7] M. Matolcsy, "The Severity of Bus Rollover Accidents," in *International Technical Conference on the Enhanced Safety of Vehicles*, Lyon, France, 2007.
- [8] National Highway Traffic Safety Administration, "Laboratory Test Procedure for FMVSS 220," US Department of Transportation, Washington, DC, 1991.

- [9] Economic Commission for Europe, "Uniform Technical Prescriptions Concerning The Approval of Large Passenger Vehicles With Regard To The Strength of Their Superstructure," United Nations, 2006.
- [10] National Highway Traffic Safety Administration, "Initiatives to Address the Mitigation of Vehicle Rollover," US Department of Transportation, 2013.
- [11] C. Liang, G. Le, "Analysis of Bus Rollover Protection Under Legislated Standards Using LS-DYNA Software Simulation Techniques," *International Journal of Automotive Technology*, vol. 11, no. 4, p. 495–506, 2010.
- [12] M. Guler, K. Elitok , B. Bayram, U. Stelzmann, "The Influence of Seat Structure And Passenger Weight on The Rollover Crashworthiness of an Intercity Coach," *International Journal of Crashworthiness*, vol. 12, no. 6, pp. 567-580, 2007.
- [13] J. Anderson, M. Sadeghi, "Influence of Passengers During Coach Rollover," in 18th International Technical Conference on the Enhanced Safety of Vehicles, Nagoya, Japan, 2003.
- [14] E. Chirwa, H. Li, P. Qian, "Modeling A 32-Seat Bus and Virtual Testing for R66 Compliance," *International Journal of Crashworthiness*, vol. 20, no. 2, pp. 200-209, 2015.
- [15] C. Bojanowski, R. Kulak, "Multi-Objective Optimization and Sensitivity Analysis of A Paratransit Bus Structure for Rollover and Side Impact Tests," *International Journal of Crashworthiness*, vol. 11, no. 6, pp. 665-676, 2011.
- [16] M. Guler,A. Atahan, B. Bayram, "Crashworthiness Evaluation of an Intercity Coach Against Rollover Accidents," *International Journal of Heavy Vehicle Systems*, vol. 18, no. 1, pp. 64-82, 2011.

- [17] G. Belingardi, D. Gastaldin, P. Martella, L. Peroni, "Multibody Analysis of M3 Bus Rollover: Structural Behaviour and Passenger Injury Risk," in 18th International Technical Conference on the Enhanced Safety of Vehicles, Nagoya, Japan, 2003.
- [18] G. Belingardi, P. Martella, L. Peroni, "Coach Passenger Injury Risk During Rollover: Influence of The Seat And The Restraint System," in 19th International Technical Conference on the Enhanced Safety of Vehicles, Washington, D.C., 2005.
- [19] P. Deshmukh, "A Thesis on Rollover and Roof Crush Analysis of Low-Floor Mass Transit Bus," Wichita State University, 2006.
- [20] B. Hare, L. Lewis, R. Hughes, "Analysis of Rollover Restraint Performance with and without Seat Belt Pretensioner at Vehicle Trip," SAE Technical Paper 2002-01-0941, 2002.
- [21] M. Klima, D. Toomey, M. Weber, "Seat Belt Retractor Performance Evaluation in Rollover Crashes," Society of Automotive Engineers, 2005-01-1702, 2005.
- [22] C. Parenteau, M. Shah, "Driver Injuries in US Single-Event Rollovers," Society of Automotive Engineers 2000-01-0633, 2000.
- [23] K. Friedman, J. Hutchinson, D. Mihora, J. Cummings, "Finite-Element Modelling of Restrained Occupant Partial Ejection under Rollover Conditions," International Journal of Crashworthiness, vol. 20, no. 3, pp. 211-216, 2015.
- [24] E. Sahraeia, K. Diggesb, D. Marzouguic, K. Roddisb, "High Strength Steels, Stiffness of Vehicle Front-End Structure, and Risk of Injury to Rear Seat Occupants," Accident Analysis & Prevention, vol. 66, pp. 43-54, 2014.
- [25] American Society of Mechanical Engineers, "Guide for Verification and Validation in Computational Solid," American National Standard, New York, 2006.

- [26] M. Ray, M. Mongiardini, C. Plaxico, C. Plaxico, "Procedures for Verification and Validation of Computer Simulations Used for Roadside Safety Applications," 2010.
- [27] M. Sprague, T. Geers, "Spectral Elements and Field Separation For An Acoustic Fluid Subject To Cavitation," *Journal of Computational Physics*, vol. 184, p. 149–162, 2003.
- [28] M. Ray, "Repeatability of Full-Scale Crash Tests and a Criteria for Validating Simulation Results," *Transportation Research Record* 1528, pp. 155-160, 1997.
- [29] ANSYS Incorporation, "ANSYS Workbench User's Guide," Canonsburg, 2009.
- [30] Livermore Software Technology Corporation, "LS-DYNA Keyword User's Manual," LSTC, Livermore, California, 2015.
- [31] Livermore Software Technology Corporation, "LSTC. LS-PrePost Online Documentation," [Online]. Available: <http://www.lstc.com/lsp/>. [Accessed 25 08 2016].
- [32] Livermore Software Technology Corporation, "LS-DYNA Support," [Online]. Available: <http://www.dynasupport.com/>. [Accessed 26 08 2016].
- [33] Livermore Software Technology Corporation, "LS-DYNA Theory Manual," LSTC, Livermore, California, 2015.
- [34] Z. Cheng, J. Thacker, W. Pilkey, W. Hollowell, S. Reagan, E. Sieveka, "Experiences in reverse-engineering of a finite element automobile crash model," *Finite Elements in Analysis and Design*, no. 37, pp. 843-860, 2001.
- [35] Y. Li, F. Lan, J. Chen, "Experimental and Numerical Study of Rollover Crashworthiness of a Coach Body Section," in *SAE 2012 Commercial Vehicle Engineering Congress*, Rosemont, Illinois, USA, 2012.

- [36] C. Liang ,G. Le, "Bus Rollover Crashworthiness under European Standard: An Optimal Analysis of Superstructure Strength using Successive Response Surface Method," International Journal of Crashworthiness, vol. 14, no. 6, pp. 623-639, 2009.
- [37] S. Guha, D. Bhalsod, J. Krebs, "LSTC Hybrid III 50th Fast Dummy, Positioning & Post-Processing," LSTC, Michigan, 2011.
- [38] S. Guha, "Occupant Safety Modeling Course Notes," LSTC, Michigan, USA, 2010.
- [39] Fastenal Engineering & Design Support, "Screw Thread Design, Rev. 3-4-09," FEDS.
- [40] R. Serway, R. Beichner, Physics for Scientists and Engineers, Orlando, FL: Saunders College Publishing, 5th Ed., (2000).
- [41] Livermore Software Technology Corporation, "Preloads in LS-DYNA," LSTC, Livermore, California, 2011.
- [42] National Highway Traffic Safety Administration, "Laboratory Test Procedure for FMVSS 210," US Department of Transportation, 1994.
- [43] Fastenal Company Engineering Department, "Technical Reference Guide," 2005.
- [44] "Engineering Material Database," 2009. [Online]. Available: <http://www.makeitfrom.com/>. [Accessed 01 10 2016].
- [45] J. Bruno, X. Trosseille, Y. Page, "Thoracic Injury Risk In Frontal Car Crashes With Occupant Restrained With Belt Load Limiter," SAE International, 2001-22-0009, 2001.